Insights into the structure and reaction mechanism of alkali and alkaline-earth metal amide - metal hydride composite systems for hydrogen storage

Von der Fakultät für Maschinenbau
der Helmut-Schmidt-Universität /
Universität der Bundeswehr Hamburg
zur Erlangung des akademischen Grades eines
Doktor-Ingenieurs
genehmigte

DISSERTATION
vorgelegt von

von
Antonio Santoru

aus
Sassari, Italien

Hamburg, 2018

Vorsitzender des Prüfungsausschusses: Univ.-Prof. Dr. rer. nat. habil. Markus Bause
1. Gutachter: Univ.-Prof. Dr.-Ing. habil. Thomas Klassen
2. Gutachter: Univ.-Prof. Dr. habil. Chiara Milanese
Tag der mündlichen Prüfung: 03.07.2018

Insights into the structure and reaction mechanism of alkali and alkaline-earth metal amide - metal hydride composite systems for hydrogen storage

Antonio Santoru

Abstract

The *in situ* formation mechanism of amides by ammonolysis of the lightest alkali and alkaline-earth metal hydrides is investigated. Novel information, particularly on the ammonolysis process of KH is given in detail. Furthermore, the hydrogen sorption properties, reaction mechanisms and phase evolution of the K-Mg-N-H system are studied *in situ*. The desorption temperature and reaction pathways of the composite systems $KNH_2 + MgH_2$, $KH + Mg(NH_2)_2$ are analysed and compared underlining differences in their thermodynamic and kinetic properties. As a consequence, the KNH_2-KH composite system is systematically explored in the entire compositional range, in order to isolate and characterize the novel intermediates evidenced during the ammonolysis of KH and during the desorption process of $K-Mg-N-H$ based systems. The investigation is enlarged to include the Rb-N-H and Rb-Mg-N-H systems, providing novel structural analogies which are discussed in detail. The insights presented in this work expand the knowledge about the crystal chemistry of metal amides, thus helping to improve the understanding of the role of K- and Rb-based additives on the hydrogen desorption/absorption properties of the Li-Mg-N-H system.

Einblicke über die Struktur und den Reaktionsmechanismus von Alkali- und Erdalkalimetallamid-Metallhydrid Komposit-Systeme zur Wasserstoffspeicherung

Antonio Santoru

Zusammenfassung

In dieser Arbeit wurde die Bildung von Amiden durch Ammonolyse der leichtesten Alkali- und Erdalkalimetallhydride untersucht. Neue Erkenntnisse, insbesondere über den Ammonolyseprozess von KH, werden im Detail gegeben. Darüber hinaus wurden die Wasser-

stoffsorptionseigenschaften, Reaktionsmechanismen und Phasenentwicklungen des K-Mg-N-H-Systems *in situ* untersucht. Sowohl die Desorptionstemperatur als auch die Reaktionswege der Komposite Systeme KNH_2 + MgH_2, KH + $Mg(NH_2)_2$ wurden analysiert und verglichen, wobei merkliche Unterschiede in ihren thermodynamischen und kinetischen Eigenschaften gefunden wurden. Das KNH_2-KH-Komposit wurde systematisch im gesamten Zusammensetzungsbereich untersucht, um die neuen Übergangphasen, die während der Ammonolyse von KH und des Desorptionsprozesses von K-Mg-N-H basierenden Systemen nachgewiesen werden konnten, zu isolieren und zu charakterisieren. Um zu studieren, in wieweit die gefunden Ergebnisse auch auf andere Systeme übertragbar sind, wurden zudem Rb-N-H- und Rb-Mg-N-H-Systeme und die entsprechendne Umwandlungen in diesen erforscht. Die in dieser Arbeit gewonnenen Erkenntnisse erweitern das Wissen über die Kristallchemie von Metallamiden und tragen somit dazu bei, die Bedeutung von K und Rb-basierten Additiven für die Desorption- und Absorptionseigenschaften von Wasserstoff des Li-Mg-N-H-Systems besser zu verstehen.

Contents

1 Introduction

1.1 Environmental aspects

In the 19th century the French mathematician and physicist Jean-Baptiste Joseph Fourier suggested that the solar radiation ("chaleur lumineuse") has the capacity to penetrate diaphanous bodies. However this property is lost once the visible light is converted into radiant heat ("chaleur obscure"). More precisely, he correctly stated that the water masses covering the globe, constitute an obstacle to the radiant heat that is emitted from the Earth in opposite direction, towards the space.[1]

Pouillet further discussed this hypothesis some years later, but an experimental proof came only with the remarkable work of Tyndall. The Irish scientist, with a series of carefully designed measurements, proved that different types of gases can absorb different amounts of radiant heat.[2, 3, 4] Tyndall is commonly regarded as the first man to prove experimentally the importance of atmospheric gases on the thermal balance of the planet, later known as greenhouse effect, and to suggest its possible effects on the climate.[5]

A very comprehensive perspective on the topic was given by the Swedish physicist and chemist Svante Arrhenius. In his work, published in 1896, he reviewed the main theories and discoveries made up to that point.[6] At that time, the scientific community was already aware that water and carbon dioxide are mostly transparent to UV radiation, while they absorb more efficiently the infrared part of the spectrum emitted from the Earth's surface. After laying down the necessary scientific basis, Arrhenius described his calculations of the temperature variations expected in the different seasons and latitudes, for various concentrations of carbon dioxide in the air.

Few years later Arrhenius published "Worlds in the making: the evolution of the universe", a book intended for a broader audience. In one chapter of this book, "Celestial bodies as abodes of organisms", he suggested that life has developed on Earth because of its mild average temperature. He also estimated that, without atmosphere, the average temperature on Earth would be as low as $-14\,^{\circ}\mathrm{C}$, well below the freezing point of water. The greenhouse effect in this view plays an important role on the thermal balance of the planet, providing the moderate climatic conditions required from living beings in order to survive.[7]

Arrhenius and Tyndall suggested that all the glaciations and climatic changes might have been caused by different amounts of carbon dioxide in the air. [4, 1, 7] They were aware that CO_2 is formed also as a result of combustion of coal and hydrocarbons, however there was not much concern on the negative impact of a possible warming. Arrhenius, in particular, was more concerned with facing a future ice age. In his opinion, the increase of carbon dioxide atmospheric concentration, due to volcanic activity and use of fossil fuels, would be helpful to prevent such event, improve the climate of colder regions and possibly augment the yield of crops, thus helping the prosperity of mankind.[7, 8]

An important milestone was achieved with the measurement of infrared absorption spectra of carbon dioxide and water.[9] In fact, these data were used from Callendar later, in 1938, to calculate more precisely the influence of anthropogenic CO_2 on the average atmospheric temperature.[10, 11, 12] Arrhenius did not separate the contributions of artificially and naturally produced CO_2. He calculated that, by doubling the amount of CO_2 in the atmosphere, the temperature would increase by 5 to 6 °C, while according to more recent models the expected increase would be from 1.5 °C to 4.5 °C.[13]

Callendar improved the equations of Arrhenius, considering different atmospheric layers in the descriptive model.[14] The calculations of CO_2 levels and corresponding temperatures showed a clear correlation; this, combined with the fact that the increase in CO_2 concentration was in good agreement with the estimated consumption of fossil fuels, induced Callendar into thinking that three quarters of the carbon dioxide artificially produced in the previous 50 years were left in the atmosphere and were directly responsible for the increase of temperature.[10] Later assessments based on radio-carbon measurements showed that carbon dioxide persists in the atmosphere only for about 10 years, before being dissolved into the oceans. Therefore, it was not possible that most of the anthropogenic CO_2 was still in the atmosphere as Callendar suggested.[15] Despite this, the values of carbon dioxide concentrations and global temperatures estimated from Callendar are still in very good agreement with the values recently calculated for the same time span.[16, 17] The reason for this apparent contradiction is most probably that Callendar didn't consider amplifying effects and forcing on the climate (except for water vapour) and he didn't include the contribution of other greenhouse gasses (methane, nitrous oxide and chlorofluorocarbons).

Concerning possible effects over the long term, Callendar's opinion was in alignment with Arrhenius'. He supposed improved growth rates of plants and an indefinite delay of "deadly glaciers".[10]

Callendar estimated that fuel reserves in his time were enough to provide a 10 fold increase of atmospheric CO_2, if fully exploited.[10] Clear preoccupations over the availability of fossil resources were expressed in 1949 by the US-American geophysicist Hubbert. In his study Hubbert underlined the limited nature of these energy sources and predicted that,

after a maximal exploitation, their use will undoubtedly decrease and tend asymptotically to zero. On the other side, the use of other forms of energy, e.g. water power, could raise asymptotically towards a maximum limit, without necessarily declining to zero over the long term.[18]

Awareness on the possible environmental problems deriving from the prolonged use of fossil fuels developed only after the International Geophysical Year in 1957-1958. The IGY was an important event from both the scientific and political point of view. 64 countries collaborated in an international research program, right after the end of the cold war and in coincidence with the peak of the 19^{th} solar cycle.[19, 20, 21] A part of the project focused on "earth's heat and water regimen" with sub-groups in climatology, oceanography and glaciology.[21] In this context, Keeling performed measurements of atmospheric CO_2 levels at the observatory of Mauna Loa (Hawaii).[14, 22]

During the IGY more than 1000 meteorological stations were deployed all over the world.[20] The huge amount of data collected, combined with the advancing computer technology and the development of general circulation models for the atmosphere, allowed noticeable improvements in the complexity of the applied model and, consequently, far more accurate predictions of the future temperature and CO_2 levels trends.[23]

The increasing importance of the topic and amount of available literature culminated with the necessary foundation of the Intergovernmental Panel on Climate Change (IPCC) in 1988. This committee was founded from the combined effort of the World Meteorological Organization (WMO) and United Nations Environment Program (UNEP). The IPCC did and still does not perform independent research, but rather assess the published literature, in order to provide the policymakers with the most rigorous scientific information. The reports written from the IPCC discuss the causes, risks and future scenarios of climate change.

Over the time, the scientific consensus on climate change has been repeatedly doubted in the media, particularly by policymakers. However the IPCC reports are by themself an expression of scientific consensus. Moreover, independent assessments on the pertinent literature confirmed the conclusions drawn by the IPCC.[24]

In the last report, published in 2014, the IPCC defined anthropogenic green house gases as the most likely and major cause of global warming. Human influence is clearly identified as the cause of atmosphere and ocean warming, decrease of snow and ice, rise of sea level and increase of heavy precipitations. Predictive models suggest that additional efforts are required in order to avoid a worsening of the negative effects cited above. In order to avoid a warming of more than 2 °C, it is necessary to significantly reduce the emissions of CO_2 and other GHGs in the first incoming decades and achieve near zero levels by 2100.[25] This goal requires a gradual replacement of fossil fuels with alternative energy sources, which do not involve the release of GHGs in the first place. Ideally, we should also be able to implement sustainable

and environmentally friendly processes that allow the reduction of CO_2 levels; of course, this way is viable only if the energy demanded by its extremely unfavourable thermodynamics is obtained by carbon-free sources.

1.2 Hydrogen economy

As discussed in the previous chapter, considering the limited nature of fossil fuels and the environmental problems deriving from their exploitation, it is necessary to find alternative energy sources. The most realistic options at the moment are the so called renewable and nuclear energies: both are independent from carbon sources and therefore do not involve carbon dioxide or other GHGs as waste products. Moreover, both are already implemented to a considerable extent in countries belonging to the Organisation for Economic Co-operation and Development (OECD). According to the International Energy Agency, in 2016 about 24 % and 18 % of the total electricity in OECD countries was produced from renewable and nuclear energy sources, respectively.[26]

Unfortunately, the production of radioactive waste requiring safe long-term storage cannot be disregarded when considering a massive use of nuclear energy. In addition, the risks of disastrous accidents associated with the operation of nuclear power plants can also be considered a major drawback. Furthermore, uranium reserves have limited availability and are non-renewable.

In fact, renewable energies can be defined as deriving from sources which are renewed on a time scale that is comparable to the lifetime of humans. The formation process of fossil fuels takes place over millions of years. Biofuels production, on the other end, requires only few months/years, therefore they are considered a renewable source; moreover, their combustion produces the same amount of CO_2 that is consumed during their formation, with a total CO_2 balance virtually equal to zero. The Sun can be regarded as an infinite source of energy, if its remaining lifetime is compared to the past existence of mankind. Moreover its energy output is not influenced from our development and it can be considered as the primary energy source. Winds and precipitations result from the conversion of solar radiation into kinetic energy of molecules. Biofuels, fossil fuels and organic matter in general can also be considered as formed via the photochemical storage of a specific fraction of the solar spectrum. Only tidal and geothermal energies stand on their own: in the first case the influence of the gravitational field of the Moon, in the second case the internal heat of the Earth, play the major role.

From the practical perspective, a big disadvantage of renewable sources, with the exception of biofuels, is their discontinuous nature. The combustion of fossil fuels provides a rather constant and manageable power output, which is compatible with the use of electricity as

energy vector. However, one major obstacle to the introduction of renewable energy sources is the incompatibility of the current electric grid with their variable power output. In order to avoid an overload of the system, wind parks are often shut down and cannot be used at their full potential. It is necessary to develop more suitable ways to store, convert and transport energy. The problem can be addressed to a limited extent by implementing smart grids, in parallel with off-grid usage. However, when the integration of renewable sources will proceed further, hydrogen could be the ideal candidate for solving this issue. In fact, hydrogen has a very high gravimetric energy density and could allow a long term storage of the energy produced from renewable sources. Moreover, only water is formed from its combustion with oxygen.[27] Unfortunately nowadays most of the hydrogen (45 megatons) is produced by steam reforming, a process that requires very high temperatures to convert hydrocarbons and water vapour in carbon monoxide and hydrogen.[28, 29] A breakthrough in the hydrogen production and storage technologies is needed in order to make the hydrogen a viable energy carrier. [29] Meanwhile, using fuel cells (FCs) and hydrogen produced from steam reforming could still make sense for both mobile and stationary applications, since lower emissions are expected, if compared with conventional fuels.[30] More ecological ways to produce hydrogen only from water are known (e.g. electrolysis or photoelectrolysis), which would allow to store the excess energy output obtained from renewable sources. Conversely, when energy is demanded but cannot be directly supplied from renewable sources, the hydrogen reserves could be used to generate electricity via fuel cell technology. Hydrogen can also be used to power fuel cell vehicles (FCVs) for mobile applications. Indeed, fuel cells are a very versatile and scalable technology which could virtually be implemented in many portable and stationary devices, alone or in combination with batteries.

A significant advantage of fuel cells over combustion engines is their higher efficiency: more than 60 % versus the 22 % or 45 % of gasoline and diesel engines, respectively. Nonetheless, for some applications it is also possible to use hydrogen as fuel in slightly modified internal combustion engines, and still achieve higher efficiency as compared to the combustion of fossil fuels.[27, 31] In both cases, fuel cells and combustion engines, energy can be obtained from the transformation of hydrogen and oxygen into water (reaction 1.3). However fuel cell technology allows to directly exploit the redox nature of this process to produce electricity. The oxidation of H_2 (reaction 1.1) occurs at the anode, while the reduction of O_2 (reaction 1.2) takes place at the cathode.

$$H_2 \longrightarrow 2\,H^+ + 2\,e^- \tag{1.1}$$

$$\frac{1}{2}\,O_2 + 2\,e^- \longrightarrow O^{2-} \tag{1.2}$$

$$H_2 + \frac{1}{2} O_2 \longrightarrow H_2O \tag{1.3}$$

Anode and cathode are connected via an external circuit, allowing the electricity produced from the redox process to be used to generate kinetic energy in an electric engine, or thermal energy with an electric resistance, depending on the type of application. In proton exchange membrane fuel cells (PEM-FCs) protons are transported from the anode to the cathode through a polymer electrolyte, while in solid oxide fuel cells (SOFCs) the oxide anions are transported from the cathode to the anode via a ceramic electrolyte.[32]

PEM-FCs and SOFCs could satisfy complementary needs and target diverse applications, since they work in very different temperature ranges (80 °C and 500 °C to 1000 °C, respectively).

In a nutshell, fuel cells offer practical and versatile options for an efficient use of the hydrogen generated from renewable energies. At this point it is necessary to consider the challenges associated with the safe and long term storage of hydrogen.

1.3 Hydrogen storage

1.3.1 Storage of hydrogen in its pure form

The combustion of hydrogen produces $142\,\mathrm{kJ\,g^{-1}}$ if we consider also the condensation enthalpy of water (upper heating value), about three times more than gasoline ($47\,\mathrm{kJ\,g^{-1}}$), which would make it a very convenient fuel.[27, 33] However, hydrogen is a gas at normal temperature and pressure conditions. It turns into liquid only at temperatures lower than $-252\,^{\circ}\mathrm{C}$ (at 1 bar of pressure), but even then, it has a density of only $70.8\,\mathrm{kg\,m^{-3}}$, quite low if compared with the value of liquid hydrocarbons (about $1000\,\mathrm{kg\,m^{-3}}$).[27] Despite its low density, in the past few years several car manufacturers (e.g. Hyundai, Toyota and Honda) managed to develop and commercialize zero emission vehicles with a driving range of more than four hundred kilometres, coupling fuel cells with compressed hydrogen tanks.

Nonetheless, developing storage units that work at a lower pressure range could attenuate the safety concerns, facilitate the refuelling process and potentially lower the costs associated with the development of hydrogen refuelling stations and tank systems.

Utilizing liquid hydrogen at cryogenic temperatures could in principle address this issue. In fact, liquid hydrogen storage units possess safety valves that prevent overpressure due to the evaporation of liquid hydrogen. BMW has already tested some FCVs based on this concept.[27] However, maintaining cryogenic temperatures in order to mitigate losses over the long term (a phenomenon known as "boil-off") is still a technological challenge.[34]

1.3.2 Materials for physical storage

The adsorption of hydrogen over materials with high surface area is a third possibility of storing H_2 molecules without causing their dissociation (physical storage). Several materials have been considered thus far, most noticeably zeolites, carbon materials, metal organic frameworks (MOFs) and polymers with intrinsic microporosity (PIMs). These materials have the disadvantage of requiring cryogenic operating temperatures in order to absorb significant amounts of hydrogen;[34, 35] at RT none of them reaches the gravimetric capacity value established from the revised requirements (May 2017) of the Department of Energy (DoE) for onboard hydrogen storage in light-duty FC vehicles. Another option to store H_2 preserving its molecular state is offered by hydrogen clathrate hydrate structures. However, this method requires high pressures (300 MPa at about 77 °C) or the use of other types of guest molecules like tetrahydrofuran (THF).[33]

1.3.3 Materials for chemical storage

The hydrogen storage materials presented in this section have in common the breaking or forming of the covalent H-H bond during the absorption and desorption processes. Since different research lines were developed in parallel, it is more convenient to categorize the type of materials rather than follow a general chronological order.

1.3.3.1 Alkali and alkaline-earth metal hydrides

Alkali and alkaline-earth metal hydrides are amongst the simplest material in this list, since they are formed by combination of a metal of the first or second group with hydrogen in simple proportions, accordingly to basic valence rules.

In terms of hydrogen storage properties, hydrides of lightweight alkali and alkaline-earth metals offer higher gravimetric capacities. However, with the exception of MgH_2 ($\Delta H \approx -75\,\mathrm{kJ/mol\,H_2}$), they are usually too stable for practical applications. Due to its gravimetric capacity of 7.66 wt%, MgH_2 has been considered an interesting candidate in the past years. One main drawback of this material though, was the sluggish desorption kinetics. This issue was addressed with the discovery of several suitable additives, mostly based on transition metals, which allowed very fast desorption kinetics (0.102 wt%/s at 300 °C for the Nb_2O_5-doped MgH_2).[36, 37, 38]

1.3.3.2 Interstitial hydrides

Some transition metals react with hydrogen forming non-stoichiometric compounds. The hydrogen molecule undergoes homolytic splitting and the hydrogen atoms occupy interstitial

sites in the crystal structure of the metal. Palladium hydride was the first one to be discovered and for this reason is one of the most known metal hydrides;[33, 39] it is still studied as model system for understanding fundamental aspects of the thermodynamic properties of metal hydrides at nanoscale.[40] Other historically important materials are intermetallic compounds that are able to form the corresponding interstitial hydrides; particularly relevant for H_2 storage are: ZrNi, TiFe and $LaNi_5$. Some interstitial hydrides display very small hydrogenation enthalpy and therefore release hydrogen in near RT conditions. Unfortunately the gravimetric capacities are very limited, less than 3 wt%. Among them, the ones that are composed of highly abundant elements (e.g. Fe-Ti) could be considered for the scale-up of stationary hydrogen storage systems, where the weight and dimensions of the tank is not a primary concern.

1.3.3.3 Complex hydrides

The term "complex hydride" might be misleading in a sense that it recalls the similar term "coordination complex" which usually refers to a class of compounds where the central atom is a transition metal (i.e. an atom or cation with partially occupied *d* sub-shell, according to the IUPAC definition) which is bounded to coordination entities called "ligands" or "complexing agents". The formula of coordination complexes is usually indicated between square brackets. According to this nomenclature borane and alanates are not coordination complexes, as opposed to some other hydrides like $Mg_2[FeH_6]$, $Mg_2[NiH_4]$ etc., which comply with the rule.

Unfortunately the term "covalent hydrides" is too general, as it includes not only BH_3, AlH_3 and their derivatives, but also CH_4, NH_3, H_2O and other compounds with a completely different chemistry. Probably for this reason the term "complex hydrides" acquired very common usage within the hydrogen storage community, to indicate compounds where the hydrogen is covalently bound to another element (not necessarily a transition metal), forming a "complex anion" (e.g BH_4^-, AlH_4^-, etc.). When the charge neutrality is reached with lightweight cations (e.g. Li^+, Na^+, Mg^{2+}, Al^{3+}...) this class of compounds offers rather high gravimetric hydrogen content, in some cases more than 10 wt%.

Among tetrahydroborates (also know as borohydrides), $LiBH_4$, $Mg(BH_4)_2$ and $Al(BH_4)_3$ possess very high gravimetric capacities (18.4 wt%, 14.8 wt% and 16.8 wt%, respectively) and lower decomposition temperatures (ca. 320 °C, 320 °C and 40 °C onset values, respectively). $Be(BH_4)_2$ is not considered a viable option due to the high toxicity of metallic beryllium.[33] Miwa et al. have shown that the theoretical decomposition enthalpy varies fairly linearly with the electronegativity of the metal.[41]

The chemistry of tetrahydroborates was noticeably enriched by the discovery of several

compounds containing multiple cations or mixed anions.[42, 43, 44, 45, 46, 47, 48, 49] Unfortunately, despite the incredible variety of compounds explored so far, most borohydrides show complicated reaction pathways, partial reversibility and, in some cases, release of harmful gasses, such as diborane and ammonia, which limits their practical application as hydrogen storage materials. Nonetheless, they show a lot of other interesting properties as ionic conductivity, semiconductivity, optical and magnetic properties etc. Detailed reviews of the synthetic strategies, structural, physical and chemical properties of this class of compounds were recently published by Paskevicius et al. and Puszkiel et al.[50, 51] Moreover, the crystal chemistry of this class of compounds was recently described evidencing the analogies to metal oxides.[52, 53, 54]

Alanates are also attractive candidates for solid state hydrogen storage, owing to their high gravimetric capacity and no risk of release of toxic gases. $LiAlH_4$ contains 10.6 wt% of hydrogen, but is a metastable compound and its existence is only allowed by its very slow decomposition kinetics. For this reason its dehydrogenation to hexa-alanate (Li_3AlH_6) is exothermic and irreversible. $NaAlH_4$ on the other end, has a rather high hydrogen content (7.5 wt%) and is thermodynamically stable. However, normally it decomposes at temperatures higher than 230 °C and its reaction kinetics are too slow for practical applications. A real breakthrough was achieved by Bogdanovic and Schwickardi in 1997 with the discovery of a suitable catalyst, $TiCl_3$.[55] With a lowered activation energy, the Ti-doped $NaAlH_4$ showed much faster desorption kinetics and good reversibility under moderate temperature and pressure conditions. Owing to these encouraging results, a considerable amount of research was conducted in the following years, trying to find other materials with similar or better sorption properties. However, despite the noticeable efforts, no other complex metal hydride could match the low desorption temperatures, low enthalpy value and good reversibility of sodium alanate. Therefore, different strategies were developed to design new hydrogen storage systems.

1.3.3.4 Reactive hydride composites (RHCs)

The expression "reactive hydride composites" refers to mixtures of metal hydrides that, upon dehydrogenation, react concertedly forming a compound with negative formation enthalpy, rather than decomposing independently to single elements. As a result, the reaction enthalpy of the system is decreased, compared to the decomposition enthalpy of the single components.[37, 38]

A similar concept was already applied from Reilly and Wiswall and is described by reaction 1.4.[56]

$$3\,MgH_2 + MgCu_2 \rightleftharpoons 2\,Mg_2Cu + 3\,H_2 \tag{1.4}$$

This approach was then extended to several other intermetallic compounds however the thermodynamic gain is usually not significant enough to motivate such a loss of gravimetric capacity: in the Mg-Cu system the final enthalpy is still $-73\,kJ/mol\,H_2$, but the hydrogen capacity drops to 2.6 wt%.

A significant step forward was made with the discovery of the $2\,LiBH_4 + MgH_2$ system.[57, 58, 59, 60] This candidates represented one of the few practically reversible hydrogen storage systems with a theoretical gravimetric hydrogen capacity higher than 10 wt%. The desorption process takes place in two steps, as indicated by reaction 1.5:

$$2\,LiBH_4 + MgH_2 \longrightarrow 2\,LiBH_4 + Mg + H_2 \longrightarrow 2\,LiH + MgB_2 + 4\,H_2 \tag{1.5}$$

The first desorption step involves the decomposition of MgH_2 alone. Without additives it is necessary to carry this process at temperatures higher than 350 °C to obtain reasonable desorption rates. Moreover, it is important to utilize a back pressure of about 5 bar of hydrogen (higher than the equilibrium pressure of $LiBH_4$). This precaution hinders the independent decomposition of $LiBH_4$ and preserves it for reacting with magnesium, to form MgB_2.[61] Interestingly, the system is fully reversible. Furthermore, differently from the desorption, the absorption seems to proceed through a one-step mechanism.[62]

Similar systems were developed using sodium and calcium borohydrides in place of lithium, but achieving only partial reversibility.[60, 63, 64, 65] Transition metals-based additives were employed successfully to hasten the sorption kinetics of the $2\,LiBH_4 + MgH_2$ system.[59, 66] Despite the noticeable improvements of both thermodynamic and kinetic properties, this system still possesses operation temperatures that are too high for mobile applications. In the next chapter, another class of material is explored, which allowed to significantly lower the sorption temperature of composite systems.

1.3.3.5 Metal amides

Since the study of metal amides is the main subject of this thesis, before presenting their properties as hydrogen storage materials, an historical perspective is given.

The discovery of metal amides dates back to a period of pioneering and fundamental findings, such as the isolation of the most common alkali metals. In fact, sodium and potassium were isolated for the first time as pure elements in 1808 by Davy, via the electrolysis of soda and potash, respectively.[67] Shortly after, Davy, Thenárd and Gay-Lussac discovered the

amides of potassium and sodium by studying the interaction of these alkali metals with ammonia.[68, 69, 70] Interestingly, these experiments first led Gay-Lussac and Thénard to doubt the elemental nature of the metallic sodium and potassium obtained by Davy, and later induced Davy to suggest that ammonia was an oxygen-containing substance.[71] Nonetheless, they are certainly remarkable, considering that chlorine was still called "oxymuriatic gas" at that time, since it was believed to be an oxide of chlorine, until Davy proved its elemental nature in 1811.[72] In order to give a broader perspective, it is also worth mentioning that the synthesis of one of the simplest organic amides, urea (carbamide) from inorganic reagents (Wöhler synthesis), was achieved only in 1828 and its importance as the first strong experimental proof against the theory of vitalism had not been yet recognized.[73, 74]

Additional studies followed the iconic work of Davy, Thenárd and Gay-Lussac. Beilstein and Geuther determined the formula of $NaNH_2$ by direct methods in 1858.[75] The empirical formula of KNH_2 was reported by Baumert and Landolt the following year.[76] Titherley confirmed these results and synthesized lithium amide ($LiNH_2$) in 1894 and rubidium amide ($RbNH_2$) in 1897.[77, 78] Moissan prepared $Ca(NH_2)_2$ in 1898 and Rengade synthesized $CsNH_2$ in 1905.[79, 80] Franklin was able to synthesize, but not isolate, $Mg(NH_2)_2$ in 1913.[81]

The works mentioned so far didn't just deal with the synthesis of metal amides. In most of the cases their reactivity towards common inorganic reagents, as well as the possibility of forming bimetallic compounds, were also studied. In parallel, the use of metal amides as ammono-base in organic chemistry was discovered and a completely new research field was founded. An extensive review of the inorganic and organic chemistry of metal amides was written by Bergstrom and Fernelius in 1933.[82]

The synthesis of metal amides in that period was mostly performed reacting the molten metal with liquid or gaseous ammonia. This process leads to the formation of the amide and release of hydrogen, as described in reaction 1.6.

$$M + NH_3 \longrightarrow MNH_2 + \frac{1}{2} H_2 \tag{1.6}$$

The alternative synthesis of metal amides from metal hydrides, was reported by Ruff and Geisel in 1906 (reaction 1.7).[83]

$$MH + NH_3 \longrightarrow MNH_2 + H_2 \tag{1.7}$$

Another possibility for forming metal amides was reported from Dafert and Miklauz in 1910.[84] They synthesized Li_3N and reported its reaction with hydrogen to form a supposed trilithium ammonium, Li_3NH_4. The following year Ruff and Goerges clarified that the total

composition Li_3NH_4, corresponds to a mixture of $LiNH_2$ and LiH, according to reaction 1.8.[85]

$$Li_3N + 2\,H_2 \longrightarrow LiNH_2 + 2\,LiH \tag{1.8}$$

They also suggested the formation of Li_2NH, according to reaction 1.9.

$$2\,LiNH_2 + 4\,LiH \longrightarrow 2\,Li_2NH + 2\,LiH\,[+\,2\,H_2] \tag{1.9}$$

Another interesting discovery from these early years, was reported by Miles.[86] He noticed that sodium amide can be converted into sodium hydride, when a flow of hydrogen is passed over it, describing the process according to reaction 1.10.

$$NaNH_2 + H_2 \longrightarrow NaH + NH_3 \tag{1.10}$$

The reversibility of this reaction under ammonia flow was proved by Guntz and Benoit.[87, 82] Moreover, Titherley realized that sodium amide heated to dull redness was able to decompose ammonia into hydrogen and nitrogen.[77]

A systematic overview of the thermodynamic and thermal properties of metal amides was reported by Juza et al. in 1937.[88, 89] The crystal structure of lithium amide was solved in 1951 by Juza and Opp.[90] This represented the first of a series of crystallographic studies on metal amides of alkali and alkaline-earth metals. The structures of sodium, potassium, rubidium and caesium amide were determined within the following eight years.[91, 92, 93] The crystallographic characterization of calcium, strontium and barium amide was reported in 1963, while the structure of magnesium amide was solved only in 1971 by Jacobs.[94, 95]

The formation of bimetallic potassium-magnesium amides had been already reported in 1913 by Franklin, whereas a first structural characterization was performed only around the 1970 by Palvadeau and Rouxel and later, after the 1980, by Jacobs et al. .[81, 96, 97, 98]

In this period, other bimetallic amides were also discovered, however most of the studies focused on structural or fundamental aspects, rather than possible applications.[99, 100]

A change of perspective on this class of compounds took place when, in 2002, Chen et al. demonstrated the promising hydrogen sorption properties of the lithium amide - lithium hydride composite system. Exposing Li_3N to only 3 bar of hydrogen pressure, with a maximum temperature of 255 °C, about 9.3 wt% of H_2 were absorbed in ca. 130 min following a two step process, as indicated from reaction 1.11.[101]

$$LiNH_2 + 2\,LiH \rightleftharpoons Li_2NH + LiH + H_2 \rightleftharpoons Li_3N + 2\,H_2 \tag{1.11}$$

An intense research activity stem from this seminal work and since then, a considerable

amount of efforts has been dedicated to the design and characterization of new metal amide based systems with improved sorption properties.

Indeed, despite its auspicious hydrogenation temperature, the Li-N-H system required temperatures as high as 430 °C in order to release all the absorbed hydrogen. Moreover the reaction enthalpy of the first step was determined to be $-66\,\mathrm{kJ/mol\,H_2}$, which is too large for practical applications.

In order to destabilize the Li-N-H system, Nakamori and Orimo tried to partially substitute Li with a more electronegative atom, such as Mg, starting from Li_3N + 10 at % Mg_3N_2, achieving a reduction of 50 K in the desorption temperature, as compared to Li_3N.[102] Further increasing the content of Mg_3N_2 to 20 at %, the system could store 9.1 wt% of hydrogen at 250 °C and 350 bar, according to the following reaction:[103]

$$4\,Li_3N + Mg_3N_2 + 12\,H_2 \rightleftarrows 3\,Mg(NH_2)_2 + 12\,LiH \tag{1.12}$$

Leng et al. tried to substitute the $LiNH_2$ with $Mg(NH_2)_2$, designing a system that could release 7 wt% of H_2 starting at 140 °C.[104] The reversible process was described as:

$$3\,Mg(NH_2)_2 + 8\,LiH \rightleftarrows Mg_3N_2 + 4\,Li_2NH + 8\,H_2 \tag{1.13}$$

Luo tried to improve the $LiNH_2$ + 2 LiH system substituting LiH with the less stable MgH_2 (their formation enthalpies are $-90\,\mathrm{kJ\,mol^{-1}}$ and $-74\,\mathrm{kJ\,mol^{-1}}$, respectively).[105]. The system obtained with this approach showed an experimental hydrogen release of 4.5 wt% as compared to the theoretical value of 5.35 wt%, calculated on the basis of reaction 1.14.

$$2\,LiNH_2 + MgH_2 \longrightarrow Li_2Mg(NH)_2 + 2\,H_2 \tag{1.14}$$

The reaction enthalpy and desorption temperature in this case were found to be as low as $39\,\mathrm{kJ\,mol^{-1}}$ and 220 °C, respectively.

Xiong et al. arrived independently to the same system developed by Luo, with the idea of changing the thermodynamics by forming new ternary imides. They also realised that, after full dehydrogenation/rehydrogenation cycles, 2 $LiNH_2$ + MgH_2 converts to $Mg(NH_2)_2$ + 2 LiH.[106] The reversible process, according to these findings, is therefore described by reaction 1.15.

$$Mg(NH_2)_2 + 2\,LiH \rightleftarrows Li_2Mg(NH)_2 + 2\,H_2 \tag{1.15}$$

The enthalpy of the desorption process, as determined by pressure-composition isotherms (PCIs) is $38.9\,\mathrm{kJ/mol\,H_2}$.[107] An extrapolation of the van't Hoff plot allows to predict an equilibrium temperature of 90 °C at 1 bar of hydrogen pressure, which is very close to the

DoE target for mobile applications in light duty vehicles.

Xiong et al. noticed already that in the PCIs of this system a sloping region is present in the low-pressure region, before the actual plateau. In fact, further studies clarified that the reversible sorption process takes place in two steps and can be described according to:[108]

$$2\,Mg(NH_2)_2 + 3\,LiH \rightleftharpoons Li_2Mg_2(NH)_3 + LiNH_2 + 3\,H_2 \tag{1.16}$$

$$Li_2Mg_2(NH)_3 + LiNH_2 + LiH \rightleftharpoons 2\,Li_2Mg(NH)_2 + H_2 \tag{1.17}$$

Other amide-hydride and amide-borohydride systems were studied, but their performance didn't compare with the ones of the Li-Mg-N-H systems, requiring higher sorption temperatures or displaying poor reversibility, due to various causes (reaction enthalpy, sluggish kinetics or formation of stable boron nitrides).

Of the various compositions examined in the Li-Mg-N-H system, the $Mg(NH_2)_2 + 2\,LiH$ (or $2\,LiNH_2 + MgH_2$) was the most studied by far, due to its promisingly low desorption and absorption temperatures. In particular, the equilibrium pressure of 1 bar of H_2 at 90 °C, thermodynamically allowed but kinetically hindered, motivated several groups to either find suitable additives that could improve the reaction kinetics at low temperature or tune the thermodynamics of the system to lower even further the equilibrium temperature.

A first considerable improvement was obtained using KH as additive in partial replacement of LiH.[109] For $Mg(NH_2)_2 + 1.9\,LiH + 0.1\,KH$ the desorption took place at a temperature about 50 °C lower and ammonia release was greatly diminished, if compared to the pristine system. Moreover the K-doped material was completely dehydrogenated and hydrogenated at 107 °C in equilibrium conditions (during PCI measurements).

This breakthrough was followed by several studies that tried to understand the role of K-based additives in the Li-Mg-N-H system using different approaches and techniques.

Wang et al. studied the KH - $Mg(NH_2)_2$ system in order to identify possible potassium-containing phases and found some incongruence with the previous studies of Palvadeau and Rouxel.[110, 96, 97] Wang et al. didn't find the mixed amide-imide, imide and nitride phases of potassium and magnesium that were reported in the earlier studies. Instead, they found a new mixed amide-imide phase, $KMgNH_2NH$. The crystal structure of this compound was unknown at that time and it was solved by Napolitano et al. only a couple of years after its discovery.[111]

Luo et al. and Durojaiye et al. studied the reaction kinetics of the K-modified $2\,LiNH_2 + MgH_2$ composite. This system shows noticeable improvements in the reaction kinetics, particularly in the temperature range 180 °C to 210 °C).[112, 113] This changes are most likely due to a decrease of ca. 30 kJ mol^{-1} in the activation energy of the desorption process,

as compared to the pristine system.

Liu et al. and Liang et al. showed that also other forms of potassium (namely potassium fluoride and hydroxide, respectively) can improve the sorption properties of the $Mg(NH_2)_2$ + 2 LiH system.[114, 115] The additive led to the lowering of both reaction enthalpy and activation energy.

In a follow up study, Li et al. showed that K-based additives can loose their effectiveness in lowering the desorption and absorption temperatures when cycled at high temperature, due to increased particle and grain sizes; in fact, the sorption properties were recovered if the material underwent additional mechanochemical treatments.[116]

Lin et al. proved that the positive effects of KH are not restricted to the 2:1 composition, but can also be extended to the $Mg(NH_2)_2$-$LiNH_2$-LiH system.[117]

Li et al. and Durojaiye et al. discovered independently that Rb-based additives are also suitable for improving the hydrogen storage properties of the Li-Mg-N-H system.[118, 119] In particular, Durojaiye et al. demonstrated that the 2 $LiNH_2$ + MgH_2 system possesses two times faster desorption kinetics when doped with RbH rather than KH. Additionally, modelling of the kinetic data showed that the desorption process is "diffusion-controlled", therefore the authors hypothesize that the bigger size of Rb allows faster diffusion through the lattice.[119, 120] Li et al. showed that the effects of RbF on the $Mg(NH_2)_2$ + 2 LiH system consist on a combined improvement of thermodynamic and kinetic properties.[118] They demonstrate that RbH is the active component, which is formed by metathesis with LiH:

$$RbF + LiH \longrightarrow RbH + LiF \tag{1.18}$$

Moreover, they suggest that the RbH interacts with $Mg(NH_2)_2$ at low temperature to form a new $RbMgNH_2NH$ phase, which is responsible for the decreased enthalpy change and lower activation energy of the system.[118] The same research group showed that KH and RbH can work effectively also together, as co-additives.[121] Recently good results were obtained also by doping the system with CsH.[122, 123, 124, 125]

Hu et al. achieved very good performances, in terms of reaction kinetics, using $LiBH_4$ as additive in the $Mg(NH_2)_2$ + 2 LiH composite.[126] Cao et al. also used $LiBH_4$ for improving the sorption properties of the Li-Mg-N-H system, but proposed a different approach, which is similar to the one utilized for RHCs: exploiting the fact that in the first reaction step of the $Mg(NH_2)_2$ + 2 LiH system lithium amide is formed, a compound was added in order to react exothermically with $LiNH_2$ and obtain a lower enthalpy for the desorption process.[127] The selected compounds were LiI, LiBr and $LiBH_4$, which can form $Li_3(NH_2)_2I$, Li_2NH_2Br and $Li_4(BH_4)(NH_2)_3$, respectively.[127] The $Mg(NH_2)_2$ and LiH molar ratio used was 2:3 (accordingly to reaction 1.16). The final reactions cam be described as:

$$2\,Mg(NH_2)_2 + 3\,LiH + \frac{1}{2}\,LiI \rightleftharpoons Li_2Mg_2(NH)_3 + \frac{1}{2}\,Li_3(NH_2)_2I + 3\,H_2 \quad (1.19)$$

$$2\,Mg(NH_2)_2 + 3\,LiH + LiBr \rightleftharpoons Li_2Mg_2(NH)_3 + Li_2NH_2Br + 3\,H_2 \quad (1.20)$$

$$2\,Mg(NH_2)_2 + 3\,LiH + \frac{1}{3}\,LiBH_4 \rightleftharpoons Li_2Mg_2(NH)_3 + \frac{1}{3}\,Li_4(BH_4)(NH_2)_3 + 3\,H_2 \quad (1.21)$$

According to the thermodynamics of each system, an equilibrium pressure of 1 bar should be reached at 60 °C, 47 °C and 64 °C, respectively.[127] These equilibrium conditions cannot be practically reached due to the kinetic limitations imposed from solid-solid reactions, however, compared to the pristine $2\,Mg(NH_2)_2 + 3\,LiH$ system, the reduced reaction enthalpy allows hydrogen desorption at temperatures 15 °C, 21 °C and 13 °C lower, respectively.[127]

The system containing $LiBH_4$ was the most promising of the three, due to its lower ammonia release and higher theoretical capacity (4.2 wt%). For these reasons, we have recently optimized its reaction kinetics using additional co-additives, achieving a hydrogenation temperature of 90 °C at 185 bar of hydrogen.[128] Different compositions were also explored by Wang et al., achieving a reaction enthalpy of 24 kJ mol H_2^{-1} for $6\,Mg(NH_2)_2 + 9\,LiH + 12\,LiBH_4$, which is outstanding considering that this theoretically allows hydrogen sorption in near ambient conditions.[129, 130]

Recently, we obtained interesting results also using transition metal amides, however additional work is required to meet the severe target imposed from the operating temperature of the PEM-FC.[131, 132, 133]

After considering some of the most important discoveries made up to now, it is necessary to define the aims of the present work.

1.4 Scope of the work

As reported in section 1.3.3.5, metal amides are a rather old class of compounds, being their discovery linked to the isolation of the most common alkali metals. However, from the intense research activity carried out in the last years in the attempt to find an ideal hydrogen storage media, several new aspects emerged, which required additional investigations to be fully understood. Furthermore, the use of more advanced techniques can sometimes provide new

insights on the properties of systems previously investigated.

With this in mind, the first part of this thesis was devoted to studying the ammonolysis process of the most common alkali and alkaline-earth metal hydrides (LiH, NaH, KH, MgH_2 and CaH_2). Most of these results confirmed what could be inferred from the previous literature, however, in case of KH, the structural evolution was somewhat unexpected, compared to the other alkali metals. The importance of KH as additive for improving the sorption kinetics of the Li-Mg-N-H system (described in section 1.3.3.5) and the scientific curiosity raised from these preliminary studies, demanded further work in this direction.

When considering the studies that, up to this point, tried to clarify the role of K-based additives, the work of Wang et al. underlined some interesting differences with the reaction pathway previously proposed by Palvadeau and Rouxel for the K-Mg-N-H system.[110, 96, 97] In particular, Palvadeau and Rouxel suggested the formation of $K_2Mg(NH_2)_2(NH)$, $K_2Mg(NH)_2$ and KMgN during the decomposition of $K_2Mg(NH_2)_4$.[96, 97] Wang et al. reported the formation of only $KMgNH_2NH$ as final product, after both the decomposition of $K_2Mg(NH_2)_4$ and the thermal desorption of KH + $Mg(NH_2)_2$.[110]The interaction of KH with $Mg(NH_2)_2$ seems to be a fundamental aspect of the role of KH in lowering the desorption temperature of the $Mg(NH_2)_2$ + 2 LiH system.[134] Moreover, the possible formation of a bimetallic nitride was not further discussed in the recent literature. Additional work was required, to shed more light in the phase evolution, sorption properties and reaction mechanism of these hydrogen storage systems. Particularly, *in situ* techniques could reveal if the crystalline bimetallic phases previously suggested are formed as stable or metastable intermediates and provide new hints for the reaction mechanism of K-containing metal amide/hydride systems.

Interestingly, the two systems, K-N-H and K-Mg-N-H, appeared to be linked by the presence of new intermediates with peculiar structural properties. Owing to the novelty of these findings, it was necessary to investigate the K-N-H system systematically, in the whole compositional range and to provide a clear structural description of these species.

At this point it became clear that potassium, differently from the lighter alkali metals, displayed some unique structural features. Considering the analogies between the crystal chemistry of potassium and rubidium amide (outlined in the pioneering work of Juza et al.[135]) and the similar performance that KH- and RbH-doped systems show in terms of hydrogen uptake and release (as shown by Li et al.[121]), the next logic step was the investigation of the rubidium case of study. In fact, Li et al. suggested the possible formation of $RbMgNH_2NH$ to explain the thermodynamic and kinetic improvements obtained by addition of RbF to the $Mg(NH_2)_2$ + 2 LiH composite.[118] However, at that time, this compound was still unknown from the structural point of view. Considering the development of the present work, a comprehensive characterization of the Rb-Mg-N-H and Rb-N-H systems and

a comparison with the potassium-based system was the most interesting and logic direction to follow.

In the next chapter, the experimental strategies undertaken to pursue the declared objectives are described in detail.

2 Experimental part

This chapter presents a list of the reagents employed for the sample preparation and describes the synthesis methods and further thermal and/or mechanochemical processing of the materials. The strategies used to characterize the samples, the experimental conditions utilized in each measurement, as well as the software employed for data analysis are also reported here.

2.1 Materials and synthesis methods

2.1.1 Ammonolysis of metal hydrides

The metal hydrides of alkali and alkaline-earth metals employed for the experiments under ammonia atmosphere were purchased with high purity from different companies. LiH (purity higher than 97 %) and MgH_2 (98 %) were purchased from Alfa Aesar. The NaH and CaH_2 employed, both 95 % purity, were produced from Sigma Aldrich.

Due to its high reactivity towards moisture, KH is usually available as suspension in mineral oil or embedded in solid paraffin. In this case the 35 % suspension under mineral oil produced from Merck was utilized. Most of the oil was removed by filtration under vacuum and the remaining slurry was washed with anhydrous diethyl ether (99 %, AlfaAesar). The powdery product obtained was left few minutes in the Büchner funnel and dried on its porous plate under vacuum to remove the residues of solvent. The removed oil was collected inside of the Büchner flask, while the volatile solvent was collected in a solvent trap cooled down with liquid nitrogen. The whole filtration/washing process took place inside of a MBraun glovebox under continuously purified and monitored argon atmosphere (oxygen and water levels lower then 1 ppm).

The as-received materials and the potassium hydride powder obtained after filtration underwent a mechanochemical processing to obtain finer and more reactive powders; to do so, they were separately transferred in hardened steel vials, ball milled in a SPEX 8000 mill for 1 h, using steel balls of ca. 1 cm diameter, with a ball to powder ratio (BPR) of 10:1

2.1.2 K-Mg-N-H system

The KH (30 % suspension under mineral oil) and the MgH_2 (98 %) utilized here were purchased from Sigma Aldrich. KH was filtered under vacuum using the same procedure and equipment previously described, but additionally washed three times using about 15 mL of anhydrous pentane (Aldrich, purity higher than 99 %) each time.

For the synthesis of the first sample, sample A, KH and MgH_2 with a molar ratio of 1:1 were transferred in a stainless steel high pressure (HP) vial (Evico Magnetics GmbH, Fig. 2.1-a). The vial was loaded with ca. 7 bar of ammonia and the milling was performed in a Pulverisette 6 planetary mill (Fritsch, Germany) at 400 RPM for 20 h.

The KNH_2 and $Mg(NH_2)_2$ used for the preparation of Sample B and Sample C, respectively, were synthesized separately by repeated mechanochemical process under 7 bar of ammonia, using the corresponding metal hydrides as starting materials. In order to increase the conversion and crystallinity of $Mg(NH_2)_2$, the product obtained after mechanochemical treatment under ammonia was further annealed under 7 bar of ammonia for more than 10 h in a stainless steel reactor manufactured from Parr Instruments (Fig. 2.1-b).

Sample B was prepared hand grinding the as synthesized KNH_2 and the as-purchased MgH_2 in molar ratio 1:1. Sample C was obtained mixing the as-synthesized $Mg(NH_2)_2$ with the filtered KH in molar ratio 1:1. In both cases an agate mortar and pestle were employed, mixing the reagents thoroughly for 10 min in order to obtain adequate dispersion and homogeneity without promoting any chemical reaction. Ball milling was not employed to avoid any mechanically induced metathesis reaction for the metastable composition of Sample B or any amorphization process in the crystalline $Mg(NH_2)_2$ of sample C. In this way, the intended compositional and microstructural state of each sample was preserved.

2.1.3 KNH_2-KH system

Pure KH was obtained from its 30 % suspension in mineral oil purchased from Sigma Aldrich after washing three times with anhydrous hexane (95 %, Sigma Aldrich) and filtering under vacuum with the same procedure described in section 2.1.2.

KNH_2 was synthesized by repeated mechanochemical treatments of the filtered KH powder in the Pulverisette 6 planetary mill under 7 bar of ammonia at 400 RPM with a BPR of about 20:1. The high pressure reaction vessel was evacuated and refilled with NH_3 four times and the total milling procedure lasted 18 h.

The KH (after filtration) and KNH_2 (as-synthesized) were then independently mechanochemically processed in the SPEX 8000 mill for 600 minutes to obtain a fine powder.

The mixtures were prepared grinding different amounts of KH and KNH_2 with an agate

Figure 2.1: Reactors used for mechanochemical (a) and thermal (b) treatments of the materials under reactive or inert atmosphere.

mortar and pestle for about 5 min. The annealed samples were prepared in the Parr reactor heating under an argon atmosphere of 1 bar at 270 °C for 1 h.

The ball milled samples were prepared milling the corresponding amounts of KH and KNH_2 in the SPEX 8000 mill for 5 h with a BPR of 10:1. Also in this case, hardened steel vials and steel balls were employed.

Potassium deuteramide (KND_2), was synthesized using metallic potassium (Aldrich, cubes under mineral oil, 99.5 %) as starting material. A chunk of potassium was cut and washed with anhydrous hexane to remove the residual oil from the surface. The surface was polished, removing a thin layer of oxidized potassium with a sharp blade. The shiny cube of metallic potassium was transferred into the Parr reactor and then annealed under 5 bar of deuterated ammonia (ND_3, Aldrich, isotopic purity of deuterium 99 atom%) at 300 °C for a total time of 16 h. The intended process can be described according to reaction 2.1.

$$K + ND_3 \longrightarrow KND_2 + \frac{1}{2} D_2 \tag{2.1}$$

Potassium deuteride was also prepared starting from metallic potassium. A piece of metallic potassium of about 1.1 g was cut, washed, polished (as previously described) and then transferred in a high pressure vial. The vial was first charged with approximately 50 bar of deuterium (D_2, Air Liquid, 99.8 mol%) and then mounted in the Pulverisette 6 planetary mill. The mechanochemical process was carried out with a BPR of 60:1 at 600 RPM for 36 h.

The mixture of KD and KND_2 was prepared by hand-grinding, with an agate mortar and pestle.

2.1.4 Rb-Mg-N-H and Rb-N-H systems

$Mg(NH_2)_2$ was obtained by ball milling of MgH_2 (Rockwood Lithium, 99.8 % of magnesium) under 7 bar of ammonia for 19 h at 400 RPM with a BPR of about 60:1. The milled powder was then annealed at 300 °C under 7 bar of ammonia for 5 h.

RbH was synthesized via ball milling of metallic rubidium (Alfa Aesar, 99.75 %) under 50 bar of hydrogen at 500 RPM for 13 h with a BPR of 180:1, followed by annealing at 180 °C under 70 bar of hydrogen for 5 h.

$Rb_2Mg(NH_2)_4$ was synthesized by ball milling of rubidium metal (Alfa Aesar, 99.75 %) and magnesium (Aldrich, 99 %) in molar ratio 2:1 under 7 bar of ammonia for 34 h at 400 RPM with a BPR of ca. 30:1. The obtained powder was further annealed at 270 °C under 7 bar of ammonia for 48 h.

$Rb_2Mg(ND_2)_4$, used for neutron diffraction experiments, was synthesized in a Parr reactor by thermal treatment of rubidium and magnesium in molar ratio 2:1 under 5 bar of

deuterated ammonia (Aldrich, isotopic purity of deuterium 99 atom%) at 300 °C for more than 48 h.

MgD_2 was prepared from previously desorbed MgH_2, by annealing under 120 bar of D_2 (Air Liquid, 99.8 mol%) at 400 °C for 24 h.

The new phase, $RbMgNH_2NH$, was obtained with two different synthesis routes. In the first one, starting from $Mg(NH_2)_2$ and RbH; in the second one, from $Rb_2Mg(NH_2)_4$ and MgH_2. The starting materials were mixed using an agate mortar and pestle and subsequently annealed in the temperature range 250 °C to 260 °C either under argon flow or dynamic vacuum, to avoid partial re-absorption of the desorbed hydrogen during the cooling down. The two processes can be described according to reaction 2.2 and 2.3, respectively.

$$Mg(NH_2)_2 + RbH \longrightarrow RbMgNH_2NH + H_2 \tag{2.2}$$

$$Rb_2Mg(NH_2)_4 + MgH_2 \longrightarrow 2\,RbMgNH_2NH + 2\,H_2 \tag{2.3}$$

$RbNH_2$ was prepared by thermal treatment of metallic rubidium under 7 bar of ammonia at 250 °C for ca. 13 h.

RbH was synthesized by mechanochemical treatment of Rb under 50 bar of hydrogen for 23 h at 600 RPM, followed by 17 h at 400 RPM, with a BPR of about 60:1.

The mixtures were all prepared by mixing the desired amounts of RbH and $RbNH_2$ with an agate mortar and pestle. The annealed samples were prepared by thermal treatment of the mixtures at 200 °C for 4 h under 1 bar of argon.

2.2 Characterization techniques

2.2.1 Manometric measurements (Sievert apparatus)

The gravimetric capacity of the different systems examined was determined by manometric measurements, performed with a PCTPro 2000 Sievert apparatus. The sample (about 150 mg) was transferred inside of a steel sample vial and closed with a screw-cap provided with porous sintered metal filter; its manipulation was performed inside of a glove box with continuously purified argon. The sample vial was placed inside of a sample holder and the empty space was reduced with steel cylinders to increase the precision of the measurement. The experiments were conducted with a heating rate of 10 °C min^{-1} under 1.5 bar of argon atmosphere.

2.2.2 Thermal desorption mass spectrometry

In order to determine the type of gases that can be released by increasing the temperature, thermal desorption mass spectrometry (TD-MS) experiments were performed. The sample (about 10 mg) was placed inside of alumina (Al_2O_3) crucibles. A Netzsch STA 409, located in a dedicated glove box, was used to heat up the sample at 5 °C min^{-1} under an argon flow of 50 mL_n/min. The evolution of hydrogen and ammonia upon heating was determined using a Hiden Analytical HAL 201 mass spectrometer connected with a steel line (about 2 m long) heated up with an electric resistance to avoid condensation of the gases.

2.2.3 *Ex situ* X-ray powder diffraction

Ex situ X-ray powder diffraction (XPD) was used throughout as characterization technique to confirm or determine the outcome of the synthesis procedures and experiments performed. It has been also a useful analytic tool to monitor the status of some samples or starting materials, in particular to exclude possible contaminations or the presence of oxide or hydroxide phases.

Most of the *ex situ* XPD experiments were performed using a diffractometer D8 Discover manufactured from Bruker (Germany), equipped with a copper X-ray source ($\lambda = 1.541\,84$ Å) and a VANTEC general area detector, in Bragg-Brentano geometry.

Since the samples and materials investigated are susceptible to a rather fast oxidation/hydrolysis process when exposed to air or moisture, a poly(methyl methacrylate) (PMMA) dome produced from Bruker was used to seal the powder under argon atmosphere. The scattering of the PMMA dome creates a noticeable bump in the final XPD pattern (at $1\,\text{Å}^{-1} < Q < 2\,\text{Å}^{-1}$).

Additionally, *ex situ* XPD measurements were performed together with Dr. Eugenio Pinatel and under the supervision of Prof. Marcello Baricco at the University of Turin (Italy), in the frame of the ECOSTORE project, using a Panalitical X'Pert Pro Multipurpose Diffractometer set in Debye-Scherrer geometry and equipped with Ni-filtered Cu radiation. The diffractograms were acquired in the 2θ range 2° to 90° with a step size $\Delta 2\theta = 0.017°$ and an exposure time of 200 s per step. The powdered samples were packed and sealed in boron silica glass capillaries of 0.8 mm internal diameter.

2.2.4 Synchrotron radiation X-ray powder diffraction

In situ synchrotron radiation X-ray powder diffraction (SR-XPD) measurements were performed at the diffraction beamline I711 in the storage ring MAX II of MAX IV Laboratories (MAX-lab, Lund, Sweden) with wavelength $\lambda \approx 0.99$ Å and a Agilant Titan detector (array of 2048x2048 pixels, 60 µmx60 µm each).[136]

Additional experiments were carried out at the diffraction beamlines P02 and P07 in the storage ring PETRA III of Deutsches Elektronen-Synchrotron (DESY, Hamburg, Germany) with wavelengths of 0.207 Å and 0.142 35 Å, respectively. In both beamlines data were recorded using a Perkin Elmer XRD1621 detector with an array of 2048x2048 pixels and pixel size of 200 µmx200 µm.[137, 138]

All facilities provided high intensity monochromatic beams and 2D image plate detectors in Debye-Scherrer geometry. This combination allows the acquisition of a diffraction pattern with high signal to noise ratio in just few seconds, therefore SR-XPD is particularly useful to study (*in situ* or *ex situ*) reaction pathways, phase transformations and structural changes. In the experiments included in this work, exposure times of 15 s or 30 s per scan were employed.

For the *in situ* experiments the samples were packed inside of single crystal sapphire capillaries with outer diameter of ca. 1 mm and inner diameter of ca. 0.6 mm. The capillary was then mounted on an in-house developed *in situ* cell using graphite or vespel ferrules within standard Swagelok connections for sealing. This special sample holder is equipped with a thermocouple, a heating element (electric resistance) and additional manual valves to allow for evacuation/loading of gases.[139] For the *in situ* SR-XPD experiments during the ammonolysis process (carried out by Pistidda et al. together with other colleagues), 6.5 bar of ammonia were loaded after evacuating the system for several minutes (a schematic view of the experimental setup is shown in Fig. 2.2); all other experiments (conducted by myself together with different colleagues) were performed under inert atmosphere (1 bar of argon).

The acquired two-dimensional annular ring diffraction images were then masked to exclude single crystal diffraction spots and finally integrated and converted to conventional 1-dimensional diffraction patterns using the Fit2D software.[141] Since the data were recorded with different wavelengths, the 2θ values were converted to scattering vector (Q) to allow for an easy comparison between different datasets. The beamline and wavelength for each dataset are specified in the corresponding figure captions. The SR-XPD data were then plotted in a contour plot using Origin;[142] this graph allows to visualize the integrated intensities as a function of scattering vector, number of scan and corresponding temperature. Rietveld refinement of selected diffraction patterns was performed with the software Material Analysis Using Diffraction (MAUD).[143, 144, 145] The structure models of known phases were found in the International Crystal Structure Database (ICSD) via software (FindIt).

An *ex situ* XPD pattern with very high signal to noise ratio and good resolution was necessary for the structure solution of $RbMgNH_2NH$. The experiment was performed by Prof. Radovan Černý and Matteo Brighi at the Swiss Norwegian Beamline (SNBL) of the European Synchrotron Radiation Facility (ESRF, Grenoble, France). The data were recorded on a Dectris Pilatus 2M detector with a monochromatic X-ray beam (0.8212 Å).[146] The software Free Objects for Crystallography (FOX) was used by myself, with the help of Prof.

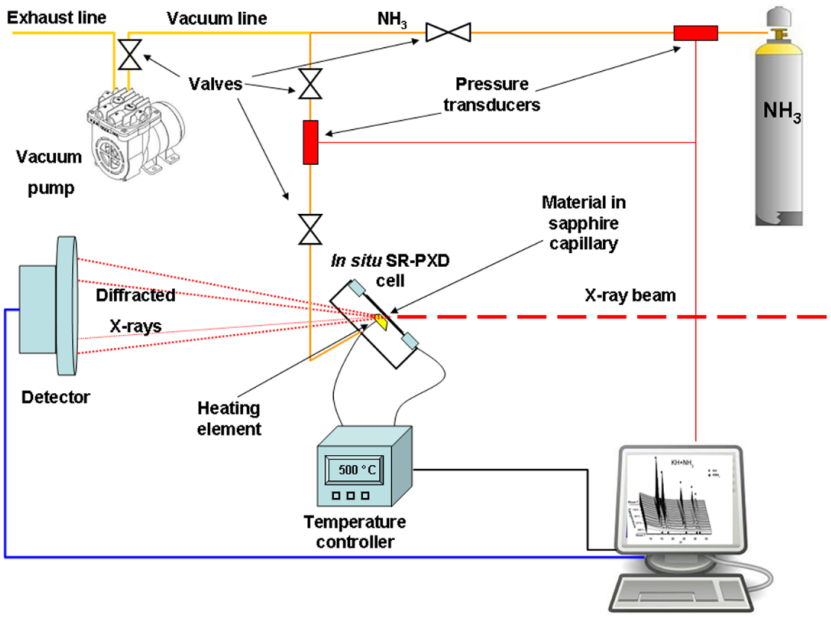

Figure 2.2: Schematic view of the experimental setup utilized for the *in situ* SR-XPD measurements under ammonia atmosphere. Reprinted with permission from Pistidda C., Santoru A., et al., J. Phys. Chem. C 119, 2, 934-943. Copyright 2015 American Chemical Society.[140]

Radovan Černý and Matteo Brighi, for indexing the Bragg reflections, determining the space group candidates and performing the global optimization of the structure using the simulated annealing algorithm.[147] Hydrogen was excluded from the structure determination process from XPD data, due to its low X-ray scattering factor. Rietveld refinement of the structure model obtained in FOX was performed by myself with MAUD and then repeated with GSAS in combination with neutron powder diffraction data (see section 2.2.5).

2.2.5 Neutron powder diffraction

Neutron powder diffraction (NPD) measurements were conducted together with Dr. Magnus H. Sørby and under the supervision of Prof. Bjørn C. Hauback with the PUS instrument at the JEEP II reactor of the Institute for Energy Technology (IFE, Kjeller, Norway) during a secondment in the frame of the ECOSTORE project.[148] Neutrons with $\lambda \approx 1.55$ Å were provided from the Ge(111) monochromator with 90° take-off angle. Two detector banks were employed for data recording; each bank features 7 vertically stacked position sensitive detectors and covers 20° in 2θ. The data were acquired in the angular 2θ range 10° to 130°, with an angular step size $\Delta 2\theta = 0.05°$.

A cylindrical air-tight vanadium sample holder of 6 mm inner diameter was used for the measurements performed at RT.

The measurement at high temperature (in isothermal condition) was conducted using a quartz sample holder of 6 mm diameter and an in-house built furnace. The quartz tube contributes to the overall pattern with additional diffraction peaks that need to be identified and excluded from the refinement process. For this reason it was necessary to collect a RT NPD pattern of the sample using first the vanadium sample holder. In fact, due to the low coherent scattering cross section of vanadium (0.018 b), this sample holder does not contribute appreciably to the final NPD pattern.[149] A second NPD pattern of the same sample was then collected using the quartz sample holder. Finally, the NPD diffractogram at high temperature was acquired. A comparison of the three patterns allowed the identification of the additional peaks of the quartz sample holder (Fig. 2.3) which were excluded using the refinement software.

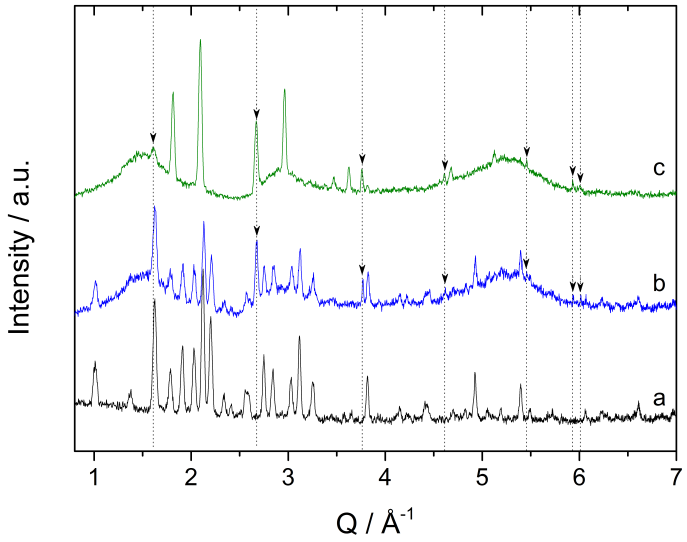

Figure 2.3: NPD pattern (λ = 1.5539 Å) of the nominal 0.5 KND_2 + 0.5 KD sample collected with the vanadium sample holder at RT (a) and with the quartz sample holder at RT (b), and at 270 °C (c). The additional peaks of the quartz sample holder (removed during the refinement stage) are indicated by the black arrows. Santoru et al., Chem. Commun., 2016, 52, 11760-11763 - Published by The Royal Society of Chemistry.[150]

The structure model of $K(ND_2)_{0.46}D_{0.54}$ was obtained by myself using FOX on the NPD pattern collected at 270 °C, after removing the peaks of the quartz sample holder. The deuteramide anions were treated as rigid bodies and the nitrogen atom was approximated to be the rotation center for simplicity. The Rietveld refinement was performed with the software General Structure Analysis System (GSAS), using the dedicated EXPGUI graphical user interface.[151, 152] The occupancies, were calculated and fixed in agreement with the exact starting composition of the KND_2-KD mixture, which was determined by Rietveld refinement of the RT PND data.

The structure model of $RbMgND_2ND$ was obtained by myself using FOX on the NPD pattern collected at RT using the vanadium sample holder. The same strategy used with the SR-XPD data (described in the previous section) was employed, except for the addition of free deuterium atoms: the amide and imide groups were formed during the global optimization without constrains. The final Rietveld refinement of the structure was performed by myself using the NPD and SR-XPD data simultaneously to have more precise results, following some directives from Dr. Magnus H. Sørby and Prof. Bjørn C. Hauback. Due to the very different statistics of the two measurements it was necessary to manually change the scale factor in favour of the NPD pattern in GSAS; additional iterations were then performed continuing to change the scale factor until reasonable structure parameters and low values of Rwp were obtained for both datasets.

The software Visualization of Electronic and STructural Analysis (VESTA) was used for building the graphical models of the crystal structures, for standardization of the crystal data and for calculation of the interatomic distances.[153]

2.2.6 Attenuated total reflection infrared spectroscopy

Attenuated total reflection infrared spectroscopy (ATR-IR) measurements were performed, upon previous discussion and agreement, by Dr. Michael Heere at IFE in the frame of the ECOSTORE project, using an Alpha-Platinum infrared spectrometer and diamond crystal manufactured from Bruker (Germany). The spectrum was recorded at RT in the wave-number range 4000 cm^{-1} to 400 cm^{-1} with a resolution of 2 cm^{-1} and with 32 scans averaged for each spectrum and the background. The pristine samples were measured, without any dilution. The spectrometer was placed inside an argon-filled glove box with controlled atmosphere.

2.2.7 Solid state nuclear magnetic resonance

Solid state nuclear magnetic resonance (SS NMR) experiments for the KNH_2-KH system were performed together with Prof. Michele R. Chierotti, under the supervision of Prof. Roberto Gobetto, after evaluation and discussion of the possible outcomes of these experiments, at the University of Turin (Italy), during a stay in the frame of the ECOSTORE project. For the $RbNH_2$-RbH system the measurements were performed by Prof. Michele R. Chierotti, after previous discussion and agreement, using the same machine and procedure. A Bruker AVANCE II 400 instrument was employed, operated at 400.23 Hz for ^1H and equipped with a 2.5 mm probe. The rotors were packed inside an argon filled glove box to protect the sample from hydrolysis. The ^1H magic angle spinning (MAS) spectra were acquired with a spinning frequency of 32 kHz with the DEPTH sequence ($\pi/2$-π-π) for suppression of the

probe background signal (^{1}H 90° = 2.5 µs; 16 scans; relaxation delays equal to 1.27-5T_1). The relaxation measurements were performed with a saturation recovery pulse sequence. 2D ^{1}H double quantum (DQ) MAS measurements were performed at 32 kHz using the back-to-back (BABA) recoupling pulse sequence with excitation time equal to the period of the rotor (^{1}H 90° = 2.5 µs; 32 scans; $t_1$increments = 46; relaxation delays equal to 1.27-5T_1). The ^{1}H scale was calibrated with adamantane (^{1}H signal at 1.87 ppm) as external standard.

3 Results and discussion

This chapter presents the results obtained during the study of selected metal amide/hydride systems, divided in four main sections based on the breadth of the topic and chronological order of the discoveries. All experiments are described and discussed, with a particular emphasis on the new insights they provide.

The first section is also the most general, since it deals with the ammonolysis process of the most common alkali and alkaline-earth metals, offering a broad overview of the main chemical and structural properties associated with this class of compounds. The second section covers the investigation performed on the reaction pathway, hydrogen storage properties and structural modifications of the K-Mg-N-H system. The third section goes into further details concerning some structural aspects of the K-N-H system, that were first discovered in the aforementioned experiments, but required a more specific approach in order to be fully understood. At the end of each of the first three sections a further discussion and a summary of the main results are given, pointing out the most important findings and the motivations that lead to continue the work in certain directions. The fourth and final section uses some of the concepts and approaches presented in the second and third section, in order to determine if they are transferable to other system. For this purpose, the Rb-Mg-N-H and Rb-N-H systems are compared to the K-Mg-N-H and K-N-H systems, respectively.

3.1 Ammonolysis of metal hydrides studied by *in situ* SR-XPD

In situ SR-XPD experiments were conducted during the ammonolysis reaction of selected alkali and alkaline-earth metal hydrides (LiH, NaH, KH, MgH_2, CaH_2). These results offer a systematic assessment of the reactivity and structural aspects associated with the formation of some of the most common metal amides, imides and nitrides and have been used as a guideline to develop our investigations along the most interesting directions.

3.1.1 Li-N-H system

The *in situ* SR-XPD experiment performed during the ammonolysis process of LiH is graphically represented with a contour plot, which shows the diffraction patterns acquired consecutively and the corresponding temperature value (Fig. 3.1-a).

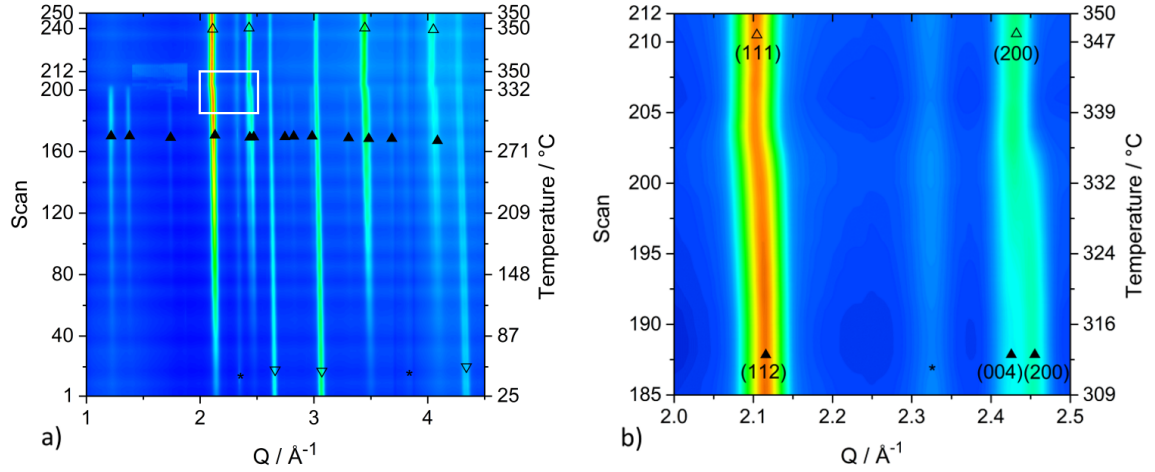

Figure 3.1: Contour plot of the *in situ* SR-XPD patterns collected during the ammonolysis reaction of ball milled LiH (a) and detail in the temperature range from 309 °C to 350 °C and in the Q-range from 2 $Å^{-1}$ to 2.5 $Å^{-1}$ (b). ▽ = LiH, ▲ = $LiNH_2$, △ = Li_2NH, ⋆ = Li_2O. The data were acquired at the diffraction beamlime I711 of MAX-lab with $\lambda = 0.992$ Å. Adapted with permission from Pistidda C., Santoru A., et al., J. Phys. Chem. C 119, 2, 934-943. Copyright 2015 American Chemical Society.[140]

In the diffraction patterns collected at RT the very strong Bragg reflections of LiH (▽, s.g. $Fm\bar{3}m$), together with the weaker peaks of Li_2O (⋆, s.g. $Fm\bar{3}m$) and $LiNH_2$ (▲, s.g. $I\bar{4}$) are identified. The presence of $LiNH_2$ peaks indicates that for LiH the ammonolysis process (reaction 3.1) can occur already at RT.

$$LiH + NH_3 \longrightarrow LiNH_2 + H_2 \tag{3.1}$$

In fact, preliminary diffraction experiments on the pristine material revealed absence of the same peaks before exposure to ammonia atmosphere, allowing to rule out a possible contamination with $LiNH_2$. During the heating process the Bragg reflections of $LiNH_2$ gradually increase in intensity while those of LiH gradually decrease, indicating a continuation of the ammonolysis reaction at the expenses of LiH.

At about 310 °C, the peaks of the tetragonal lithium amide phase reach their maximum intensity and then start to decrease, while the peaks of the cubic imide phase (△, $Fm\bar{3}m$) appear. At 340 °C the peaks of $LiNH_2$ completely disappear. In order to better visualize this transformation, a detail of the contour plot is provided in the temperature range from

309 °C to 350 °C and in the Q-range from 2 Å^{-1} to 2.5 Å^{-1} (Fig. 3.1-b). It can be noticed that the (112) Bragg peak of the amide phase undergoes a continuous shift toward the (111) Bragg reflection of the corresponding imide; at the same time the peaks corresponding to the (004) and (200) crystal family planes of the tetragonal phase gradually converge to the (200) reflection of the cubic phase. Analogous structural modifications were already observed and explained by David et al. and later confirmed by Makepeace et al. in studies of the Li-N-H system by high resolution SR-XPD.[154, 155] The authors showed that these changes are due to the formation of non-stoichiometric phases, with formula $Li_{1+x}NH_{2-x}$.

3.1.2 Na-N-H system

The ammonolysis process of NaH under gaseous NH_3 was investigated, correspondingly, by *in situ* SR-XPD and the results of this experiment are displayed in Fig. 3.2.

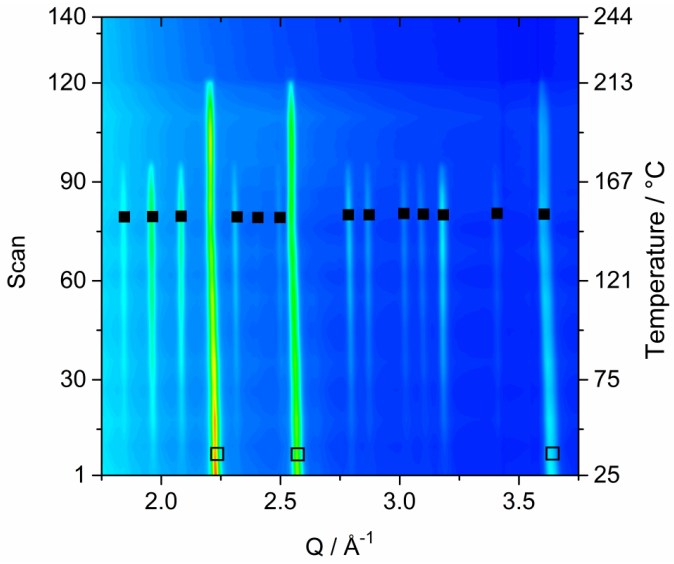

Figure 3.2: Contour plot of the *in situ* SR-XPD patterns collected during the ammonolysis reaction of ball milled NaH. □ = NaH, ■ = $NaNH_2$. Data from MAX-lab, $\lambda = 0.992$ Å. Adapted with permission from Pistidda C., Santoru A., et al., J. Phys. Chem. C 119, 2, 934-943. Copyright 2015 American Chemical Society.[140]

At RT the presence of the diffraction peaks of NaH (s.g. $Fm\bar{3}m$) can be noticed, as expected. Similarly to the Li-N-H system, the $NaNH_2$ peaks (s.g. $Fddd$) start to appear almost at RT (28 °C in this case). During the heating process the peaks attributed to $NaNH_2$ continuously increase, while the diffracted intensities of NaH decrease. The process can be therefore described according to reaction 3.2.

$$NaH + NH_3 \longrightarrow NaNH_2 + H_2 \tag{3.2}$$

The evolution of the diffractograms indicates that sodium amide is formed by reaction of the metal hydride with ammonia, without involving any intermediate crystalline structure.

When the temperature reaches 180 °C, the diffraction peaks of $NaNH_2$ disappear, and at 215 °C also the signal of NaH vanishes. The melting temperature previously reported for $NaNH_2$ is significantly higher than 180 °C (T = 208 °C and T > 190 °C according to McGee and Juza, respectively)[156, 91]; a much lower temperature of melting was previously reported by Titherley (155 °C).[77] Despite these differences, the fact that the background signal increases simultaneously with the disappearance of $NaNH_2$ peaks, suggests that a molten phase is present, most certainly $NaNH_2$.

3.1.3 K-N-H system

The contour plot for the reaction between KH and NH_3 is shown in Fig. 3.3.

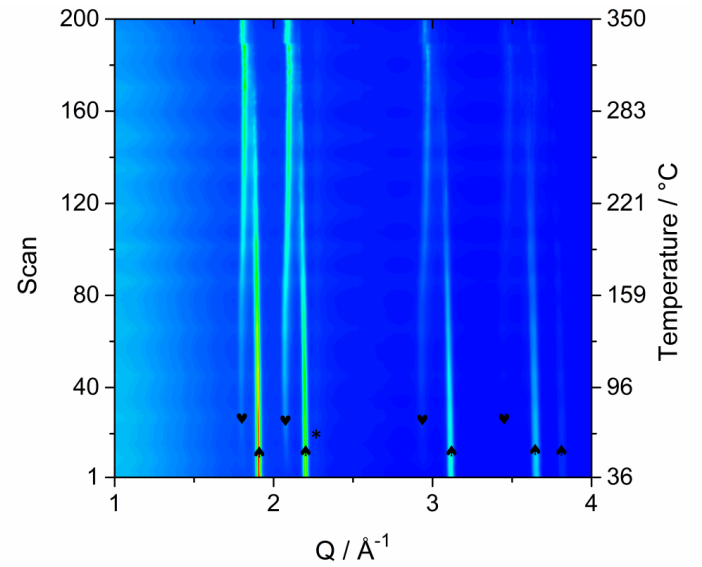

Figure 3.3: Contour plot of the *in situ* SR-XPD patterns collected at MAX-lab (λ = 0.992 Å) during the ammonolysis reaction of ball milled KH. ♠ = KH-like, ♥ = KNH_2-like, * = KOH. Adapted with permission from Pistidda C., Santoru A., et al., J. Phys. Chem. C 119, 2, 934-943. Copyright 2015 American Chemical Society.[140]

In the first diffraction pattern at RT the Bragg reflections of cubic KH (s.g. $Fm\bar{3}m$) are easily identifiable while peaks of monoclinic KOH (s.g. $P2_1/m$) are only barely detectable. During the first part of the heating process the appearance of seemingly cubic KNH_2 (s.g. $Fm\bar{3}m$) is noticeable, starting almost at RT; at the same time the intensity of KH peaks diminishes. The formation of the cubic phase of KNH_2 at such low temperatures is unexpected. In fact, in the temperature range between RT and 54 °C, the stable polymorph of KNH_2 is monoclinic (s.g. $P2_1/m$). A phase transformation to the tetragonal geometry (s.g $P4/nmm$)

should occur at 54 °C and finally, only at higher temperatures (ca. 75 °C), the cubic polymorph should prevail.[157] As the temperature increases, the peaks associated to the cubic KNH_2-like phase grow stronger, while KH peaks become gradually weaker. Interpreting these results similarly to the cases previously examined (Li-N-H and Na-N-H system), it would lead to conclude that an ammonolysis process is taking place, which consumes potassium hydride in order to form the corresponding amide (reaction 3.3).

$$KH + NH_3 \longrightarrow KNH_2 + H_2 \tag{3.3}$$

However, another aspect of this *in situ* SR-XPD experiment is worth noticing. In the previous experiments (Fig. 3.1 and Fig. 3.2), as expected, the Bragg reflections of the amide and hydride phases gradually shifted to lower Q-values over the heating process, which is due to the thermal expansion of the crystal lattice. However in this case (Fig. 3.3) a similar shift seems to occur only in the first part of the heating process. Indeed, above 160 °C it is noticeable how all peaks of the KNH_2-like phase start to move to higher Q-values, which implies an unexpected contraction of the cubic lattice.

3.1.4 Mg-N-H system

The contour plot reported in Fig. 3.4 shows the diffractograms collected *in situ* for the ammonolysis of MgH_2.

The co-existence of β-MgH_2 (s.g. $P4_2/mnm$) and γ-MgH_2 (s.g. *Pbcn*) at RT is clearly visible. The γ-phase is the high pressure polymorph of MgH_2. γ-MgH_2 forms during the ball milling process, since the impact of the balls can locally increase the pressure favouring its instantaneous formation. In the first part of the heating no events can be noticed. At about 140 °C a sudden decrease of the peak intensities of the γ-MgH_2 takes place, together with the increase of β-MgH_2. This change in the diffraction patterns indicates that the metastable phase of γ-MgH_2 is starting to convert into the thermodynamically more stable phase of β-MgH_2. The further disappearance of the peaks of γ-MgH_2 is associated with the formation of $Mg(NH_2)_2$ (s.g. $I4_1/acd$), starting at about 230 °C. When the temperature reaches 350 °C the complete consumption of γ-phase can be noticed. The evolution of the diffractograms indicates that the ammonolysis reaction proceeds mostly at the expenses of the metastable γ-MgH_2 and can be described according to reaction 3.4:

$$\gamma\text{-}MgH_2 + 2\,NH_3 \longrightarrow Mg(NH_2)_2 + 2\,H_2 \tag{3.4}$$

During the isothermal period we assist to the appearance and continuous increase of the Bragg peaks associated with MgNH (s.g. $P6/m$), which is accompanied with the clear decrease of

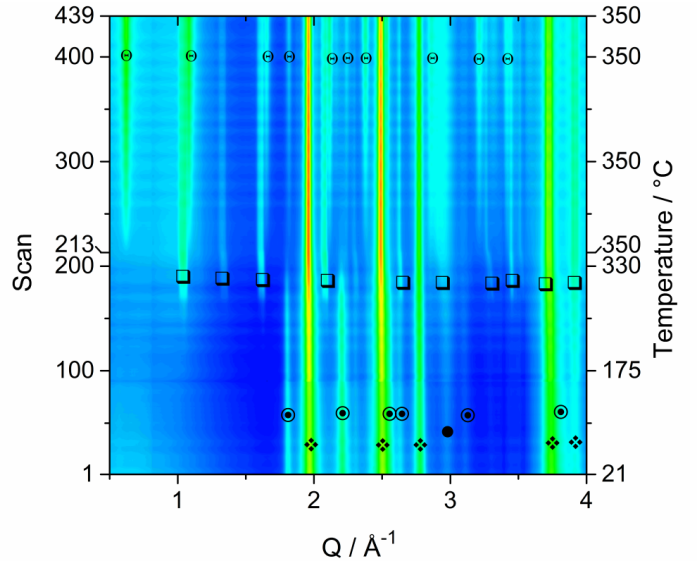

Figure 3.4: Contour plot of the *in situ* SR-XPD patterns acquired during the ammonolysis reaction of ball milled MgH_2. ❖ = β-MgH_2, ◉ = γ-MgH_2, ● = MgO, ❑ = $Mg(NH_2)_2$, Θ = MgNH. Data collected at the diffraction beamlime I711 of MAX-lab with $\lambda = 0.992$ Å. Adapted with permission from Pistidda C., Santoru A., et al., J. Phys. Chem. C 119, 2, 934-943. Copyright 2015 American Chemical Society.[140]

β-MgH_2. The reflections of $Mg(NH_2)_2$ are rather constant during the whole isothermal period. Therefore the diffractograms suggest that the formation of MgNH occurs mainly due to a direct reaction involving β-MgH_2. For this reason, the process can be described according to reaction 3.5.

$$\beta\text{-}MgH_2 + NH_3 \longrightarrow MgNH + 2\,H_2 \tag{3.5}$$

The relative amount of crystalline phases (obtained by Rietveld refinement) as a function of the scan number (and corresponding temperature) is reported in Fig. 3.5. From this plot it is easier to appreciate the partial conversion from γ- to β-MgH_2, the formation of $Mg(NH_2)_2$ occurring mostly at the expenses of γ-MgH_2 (reaction 3.4) and the partial consumption of β-MgH_2 to form MgNH (reaction 3.5).

3.1.5 Ca-N-H system

The results of the *in situ* SR-XPD investigation on the ammonolysis reaction of CaH_2 are presented in Fig. 3.6. During the first part of the heating, only a slight shift of the Bragg peaks to lower Q-values is observed, due to the expected thermal expansion. At temperatures above 145 °C the reflections of CaNH (s.g. $Fm\bar{3}m$) start to appear and slowly increase in intensity, while a contemporary decrease can be noticed in the intensity of CaH_2 peaks (s.g. *Pnma*). The formation of $Ca(NH_2)_2$ in this temperature range is not expected.[158] The ammonolysis

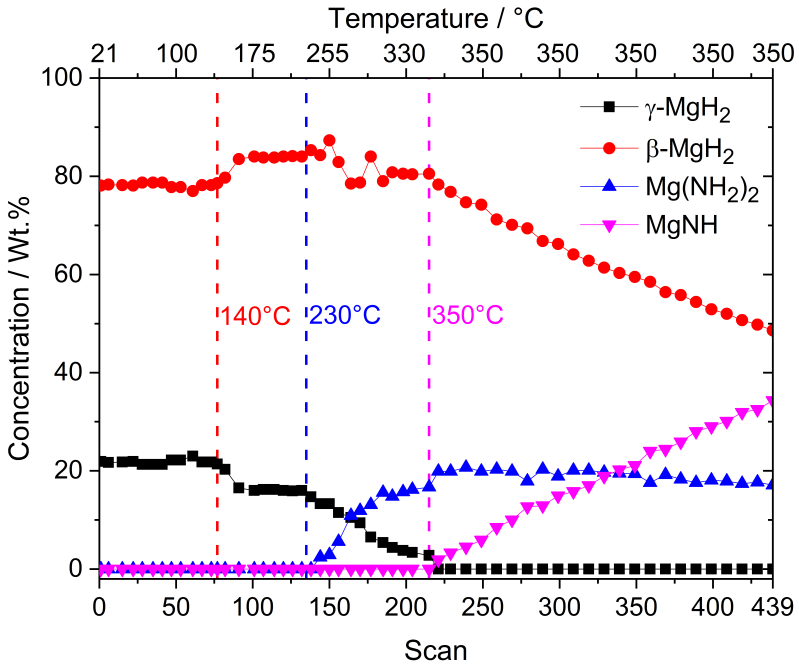

Figure 3.5: Compositional changes of the crystalline phases obtained by Rietveld refinement of the *in situ* SR-XPD patterns. Adapted with permission from Pistidda C., Santoru A., et al., J. Phys. Chem. C 119, 2, 934-943. Copyright 2015 American Chemical Society.[140]

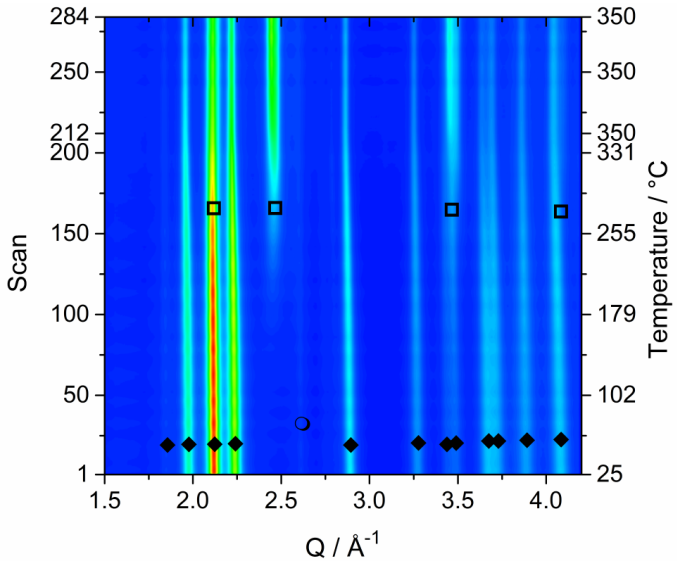

Figure 3.6: Contour plot of the *in situ* SR-XPD patterns acquired at the diffraction beamlime I711 of MAX-lab with $\lambda = 0.992$ Å during the ammonolysis reaction of ball milled CaH_2. ◆ = CaH_2, □ = CaNH, ❍ = CaO. Adapted with permission from Pistidda C., Santoru A., et al., J. Phys. Chem. C 119, 2, 934-943. Copyright 2015 American Chemical Society.[140]

reaction of CaH_2 can be therefore described as in reaction 3.6:

$$CaH_2 + NH_3 \longrightarrow CaNH + 2\,H_2 \tag{3.6}$$

In the range of temperatures between 325 - 340 °C the reflections of the calcium imide phase develop asymmetric features, which can be noticed more easily at higher Q (e.g. at Q = 3.5 Å). This could be due to a phase transition to a structure with lower symmetry. Another possibility would be the formation a calcium imide phase with slightly different atomic composition.

3.1.6 M-N-H systems: general discussion and summary

The SR-XPD experiments described in this section are the first reported attempt to systematically characterize *in situ* the ammonolysis process of the most common alkali and alkaline-earth metals.

For LiH, NaH and KH the ammonolysis reaction starts to take place already at RT, while in case of MgH_2 and CaH_2 much higher temperatures (220 °C and 145 °C respectively) are necessary to initiate the process under 6.5 bar of ammonia.

For the Li-N-H system, our results confirm the reaction mechanism previously proposed from David et al.[154] and Makepeace et al.[155] for the conversion of $LiNH_2$ into Li_2NH under hydrogen atmosphere and extend its validity to the ammonia atmosphere. The authors realized that the tetragonal lithium amide phase can be considered an ordered superstructure (a x a x $2a$) of the disordered cubic structure of lithium imide, with only half of the lithium sites occupied. The formation of intermediate $Li_{1+x}NH_{2-x}$ follows a non-stoichiometric mechanism, involving the creation of Frenkel defects.[154]

Concerning the Na-N-H system, $NaNH_2$ is formed from the ammonolysis process without involving any other crystalline intermediate and it is confirmed to be the alkali metal amide with the lowest melting point; no high temperature polymorphs are observed before its melting. The difference between the melting temperature of about 180 °C found in our work (Pistidda C., Santoru A. et al., 2015[140]) and the one of 208 °C previously reported (McGee et al.[156], 1921) can be understood thanks to a recent work published by Jepsen et al.[159] in 2016. In their *in situ* SR-XPD measurement of commercial $NaNH_2$ (containing 1% of NaOH) after ball milling, it can be noticed that the peaks of $NaNH_2$ almost disappear already at 184 °C, a temperature value, which is very similar to the one found in our experiment.[159] Moreover, in the same study, Jepsen et al. showed that in the $NaNH_2$-NaOH system, lower melting temperatures are found, compared the the melting temperature of the pristine components;[159] this may explain the significantly lower value (155 °C) reported in

the pioneering work of Titherley[77].

In the K-N-H system, the room temperature polymorph of KNH_2 is not formed, but rather a cubic phase which closely resembles the high temperature polymorph of KNH_2. Moreover, the shift of the peaks of this phase to higher Q-values at increasing temperature, implies a contraction of the cubic cell, in contrast to the expected thermal expansion; this fact suggests the possibility of forming non stoichiometric phases, rather than well defined compositions. A possible explanation for this can be proposed considering the profound structural similarities between KH and cubic KNH_2. Both structures have the same space group ($Fm\bar{3}m$), same coordination number (c.n. $= 6$), same cation (K^+), anions with same total electric charge (-1) and similar cell parameters (less than 10 % difference). Therefore it is reasonable to hypothesize the formation of amide-hydride phases with intermediate compositions, i.e. $K(NH_2)_xH_{1-x}$, which could explain the observed shift of the Bragg reflections of the two cubic phases.

For the Mg-N-H system, the *in situ* experiment offers direct evidence of the importance of the metastable γ-MgH_2 in the synthesis of $Mg(NH_2)_2$. In order to explain the different reactivity of β- and γ-MgH_2, it is important to consider that the γ-phase is known to occupy the finest material particle population, when prepared by mechanochemical methods;[160] moreover, this polymorph is metastable and therefore more reactive. γ-MgH_2 appears to be a key intermediate in the synthesis of $Mg(NH_2)_2$ at lower temperatures (e.g. via the ball milling technique).

The ammonolysis reaction in the Ca-N-H systems leads to the formation of calcium imide above 145 °C; the evolution of the diffractograms at higher temperatures suggests that subtle structural/compositional modifications start to take place, probably involving non-stoichiometric phases formed from the interaction of the newly formed imide with the unreacted hydride phase. Indeed, CaNH can react with CaH_2 according to reaction 3.7, forming calcium nitride hydride:

$$CaH_2 + CaNH \longrightarrow Ca_2NH + H_2 \tag{3.7}$$

Since the cell parameter of Ca_2NH (s.g. $Fd\bar{3}m$) is roughly double than that of CaNH (10.13 Å vs 5.14 Å respectively), the unit cell of Ca_2NH can be considered a supercell (2a x 2a x 2a) of the unit cell of CaNH. For this reason, non-stoichiometric phases may be formed, causing these subtle changes evidenced in the diffraction patterns. In particular, the partial H_2 pressure developed during the ammonolysis process (reaction 3.6) might hinder the completion of reaction 3.7, allowing the formation of phases with intermediate compositions. Due to the low number of Bragg reflections available and great extent of overlap, a more detailed description of the ammonolysis reaction is not possible at this point.

In a whole, the most common M-N-H systems were studied, with a particular focus on the processes that lead to the formation of the corresponding metal amides and imides. In the last decades, most of these compounds were subjected to extensive investigations regarding their potential as hydrogen storage materials. Even if the possibility of using the ammonolysis reaction to produce hydrogen was suggested,[161] reactive composites of amides and hydrides are considered to be more technologically appealing. Indeed, due to their exceptional properties, such systems can be directly utilized in hydrogen storage tanks coupled to fuel cells and tested for mobile applications at prototype level.[162] In this regard, the diverse chemistry of bimetallic systems allowed important improvements in the thermodynamic and kinetic properties as compared to simpler amide-hydride systems (e.g. Li-Mg-N-H systems vs Li-N-H systems respectively).[104, 105, 102, 106] In the next chapter several bimetallic amide-hydride composite systems are introduced, emphasizing the new insights deriving from the present investigation.

3.2 K-Mg-N-H system

As anticipated in section 1.3.3.5, a first significant improvement in the desorption properties of the Li-Mg-N-H system was obtained by partially replacing LiH with KH. The starting desorption temperature, as determined by temperature programmed desorption (TPD), under argon flow is 132 °C for the $Mg(NH_2)_2$ + 1.9 LiH + 0.1 KH composite. If compared with the value of 186 °C, determined for the pristine $Mg(NH_2)_2$ + 2 LiH system using the same experimental procedure, the former is about 50 °C lower.[109] In the same work, Wang et al. revealed that they chose potassium for its ability to form bimetallic amides with magnesium.[109] In a follow-up paper, Wang et al. thoroughly investigated the properties of the K-Mg-N-H system, evidencing the formation of a kinetic product (less stable, but kinetically favourable), $K_2Mg(NH_2)_4$, and the formation of a thermodynamic product, $KMgNH_2NH$ (more stable, but kinetically hindered).[110] However, the studies performed by Palvadeau and Rouxel reported the formation of the $K_2Mg(NH_2)_2(NH)$ and $K_2Mg(NH)_2$ phases in the temperature range of 180 - 250 °C, and then the formation of KMgN at about 330 °C.[96, 97] Our investigation, based on *in situ* and *ex situ* XPD experiments, manometric measurements and mass spectroscopy, provides new information on the desorption properties, phase evolution and reaction mechanism of K-Mg-N-H-based systems.

3.2.1 KH-MgH_2-NH_3 system

The first experiment was performed to study the reactivity of the KH-MgH_2-NH_3 system under mechanochemical processing: KH and MgH_2 (molar ratio 1 : 1) were ball milled

for 20 h under 7 bar of ammonia at 400 RPM (sample A). The intermediates and products formed during the mechanochemical treatment were determined by means of *ex situ* XPD. The XPD pattern (Fig. 3.7) of the sample after ball milling reveals the formation of KNH_2, $K_2Mg(NH_2)_4$ as well as the presence of unreacted MgH_2.

The other starting reagent, KH, is not detected because it reacted completely with ammonia forming potassium amide (reaction 3.8). These results suggest that the reactivity of MgH_2 towards NH_3 is lower compared to that of KH when the reaction is induced by ball milling. Interestingly, in the previous chapter, the same marked difference in reactivity is shown when the reactions are induced by thermal rather than mechanical input. Considering this pronounced difference in the reactivity of KH and MgH_2 it is reasonable to suggest that KH would be the first to react with ammonia; for this reason a multi-step reaction pathway, involving the formation of KNH_2 and $Mg(NH_2)_2$ as intermediate products, can be envisaged as follows:

$$KH + NH_3 \longrightarrow KNH_2 + H_2 \tag{3.8}$$

$$MgH_2 + 2\,NH_3 \longrightarrow Mg(NH_2)_2 + 2\,H_2 \tag{3.9}$$

$$2\,KNH_2 + Mg(NH_2)_2 \longrightarrow K_2Mg(NH_2)_4 \tag{3.10}$$

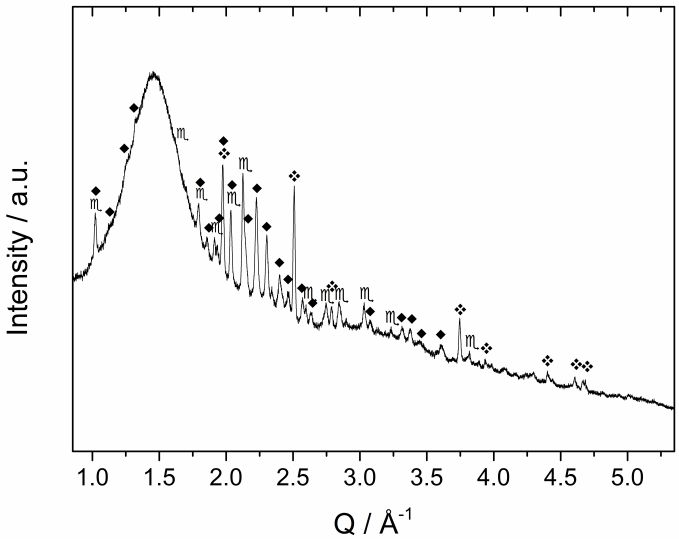

Figure 3.7: XPD pattern of sample A as obtained after mechanochemical treatment. ℳ = KNH_2 ($P2_1/m$), ♦ = $K_2Mg(NH_2)_4$, ❖ = MgH_2. Data acquired with the D8 Discover diffractometer, equipped with a copper X-ray source (λ = 1.541 84 Å). Picture readapted from Santoru et al., Phys. Chem. Chem. Phys., 2016, 18, 3910-3920 - Published by the PCCP Owner Societies.[163]

Nonetheless, a direct single step reaction of KH, MgH_2 and NH_3, forming $K_2Mg(NH_2)_4$ and H_2 (in competition with the multi-step pathway proposed above), cannot be completely ruled out by *ex situ* methods. It is also interesting to notice that the Bragg reflections associated

with the $Mg(NH_2)_2$ phase (reaction 3.9) are not present in the RT diffraction pattern of sample A (Fig. 3.7), probably due to its further interaction with KNH_2 to form $K_2Mg(NH_2)_4$ (reaction 3.10). However, $Mg(NH_2)_2$ is known to be formed in the amorphous/nano-crystalline state, when subjected to intense ball milling treatment for either its synthesis or processing; for this reason, the presence of this compound cannot be completely excluded based on the XPD experiment reported in Fig. 3.7.[164]

The desorption properties of sample A were studied by manometric analysis as well as mass spectroscopy. According to Fig. 3.8-a, the desorption takes place reaching a single plateau, releasing 1.8 wt% of hydrogen after 50 minutes: the process is slow below 200 °C but becomes vigorous above 210 °C (more than 1.2 wt% of H_2 release in about 5 minutes). Apparently, mainly hydrogen is released (Fig. 3.8-b).

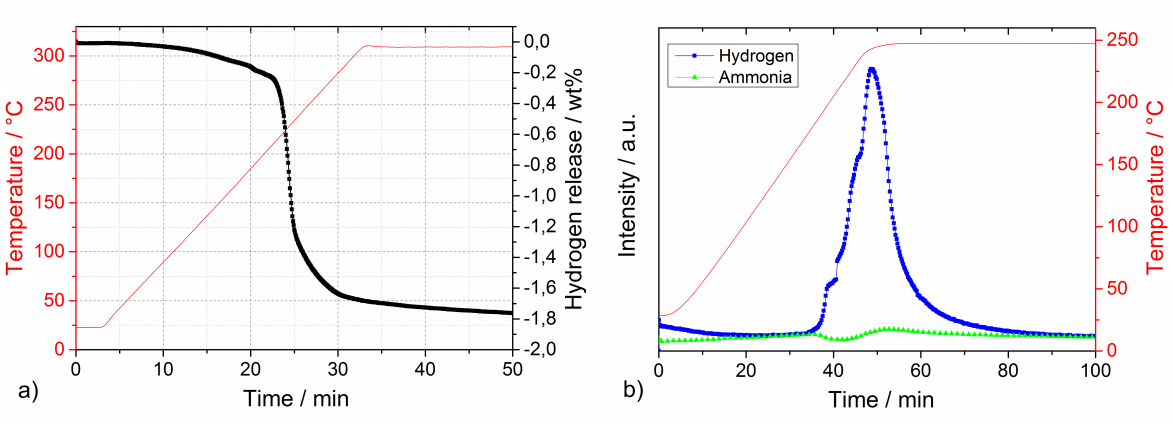

Figure 3.8: Desorption properties of sample A determined by a Sieverts apparatus (a) and thermal desorption mass spectrometry (TD-MS) (b). Picture readapted from Santoru et al., Phys. Chem. Chem. Phys., 2016, 18, 3910-3920 - Published by the PCCP Owner Societies.[163]

Ex situ XPD performed on sample A after desorption in the manometric apparatus revealed the presence of $KMgNH_2NH$ (Fig. 3.9-a). After re-absorption the absence of the peaks of $KMgNH_2NH$ is clear in the corresponding diffractogram (Fig. 3.9-b), while the reflections of KH and $Mg(NH_2)_2$ can be easily identified.

These measurements indicate that the hydrogenation process proceeds according to reaction 3.11, in agreement with the data reported by Wang et al.,[110] even if the sample preparation and the desorption process were different.

$$KMgNH_2NH + H_2 \longrightarrow KH + Mg(NH_2)_2 \tag{3.11}$$

This result suggests that the system obtained upon ball milling is metastable, whereas, similarly to the $2\,LiNH_2$-MgH_2 / 2LiH-$Mg(NH_2)_2$ systems previously described (section 1.3.3.5), KH-$Mg(NH_2)_2$ corresponds to the thermodynamically stable state. The *ex situ* XPD

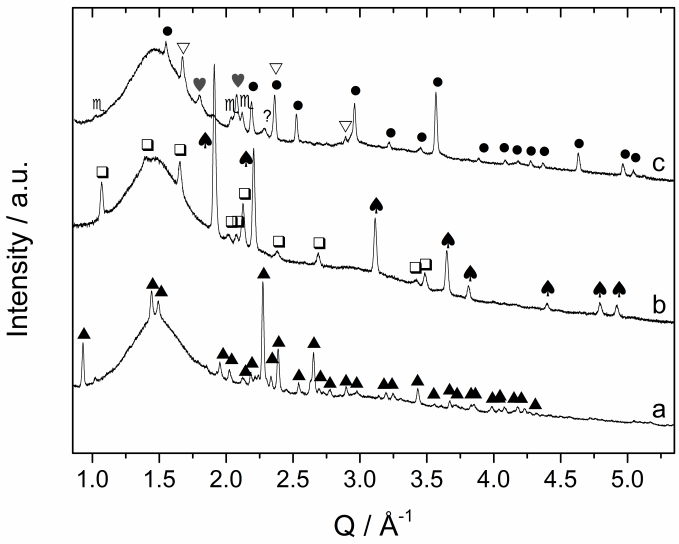

Figure 3.9: Room temperature XPD pattern of sample A (a) after desorption at 310 °C in the Sievert apparatus; (b) after absorption; and (c) after thermal decomposition at 450 °C under static vacuum. ▲ = $KMgNH_2NH$, ❑ = $Mg(NH_2)_2$, ♠ = KH, ♏ = KNH_2 ($P2_1/m$), ❖ = MgH_2, ? = unknown, ● = Mg_3N_2, ♥ = KNH_2-like, ▽ = K. The data were acquired with the D8 Discover diffractometer (λ = 1.541 84 Å). Santoru et al., Phys. Chem. Chem. Phys., 2016, 18, 3910-3920 - Published by the PCCP Owner Societies.[163]

performed after thermal treatment of the $KMgNH_2NH$ product up to 450 °C under static vacuum, disproves the formation of KMgN (Fig. 3.9-c) as the decomposition product of the amide-imide phase and reveals the formation of a new cubic phase (marked as ♥ in Fig. 3.9-c) similar to the intermediate phases of the K-N-H system presented in section 3.1.3.

In order to investigate the desorption mechanism of sample A and clarify if the previously reported bimetallic amide-imide, imide and nitride phases can be formed as intermediates or metastable components, an *in situ* SR-XPD experiment was performed.

Fig. 3.10-a shows the SR-XPD patterns collected increasing the temperature from RT to 420 °C. The first variation in the diffraction patterns is related to a phase transformation of potassium amide: in the temperature range 50 °C < T < 80 °C the monoclinic cell rearranges into a cubic geometry through an intermediate tetragonal polymorph of KNH_2 ($P4/nmm$).

With a further increment of the temperature up to 167 °C, the Bragg reflections of $Mg(NH_2)_2$ appear (Fig. 3.10-a), most probably due to re-crystallization of an amorphous product formed during the synthesis of the sample (as previously hypothesized). The formation of crystalline $Mg(NH_2)_2$ could also arise from a metathesis reaction between magnesium hydride and amide anions containing phases (KNH_2 or $K_2Mg(NH_2)_4$). However, only the peak intensities of $Mg(NH_2)_2$ increase in this step: the Bragg reflections of the co-product that would be generated should appear as well, and the intensity of the peaks of the amide phase should decrease as well, but according to the details reported in Fig. 3.10-b this is not

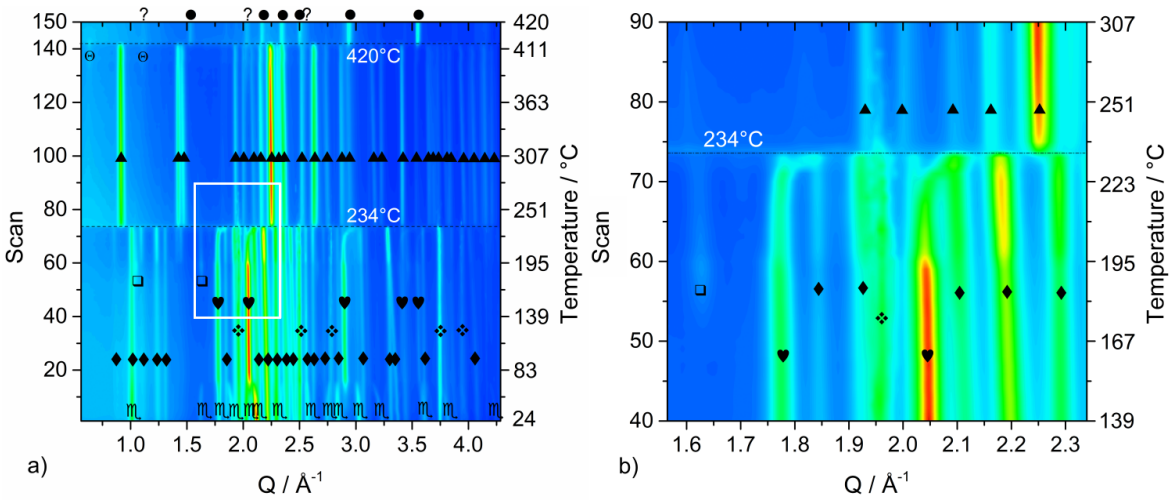

Figure 3.10: Contour plot of the SR-XPD experiment conducted at MAX-lab ($\lambda = 0.978\,89$ Å) on sample A (a). Detail in the Q-range 1.55 $Å^{-1}$ to 2.35 $Å^{-1}$ and scans 40 to 90 (b). ♏ = KNH_2 ($P2_1/m$), ♦ = $K_2Mg(NH_2)_4$, ❖ = MgH_2, ♥ = KNH_2 ($Fm\bar{3}m$), ❑ = $Mg(NH_2)_2$, ▲ = $KMgNH_2NH$, Θ = MgNH, ? = unknown phase, ● = Mg_3N_2. Picture readapted from Santoru et al., Phys. Chem. Chem. Phys., 2016, 18, 3910-3920 - Published by the PCCP Owner Societies.[163]

the case. Furthermore, the broad signal in the low Q-range ($Q < 1.5$ $Å^{-1}$, Fig. 3.10-a), due to the incoherent scattering from amorphous and/or nano-crystalline phases, disappears in the same temperature range.

The subsequent decreased intensity of $Mg(NH_2)_2$ and KNH_2 reflections is associated with an increment of $K_2Mg(NH_2)_4$ peaks when the temperature reaches 195 °C (see Fig. 3.10-b for details). Most probably the $K_2Mg(NH_2)_4$ phase is formed by the interaction of KNH_2 with $Mg(NH_2)_2$ according to reaction 3.10.

Increasing the temperature further, at 234 °C a sudden transition in the contour plot is visible (detail in Fig. 3.10-b). This event coincides with the disappearance of the $K_2Mg(NH_2)_4$ peaks. The transition is rather fast for being ascribable to a solid state reaction: most likely the observed phenomenon is due to the melting of $K_2Mg(NH_2)_4$. This hypothesis is supported by the fact that the background intensity increases noticeably in the low Q-range ($Q < 1.3$ $Å^{-1}$). Magnesium hydride particles dispersed in the liquid $K_2Mg(NH_2)_4$ phase react releasing hydrogen and forming $KMgNH_2NH$ according to reaction 3.12.

$$K_2Mg(NH_2)_4 + MgH_2 \longrightarrow 2\,KMgNH_2NH + 2\,H_2 \tag{3.12}$$

Indeed, the intensity change for the peaks of the two solid phases MgH_2 and $KMgNH_2NH$ is in agreement with the kinetics measured by manometric measurements and TD-MS (Fig. 3.8). Surprisingly, neither $K_2Mg(NH_2)_2(NH)$ nor $K_2Mg(NH)_2$ (reported by Palvadeau and Rouxel) are identified as crystalline components in the patterns in the range of 180 -

250 °C.[97] The theoretical capacity of reaction 3.12 is 2.1 wt%. The difference from the experimental value of 1.8 wt%, determined by a Sievert apparatus, could be ascribable to the hydrogen release occurred during ball milling, similarly to the study of Wang et al.[110]

Another interesting aspect of the desorption process is revealed by the *in situ* experiment reported in Fig. 3.10: below 234 °C, a shift of the cubic KNH_2 peaks to higher Q-values occurs, implying that a fast contraction of the cubic KNH_2 cell volume takes place. This event is in contrast to the predictable thermal expansion of potassium amide unit cell and may be due to an interaction with magnesium hydride; the mechanism of this interaction is explored and discussed in detail in the next section.

The amide-imide phase shows a rather high thermal stability (Fig. 3.10), and the decomposition takes place only at 420 °C in good agreement with the decomposition temperature found by Wang et al.[110] Due to decomposition, Mg_3N_2 is formed as an end-product while MgNH is most likely a reaction intermediate for the formation of Mg_3N_2. Also a minor unknown component is produced, differently from the phases previously reported by Palvadeau and Rouxel.[96, 97] Additionally, KMgN is not detected in our diffraction experiments (Fig. 3.9-c and Fig. 3.10-a).

Complementary *in situ* and *ex situ* XPD allowed to prove that the K-containing products at these temperatures are formed in a molten state: indeed they can be observed in the *ex situ* experiment (Fig. 3.9-c) but are undetectable as coherent scattering in the *ex situ* experiment; only an increasing diffuse scattering can be noticed, markedly in the low Q-region ($Q < 1.5\,\text{Å}^{-1}$, Fig. 3.10-a).

3.2.2 KNH_2-MgH_2 system

The singular behaviour evidenced in the previous section for the potassium amide crystal structure (just below 234 °C and above 420 °C, in Fig. 3.10-b and Fig. 3.9-c, respectively) and the scarce information available in the literature motivated further work to explain the previous results. The potassium amide and magnesium hydride mixture is here studied for the first time by *in situ* SR-XPD to understand the mechanisms laying behind this phenomenon. According to the work carried out in recent years by P. Chen et al., the hydrogen release in amide- hydride mixtures arises from the $H^{\delta+}$-$H^{\delta-}$ interaction.[107] The maximum hydrogen capacity is therefore obtained by selecting the system compositions with an equal amount of hydrogen atoms in the oxidation states (+I) and (-I). As a consequence of this strategy for designing systems with higher hydrogen capacities, nitride phases are usually formed upon decomposition and all the hydrogen is released.[101, 103] Following this approach a study of the KNH_2+MgH_2 system (sample B) could reject or confirm the existence of a KMgN phase resulting from the interaction between an equal number of hydrogen atoms with partial

positive and negative charges.

The starting diffraction pattern of Sample B shows the presence of KNH_2 and MgH_2 as the major components (Fig. 3.11-a); in addition, a small amount of Mg already present in the as-received MgH_2 is visible.

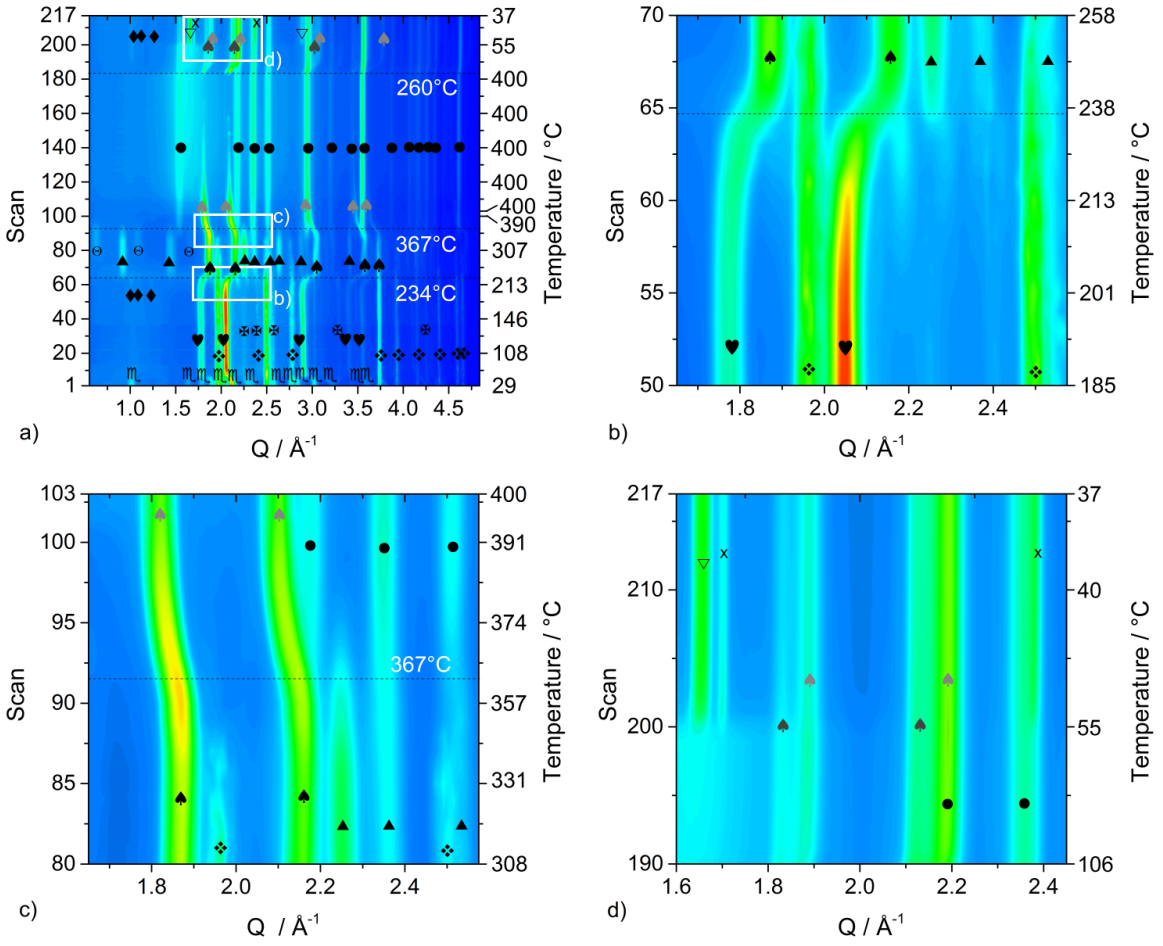

Figure 3.11: Contour plot of the SR-XPD experiment conducted at MAX-lab ($\lambda = 0.9938$ Å) on the ground KNH_2 + MgH_2 mixture (sample B) (a), details showing the transformations related to the first and second desorption step (b and c respectively) and cooling process (d). ♏ = KNH_2 ($P2_1/m$), ❖ = MgH_2, ♥ = KNH_2 ($Fm\bar{3}m$), ✠ = Mg, ♦ = $K_2Mg(NH_2)_4$, ▲ = $KMgNH_2NH$, ♠ = KH, Θ = MgNH, ♠ and ♥ = $K(NH_2)_xH_{1-x}$, ● = Mg_3N_2, ▽ = K, x = K-phase. Picture readapted from Santoru et al., Phys. Chem. Chem. Phys., 2016, 18, 3910-3920 - Published by the PCCP Owner Societies.[163]

According to the *in situ* SR-XPD data in Fig. 3.11, the temperature of the first desorption step (234 °C) is basically unchanged, compared to that of Sample A (Fig. 3.10). However, due to its ratio of metal-nitrogen atoms, the desorbed state of KNH_2 + MgH_2 cannot be consistent with the pure $KMgNH_2NH$ phase. Indeed, according to Fig. 3.11-b, not only $KMgNH_2NH$ but also KH and residual MgH_2 are found. For this reason the desorption, expected in this temperature range according to the *in situ* SR-XPD experiment (Fig. 3.11), can be envisaged

as follows:

$$2\,KNH_2 + 2\,MgH_2 \longrightarrow KMgNH_2NH + KH + MgH_2 + H_2 \tag{3.13}$$

Reaction 3.13 releases 1.2 wt% of hydrogen, which is in agreement with the value of 1.2 wt% found by the manometric measurements at the temperature of 240 °C (Fig. 3.12).

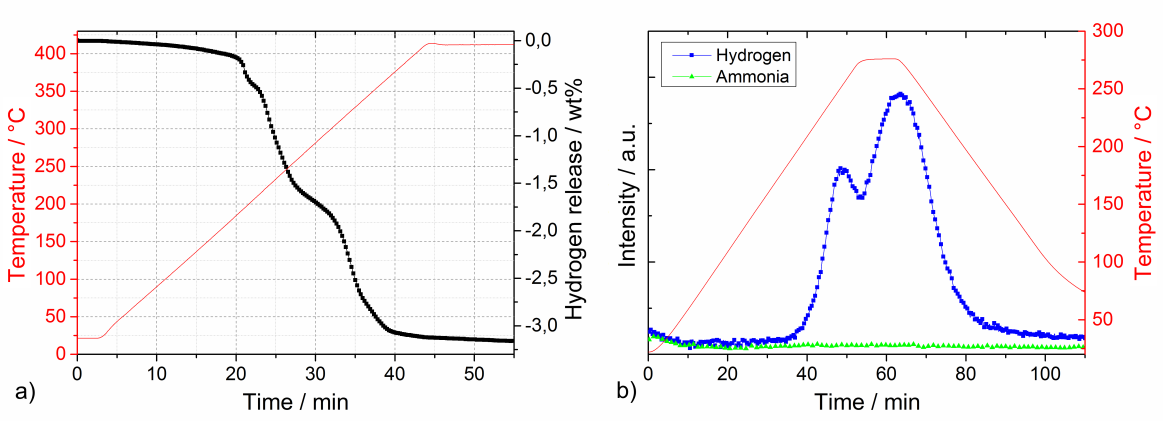

Figure 3.12: Desorption properties of sample B determined by: (a) Sieverts apparatus and (b) thermal desorption mass spectrometry. Picture readapted from Santoru et al., Phys. Chem. Chem. Phys., 2016, 18, 3910-3920 - Published by the PCCP Owner Societies.[163]

However, there is no clear plateau at this point and the desorption continues with the same rate until 1.6-1.7 wt% of hydrogen is released (Fig. 3.12). The additional desorption may depend on the formation of an amorphous imide as an intermediate phase. In fact, the *ex situ* XPD pattern of the sample collected after the desorption of about 1.7 wt% of hydrogen (Fig. 3.13-a), reveals the presence of the same phases shown in the *in situ* measurement at about 250 °C (Fig. 3.11-b).

The evolution of the diffractograms reported in Fig. 3.11-b suggests that above 200 °C, the unit cell of KNH_2 undergoes a continuous contraction until it is converted into KH. This phenomenon, previously observed for sample A at similar temperature is therefore ascribable to the interaction of KNH_2 and MgH_2. The contraction of the cell volume at higher temperature (Fig. 3.11-b) may be explained by a substitution mechanism of amide groups with smaller anions, namely by hydride anions from MgH_2.

A further increase of the temperature up to 234 °C led to the appearance of weak peaks of $K_2Mg(NH_2)_4$, anticipating the desorption processes (Fig. 3.11-a). Then at 367 °C all the reflections attributable to $KMgNH_2NH$, MgH_2 and MgNH disappeared, magnesium nitride was formed and a fast expansion of the KH lattice took place (Fig. 3.11-c). According to the data reported in the literature, a thermal expansion of the KH cell volume of about 1 % can be calculated in the temperature range between 308 and 400 °C.[165] Conversely, in our

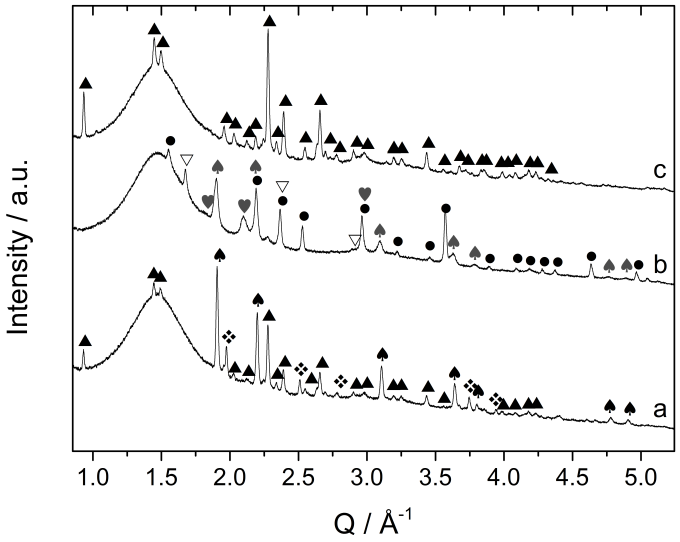

Figure 3.13: Room temperature diffractograms of: sample B collected after desorption in the Sievert apparatus until 255 °C (a) and 410 °C (b) respectively; sample C collected after desorption in a heating ramp RT - 300 °C in the Sievert apparatus (c). ❖ = MgH_2, ♠ = KH, ▲ = $KMgNH_2NH$, ● = Mg_3N_2, ♠ and ♥ = $K(NH_2)_xH_{1-x}$, ▽ = K; Bruker D8 Discover, $\lambda = 1.541\,84$ Å. Santoru et al., Phys. Chem. Chem. Phys., 2016, 18, 3910-3920 - Published by the PCCP Owner Societies.[163]

experiment (Fig. 3.11-c), for the same temperature range, a considerably bigger expansion of the cell volume takes place: the calculated expansion is about 8.5 %. Amide anions from $KMgNH_2NH$ are most probably responsible for this event, while the imide groups further react with hydride anions forming the nitride phase and releasing hydrogen. The process may be described according to reaction 3.14.

$$3\,KMgNH_2NH + 3\,KH + 3\,MgH_2 \longrightarrow 2\,Mg_3N_2 + 6\,K(NH_2)_{1/3}H_{2/3} + 5\,H_2 \qquad (3.14)$$

The total desorption process can then be written as:

$$3\,KNH_2 + 3\,MgH_2 \longrightarrow Mg_3N_2 + 3\,K(NH_2)_{1/3}H_{2/3} + 4\,H_2 \qquad (3.15)$$

During the isothermal period at 400 °C (Fig. 3.11-a) the potassium amide-hydride solid solution melts completely. During fast cooling down the solidification of two cubic phases with slightly different cell parameter is observed at 260 °C together with a decrease of the incoherently scattered intensity (Fig. 3.11-a, Q-range: 1.3 $Å^{-1}$ to 1.8 $Å^{-1}$, patterns 180 to 200). When the temperature reaches about 55 °C potassium, which was present in a molten state, crystallizes and also the residual broad signal between 1.5 $Å^{-1}$ and 1.75 $Å^{-1}$ completely disappears (Fig. 3.11-d, patterns 200 to 217). Other peaks (indicated by "X" in Fig. 3.11-d) also appear at the same moment: the temperature is rather close to the melting point of

metallic potassium (63.5 °C). $K_2Mg(NH_2)_4$ is also detected in traces. The appearance of metallic potassium is most probably due to the partial decomposition of the K-N-H phases. The results on the final products were cross-checked with the *ex situ* XPD acquired on the sample desorbed in the Sievert apparatus (Fig. 3.13-b), showing that the "X-phase" and $K_2Mg(NH_2)_4$ are not formed if the cooling down is performed slowly. Therefore the X-phase may be a metastable phase of potassium and its formation, together with $K_2Mg(NH_2)_4$, is probably due to the fast cooling down in the ammonia-rich atmosphere resulting from the precedent decomposition of $K(NH_2)_xH_{1-x}$. The formation of metallic potassium poses serious concerns on the safety issues associated with the long term storage of this material, particularly if contamination with aluminium takes place: even if the samples are stored in a glove-box under inert atmosphere the formation of explosive compounds may occur.[166] The theoretical value of gravimetric capacity according to reaction 3.15 (3.3 wt%) is close to the experimental value of 3.2 wt% determined by the Sievert apparatus (Fig. 3.12-a). The hydrogen desorption expected from the *ex situ* XPD and manometric measurement was confirmed by a TD-MS experiment (Fig. 3.12-b). Noteworthy, even if ball milling is known to be beneficial for limiting the release of ammonia (e.g. in the magnesium amide-magnesium hydride system)[167], for the potassium amide-magnesium hydride composite the ammonia release upon desorption is rather low compared to the H_2 signal, even if the material was not prepared via ball milling (see experimental details in section 2.1.2).

3.2.3 KH-$Mg(NH_2)_2$ system

According to the work of Wang et al. when a mixture of KH and $Mg(NH_2)_2$ is heated at 2 °C min^{-1} under static vacuum conditions, the components start to interact with each other releasing hydrogen at temperatures below 100 °C, reaching a maximum rate of hydrogen release at about 125 °C.[110] However by exchanging the reactants (i.e. KNH_2 + MgH_2) we proved that the interaction is shifted to higher temperatures (ca. 210 °C). Using the thermodynamic data reported in the literature, a standard enthalpy change of ca. -138 kJ mol^{-1} can be calculated for the metathesis reaction (3.16).[168]

$$2\,KNH_2 + MgH_2 \longrightarrow Mg(NH_2)_2 + 2\,KH \tag{3.16}$$

The KNH_2 + MgH_2 composite is metastable at room temperature and hydrogen release should occur as an exothermic event: therefore the higher temperature of hydrogen release in our experiment is due to higher kinetic barriers and it does not depend on the thermodynamic properties of the system. Moreover even though the metathesis reaction is exothermic and therefore favourable, no metathesis was observed: according to our *in situ* diffraction

experiments if KH is not present in the system, the desorption takes place at about 230 °C, even when ball milling is employed for the material synthesis (sample A). The collected results suggest that thermodynamic differences arising from different compositions have only a minor effect on the desorption temperature measured during a kinetic experiment and that the formation of the most stable phases ($Mg(NH_2)_2$ and KH) is kinetically hindered during the desorption process: in our experiment (Fig. 3.11-a) the direct desorption took place. These considerations motivated the study of the KH + $Mg(NH_2)_2$ system, via an *in situ* SR-XPD experiment under the same conditions used for studying the KNH_2 + MgH_2 system. According to the study of Wang et al.[110] when KH and $Mg(NH_2)_2$ are heated at 2 °C min^{-1} under static vacuum conditions they react together as follows (reactions 3.17 and 3.18):

$$3\,Mg(NH_2)_2 + 2\,KH \longrightarrow K_2Mg(NH_2)_4 + 2\,MgNH + 2\,H_2 \tag{3.17}$$

$$K_2Mg(NH_2)_4 + 2\,MgNH + KH \longrightarrow 3\,KMgNH_2NH + H_2 \tag{3.18}$$

However under near-equilibrium conditions (i.e. PCI measurements) direct formation of $KMgNH_2NH$ is suggested, based on the ex situ XRD results, according to reaction 3.19.[110]

$$Mg(NH_2)_2 + KH \rightleftharpoons KMgNH_2NH + H_2 \tag{3.19}$$

Due to these results Wang et al. revealed the presence and competition of two different pathways: if enough time was given to the system to reach the thermodynamic equilibrium (at a certain temperature and pressure), the thermodynamic product $KMgNH_2NH$ was formed - reaction 3.19; otherwise, during kinetic measurements, the kinetic products - less stable but accounting for a lower activation energy - are formed (reaction 3.17). In our experiment $Mg(NH_2)_2$ and KH started to interact at temperatures lower than 100 °C, forming an amide-rich and an amide-poor cubic phase (Fig. 3.14).

Indeed, the trend of KH unit cell parameter is fairly linear in the low temperature region as displayed in Fig. 3.15, but above 100 °C a fast expansion takes place; at the same time a fast contraction occurs for the KNH_2-like structure.

No other crystalline Mg co-products are noticeable, but only an increase of the diffuse scattering, which supports the formation of an amorphous Mg-N-H product during desorption (Fig. 3.14-b, patterns 40 to 50). Indeed, the formation of an amorphous phase was already observed in structural studies of magnesium amide-magnesium imide phases.[164, 169] Above 200 °C, $Mg(NH_2)_2$ and the potassium-containing structures react forming $KMgNH_2NH$ (Fig. 3.14-a).

Moreover, the absence of molten phases possibly formed above 200 °C was confirmed by *ex situ* XPD collected at room temperature after the desorption was completed, proving

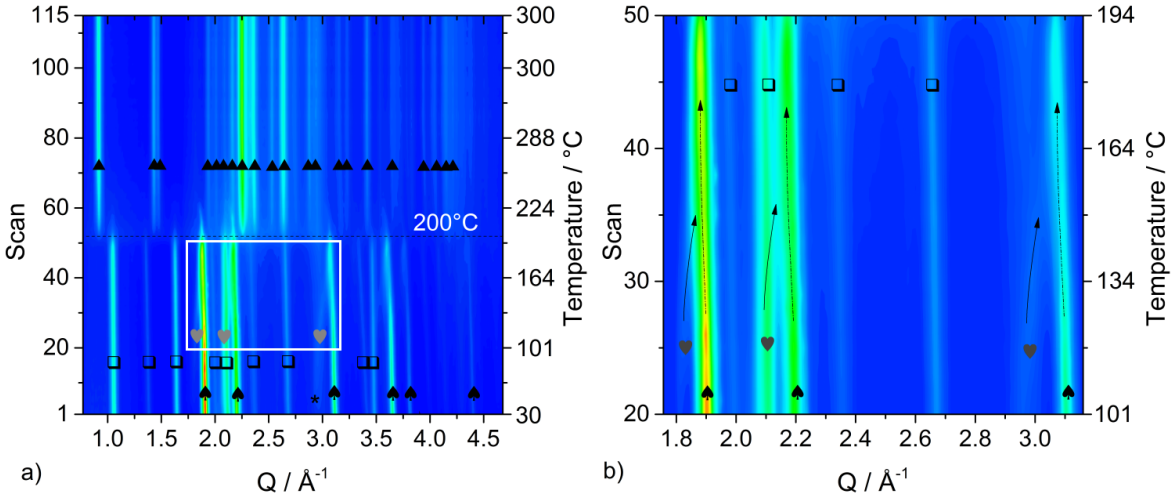

Figure 3.14: *In situ* SR-XPD experiment conducted at the diffraction beamline I711 of MAX-lab ($\lambda = 0.995\,48\,\lambda$) on sample C (a) and details showing the structural modifications taking place above 100 °C (b). ♠ = KH, ❑ = $Mg(NH_2)_2$, ♥ = $K(NH_2)_xH_{1-x}$, ▲ = $KMgNH_2NH$, ⋆ = MgO. Picture readapted from Santoru et al., Phys. Chem. Chem. Phys., 2016, 18, 3910-3920 - Published by the PCCP Owner Societies.[163]

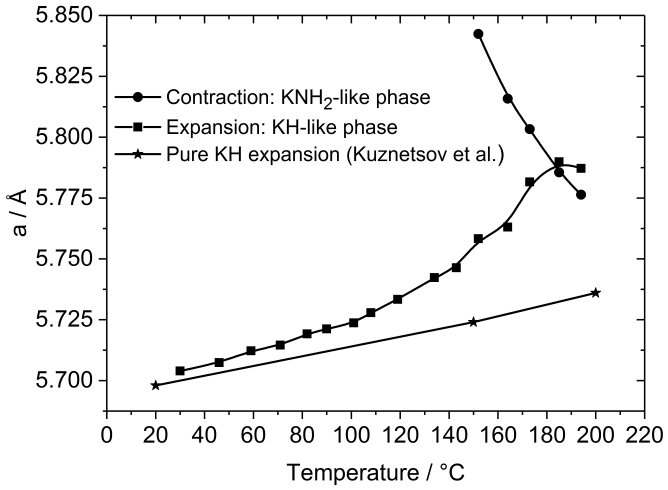

Figure 3.15: Cell parameter "a" of the cubic phases involved in the desorption process, plotted as a function of the temperature. Data from Kuznetsov et al. were reported for comparison.[165] Above 100 °C the expansion diverged from linearity, and another cubic phase is formed. Picture readapted from Santoru et al., Phys. Chem. Chem. Phys., 2016, 18, 3910-3920 - Published by the PCCP Owner Societies.[163]

that $KMgNH_2NH$ is the only final product (Fig. 3.13-c), in agreement with reaction 3.19 and with the *in situ* data (Fig. 3.14-a).

The hydrogen desorption starts at temperatures as low as 100 °C and occurs reaching a single plateau, with a total capacity loss of about 2 wt% (Fig. 3.16-a) and mainly hydrogen is released (Fig. 3.16-b).

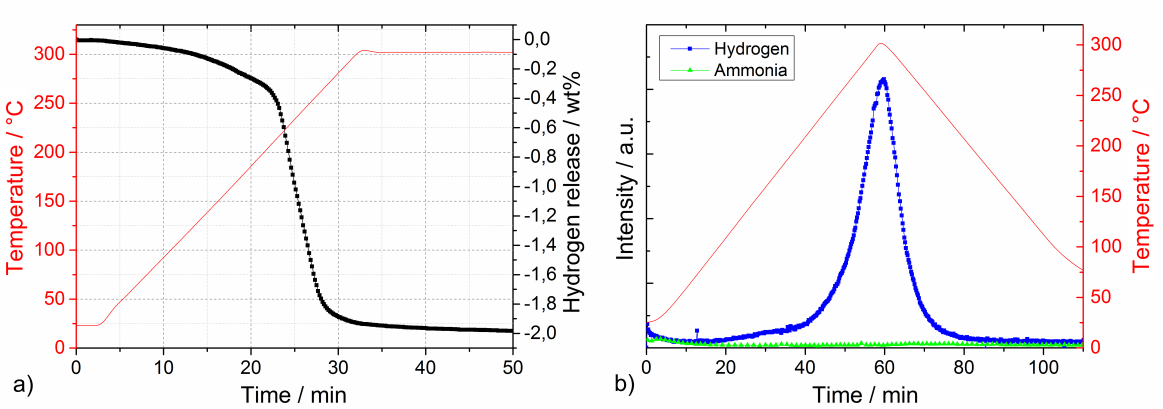

Figure 3.16: Manometric measurement (a) and TD-MS measurement (b) performed on sample C. Picture readapted from Santoru et al., Phys. Chem. Chem. Phys., 2016, 18, 3910-3920 - Published by the PCCP Owner Societies.[163]

3.2.4 K-Mg-N-H system: general discussion and summary

The *in situ* SR-XPD experiments presented in this chapter disprove the formation of $K_2Mg(NH_2)_2NH$, $K_2Mg(NH)_2$ and KMgN as reaction products or intermediates during the desorption of the K-Mg-N-H system.

Moreover, similarly to the compounds observed during the ammonolysis of KH (section 3.1.3), these results suggest the formation of K-N-H containing phases with intermediate compositions. These compositional modifications occur as a continuous process during hydrogen release for both the $KNH_2 + MgH_2$ and $KH + Mg(NH_2)_2$ systems. However for the $KH + Mg(NH_2)_2$ system an alteration of KH cell volume already starts to take place at low temperatures (about 100 °C). Since similar conditions were used for the sample preparation and desorption, it is possible to say that this intermediate is more easily formed from the interaction of KH at the interface with $Mg(NH_2)_2$ rather than at the KNH_2-MgH_2 interface. This is in agreement with the conclusion drawn in another study, which claims that the role of KH in lowering the desorption temperature of the $Mg(NH_2)_2 + 2\,LiH$ system, consists in facilitating the interface reaction by interacting with magnesium amide.[134]

For the $KH + Mg(NH_2)_2$ system, the trend of the cell parameters displayed in Fig. 3.15 clearly shows the lattice of the KH-like structure expanding and that of the KNH_2- like

structure contracting, until they reach similar dimensions. In this case, the amide anions necessary for the formation of the KNH_2-like structure could only come from a reaction between KH and $Mg(NH_2)_2$, by direct exchange or NH_3-mediated mechanism, as shown in Fig. 3.17.

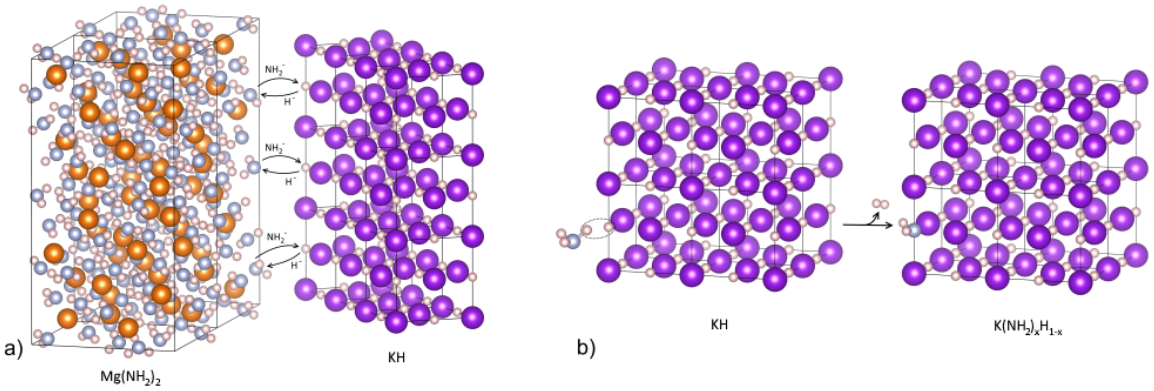

Figure 3.17: Possible reaction mechanisms in agreement with the expansion of the cubic cell of KH: (a) direct exchange of amide-hydride anions at the interface of KH and $Mg(NH_2)_2$; (b) NH_3-mediated mechanism - ammonia released from $Mg(NH_2)_2$ reacts with KH to form one H_2 molecule (the resulting amide anion is retained in the crystal structure). Picture readapted from Santoru et al., Phys. Chem. Chem. Phys., 2016, 18, 3910-3920 - Published by the PCCP Owner Societies.[163]

Interestingly, both mechanisms are compatible with the formation of K-N-H phases with intermediate stoichiometries. In this regard, the hypothesis of a K-N-H solid solution appears reasonable considering the similarities between KH and KNH_2. David et al. and Makepeace et al. have reported a cubic solid solution $Li_{2-x}NH_{1+x}$ as an intermediate of the $LiNH_2/Li_2NH$ structures resulting from the interaction of $LiNH_2$ and LiH.[154, 155] This possibility was considered also for the present case of the K-N-H system, however, due to the different chemistry of the K-N-H system, no stable K_2NH phases are known in literature. Furthermore the position and relative intensities of the Bragg reflections match the ones of KNH_2 and KH phases as the starting and end-products, respectively (Fig. 3.11-b). The changing intensity of the (111) and (200) Bragg reflections also supports the structural modification and substitution of amide anions by entities with lower scattering strength (e.g hydride anions) in the lattice of potassium amide. In summary, by evaluating different chemistry of $LiNH_2$-LiH with respect to the KNH_2-KH case, it is reasonable to propose a mechanism of amide-hydride anions exchange involving the formation of a solid solution. Moreover, an exchange of amide and hydride anions could explain the structural modifications observed during the *in situ* SR-XPD experiments performed for the ammonolysis process of KH (section 3.1.3) and desorption properties of K-Mg-N-H systems. However, in order to confirm this hypothesis, more specific and systematic experiments were needed. With this in mind, the KNH_2-KH system was investigated with complementary techniques. The outcome of this study is presented in the

next chapter.

3.3 KNH_2-KH system

Potassium hydride is known to crystallize in a cubic rock-salt type structure with space group (s.g.) $Fm\bar{3}m$ and no polymorphic changes are expected in the temperature range from RT to 390 °C.[165] For potassium amide, the stable polymorph at RT is monoclinic with the s.g. $P2_1/m$. Upon heating this phase transforms into a tetragonal structure in $P4/nmm$ at 54 °C. The latter phase is stable only in a narrow temperature range: already above 75 °C the stability of the cubic phase ($Fm\bar{3}m$) prevails.[157] An increase of symmetry is therefore reached with the two phase transitions at a higher temperature. The symmetry changes are associated with an increasingly high orientational disorder of the amide anions, as proven by NPD, quasielastic incoherent neutron scattering and orientation-dependent deuterium spin lattice relaxation.[170, 171, 172, 173] If the maximum temperature upon heating is kept below the decomposition temperature of KNH_2 (ca. 340 °C), the two phase transitions and the associated rotational dynamics should be reversible upon cooling.

3.3.1 *Ex situ* XPD

To prove the formation of a K-N-H solid solution, KNH_2-KH mixtures (obtained by hand-grinding with mortar and pestle) in different molar ratios (xKNH_2 + (1-x)KH, with x = $\{0.1, 0.3, 0.5, 0.7, 0.9\}$) were annealed at 270 °C for 1 h under Argon atmosphere.

The diffractograms of the annealed samples are displayed in Fig. 3.18.

The most noticeable aspect is that, in the XPD pattern of the compositions x = $\{0.1, 0.3, 0.5, 0.7\}$, the reflections of monoclinic KNH_2 (s.g. $P2_1/m$, indicated as "♏" in Fig. 3.18) are not present. This result clearly indicates that KNH_2 reacted with KH. However, the presence of a single phase, as expected from the formation of a continuous solid solution, occurs only for x = 0.1 (♣, Fig. 3.18). Indeed, for the compositions x = $\{0.3, 0.5, 0.7\}$, the diffractograms reveal the presence of two coexisting and clearly discernible cubic phases. It is interesting to notice that, considering the relative intensities and peak positions, one phase can be considered a KH-like phase (♠) while the other one a KNH_2-like phase (♥), both with space group $Fm\bar{3}m$.

For the composition x = 0.9 the KH-like phase cannot be identified, rather a coexistence of the monoclinic KNH_2 phase ($P2_1/m$) and the cubic KNH_2-like phase ($Fm\bar{3}m$) can be inferred.

The diverse results obtained over the explored compositional range do not agree with the continuous structural evolution evidenced in the *in situ* SR-XPD measurements presented

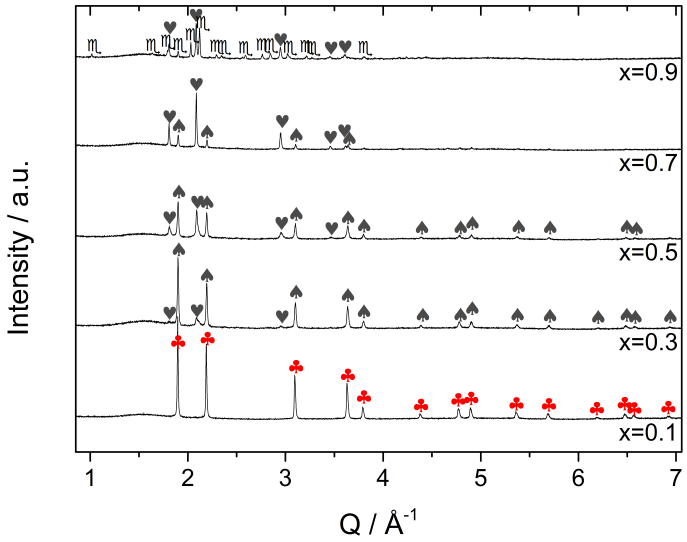

Figure 3.18: Room temperature diffractograms on the $xKNH_2$ + (1-x)KH samples collected after thermal treatment to 270 °C. ♠ = KH-like phase ($Fm\bar{3}m$), ♥ = KNH_2-like phase ($Fm\bar{3}m$), ♣ = $K(NH_2)_xH_{1-x}$ (full solubility, $Fm\bar{3}m$), ♏ = KNH_2 ($P2_1/m$); Panalitical X'Pert Pro, Cu $K\alpha_1$ = 1.5406 Å, $K\alpha_2$ = 1.5444 Å. Readapted from Santoru et al., Chem. Commun., 2016, 52, 11760-11763 - Published by The Royal Society of Chemistry.[150]

in the previous chapter. At this point it was reasonable to suppose that the hand-grinding procedure was not sufficient to promote good contact between the reactants (KH and KNH_2). Ball milling is known to be an effective processing technique to improve the mutual dispersion of the starting components and reduce the particle and grain size, thus shortening the diffusion paths, which are often crucial for the completion of solid state reactions in a short time period. For this reason an attempt was made, to synthesize the solid solution by mechanochemical treatment. The XPD patterns collected after ball milling are displayed in Fig. 3.19.

The diffractograms of the ball milled samples revealed coexistence of the two KH- and KNH_2-like cubic phases, for the compositions $x = \{0.2, 0.4, 0.6, 0.8\}$. Only for $x = 0.8$ the KH like-phase is almost undetectable. The structural changes observed in the previous chapter suggested the possibility of forming a continuous solid solution, while the *ex situ* XPD experiments presented so far can be regarded as evidence for partial solubility only. Indeed, a single phase product could be obtained only for $x = 0.1$. Since the experimental evidence reported in chapter 3.2 consists of *in situ* experiments, it is likely that the temperature can greatly influence the formation of the solid solution. In order to clarify this point and collect more information on the KNH_2-KH system, *in situ* SR-XPD experiments were performed systematically over the whole compositional range. These results and their interpretation are discussed in the next section.

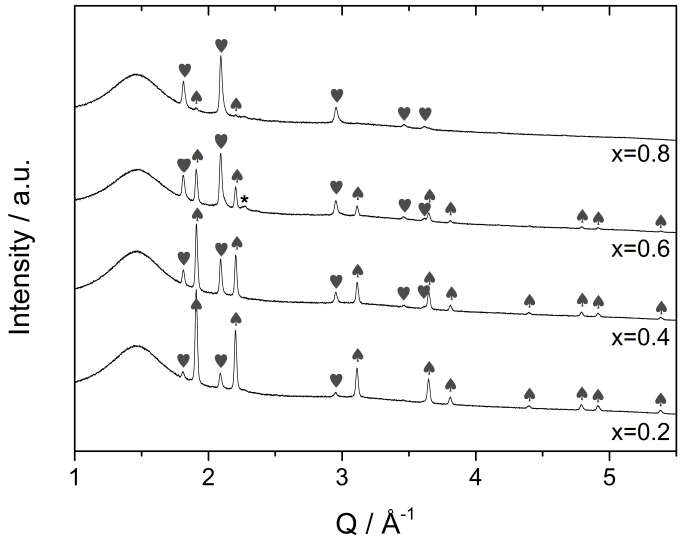

Figure 3.19: Room temperature diffractograms on the xKNH_2 + (1-x)KH samples collected after ball milling. ♠ = KH-like phase ($Fm\bar{3}m$), ♥ = KNH_2-like phase ($Fm\bar{3}m$), ⋆ = KOH. Bruker D8 Discover, $\lambda = 1.541\,84$ Å. Santoru et al., Chem. Commun., 2016, 52, 11760-11763 - Published by The Royal Society of Chemistry.[150]

3.3.2 *In situ* SR-XPD

A contour plot of the *in situ* SR-XPD investigation performed on the 0.5 KNH_2 + 0.5 KH sample is reported in Fig. 3.20.

At RT the peaks of KNH_2 ($P2_1/m$) and KH ($Fm\bar{3}m$) are visible. Increasing the temperature, the phase transformations of KNH_2 to the tetragonal ($P4/nmm$) and cubic ($Fm\bar{3}m$) polymorphs occur as expected in the range of temperatures from 50 °C to 80 °C.

Above 100 °C it can be noticed a continuous shift of the cubic KNH_2 diffraction peaks to higher Q-values; conversely the reflections of KH shift to lower Q-values. The process continues gradually until the two series of reflections merge into one. At 270 °C the transformation is completed and the newly formed cubic phase appears to be stable.

During the cooling process no particular changes are observed, except for the expected shift of the peaks to higher Q-values, which is due to the thermal contraction of the cubic cell. The structural evolution just described suggests that a progressive anionic substitution process takes place upon heating. The fact that at 270 °C a single series of Bragg peaks is present indicates that the formation of a single phase with defined composition can be obtained by increasing the temperature. This finding further explains the discrepancies between *in situ* and *ex situ* experiments underlined before.

In order to have a complete picture of the system, *in situ* SR-XPD analysis of samples with different KNH_2 molar fractions, including the pristine KH (x = 0) and KNH_2 (x = 1), were carried out. The results are summarized in Fig. 3.21.

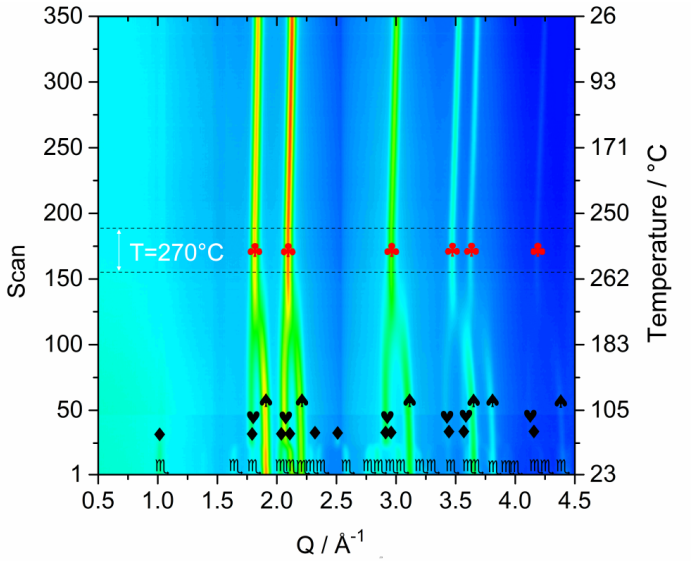

Figure 3.20: *In situ* SR-XPD experiment performed at MAX-lab ($\lambda = 0.995\,48$ Å) on the 0.5 KNH_2 + 0.5 KH sample. ♏ = KNH_2 ($P2_1/m$), ♦ = KNH_2 ($P4/nmm$), ♥ = KNH_2 ($Fm\bar{3}m$), ♠ = KH ($Fm\bar{3}m$), ♣ = $K(NH_2)_xH_{1-x}$ ($Fm\bar{3}m$, full solubility). Readapted from Santoru et al., Chem. Commun., 2016, 52, 11760-11763 - Published by The Royal Society of Chemistry.[150]

It is noteworthy to notice that the pristine materials behave as expected: for KH no phase transformations occur in the investigated temperature range, while for KNH_2 the phase transformations occur as foretold during heating and complete reverse during the cooling process.

For the xKNH_2 + (1-x)KH samples with x = $\{0.1, 0.3, 0.7, 0.9\}$, the phase transformation of KNH_2 takes place as expected, during the first part of the heating process (Fig. 3.21). Moreover, as the temperature further increases, the two sets of Bragg reflections belonging to the cubic KNH_2 and KH phases progressively shift towards each other and merge in a single series of peaks, similarly to what was observed for the sample with x = 0.5 (Fig. 3.21 and 3.20, respectively). It can also be noticed that, similarly to the sample with $x = 0.5$, no polymorphic changes occur during the cooling process of the samples with x = $\{0.1, 0.3, 0.7\}$: the cubic structure is retained until RT. Only for x = 0.9 a phase transformation to the tetragonal geometry can be noticed at the end of the *in situ* experiment (Fig. 3.21).

3.3.3 NPD

In order to confirm the formation of an amide-hydride solid solution, deuterated samples were synthesized and investigated by NPD. The RT NPD pattern acquired on the hand-ground sample 0.5 KND_2 + 0.5 KD confirms the presence of only KND_2 and KD (Fig. 3.22).

The wavy background is due to the quartz sample holder, which was then used for collecting the pattern at 270 °C. The quartz sample holder also contributes with some peaks,

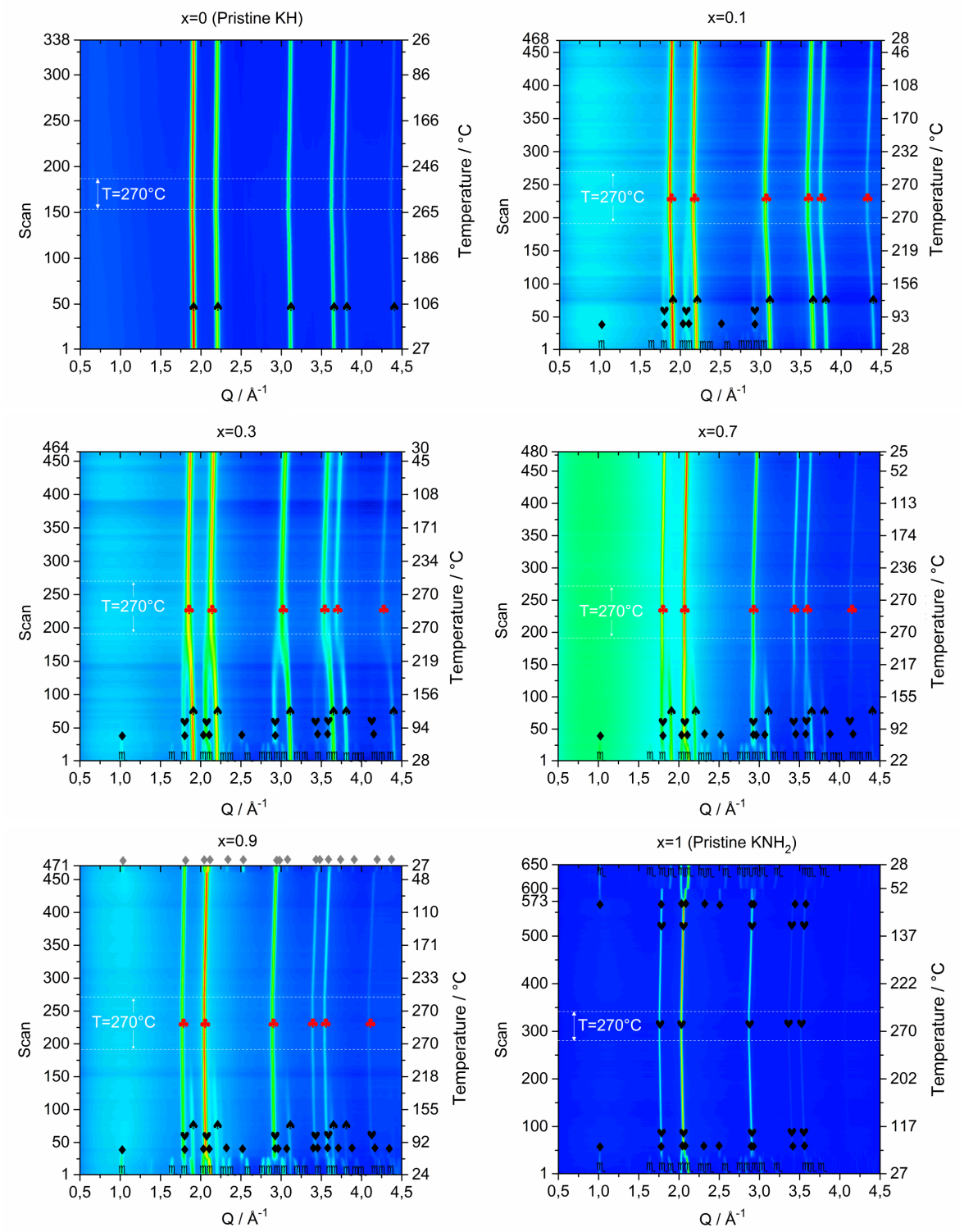

Figure 3.21: *In situ* SR-XPD experiments on the $xKNH_2$ + (1-x)KH system. ♏ = KNH_2 ($P2_1/m$), ♦ = KNH_2 ($P4/nmm$), ♥ = KNH_2 ($Fm\bar{3}m$), ♠ = KH ($Fm\bar{3}m$), ♣ = $K(NH_2)_xH_{1-x}$ ($Fm\bar{3}m$, full solubility), ♦ = $K(NH_2)_xH_{1-x}$ ($P4/nmm$). Measurement of sample x = 0 performed at MAX-lab (λ = 0.9941 Å), all other measurements performed at PETRA III, beamline P02 (λ = 0.2075 Å for x = 1, λ = 0.207 79 Å for x = $\{0.1, 0.3, 0.7, 0.9\}$). Readapted from Santoru et al., Chem. Commun., 2016, 52, 11760-11763 - Published by The Royal Society of Chemistry.[150]

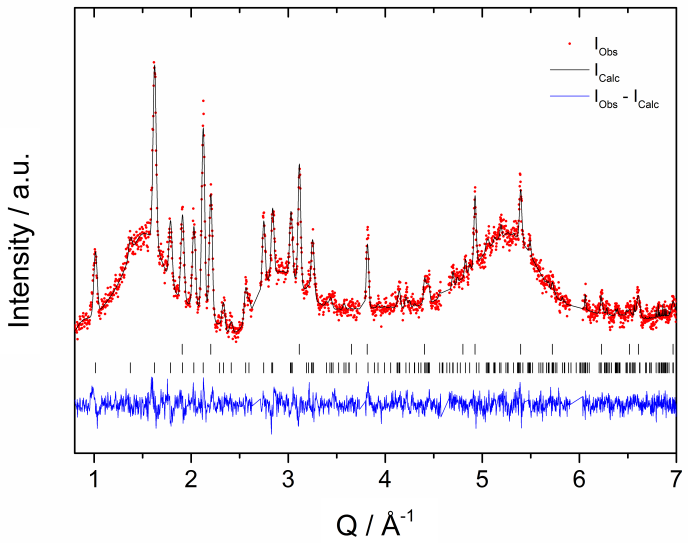

Figure 3.22: RT NPD pattern (IFE, PUS instrument, $\lambda = 1.5539$ Å) of the 0.46 KND_2 + 0.54 KD sample (red dots) and corresponding Rietveld refinement (black line). The upper and lower rows of tick marks indicate the Bragg peaks of KD ($Fm\bar{3}m$) and KND_2 ($P2_1/m$) respectively. Rwp(%) = 5.52 (corrected for background). Santoru et al., Chem. Commun., 2016, 52, 11760-11763 - Published by The Royal Society of Chemistry.[150]

which is necessary to remove prior to the refinement (see the experimental details in section 2.2.5 for further information). The NPD pattern collected under isothermal conditions at 270 °C reveals the presence of a single cubic phase (Fig. 3.23), in agreement with the *in situ* SR-XPD experiment (Fig. 3.20).

A structural model can be obtained from the NPD measurements at 270 °C, assuming deuteramide-deuteride anionic substitution (i.e. the formation of a solid solution). The occupancies of the anions were calculated and fixed in order to have the same anionic composition that was found from the refinement of the RT NPD pattern (Fig. 3.22). The amide anions were treated as rigid bodies. With these assumptions the Rietveld refinement can be performed successfully (Fig. 3.23), confirming the formation of a deuteramide-deuteride solid solution.

The experimental proofs presented so far are all consistent and in agreement with the initial hypothesis of an amide-hydride solid solution. However, due to the novelty of this compound, a spectroscopic technique was additionally employed to confirm the information obtained by powder diffraction methods.

3.3.4 MAS SSNMR

The similarity of the chemical environment between the starting materials and the xKNH_2 + (1-x)KH samples at different compositions (x = $\{0.1, 0.5, 0.9\}$) after annealing was verified

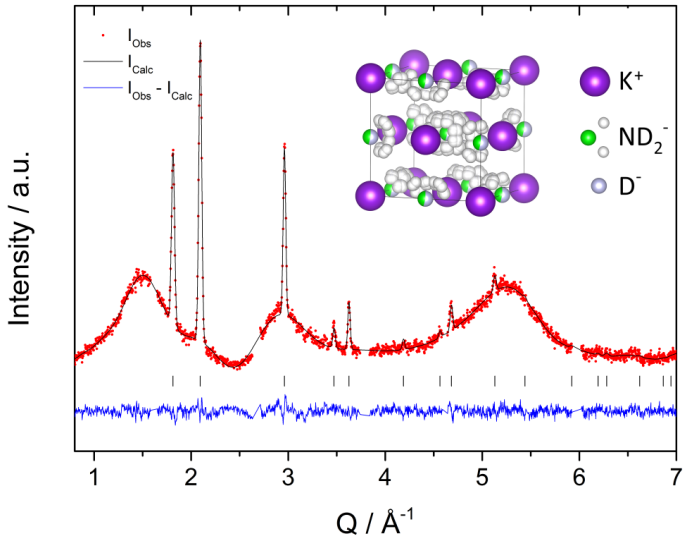

Figure 3.23: NPD pattern (IFE, PUS instrument, $\lambda = 1.5539$ Å) of the $K(ND_2)_{0.46}D_{0.54}$ phase at T = 270 °C (red dots) and corresponding Rietveld refinement (black line) using the structural model displayed in the picture. Rwp(%) = 2.8 (corrected for background). Readapted from Santoru et al., Chem. Commun., 2016, 52, 11760-11763 - Published by The Royal Society of Chemistry.[150]

by ^{1}H MAS SSNMR.

In the ^{1}H MAS SSNMR spectra of pristine KNH_2 and KH, which are taken as reference, the ^{1}H signals have very different chemical shifts (Fig. 3.24). In the spectra of the mixtures, no significant change in the chemical shift of the protons is observed after annealing and the integral values perfectly reflect the total composition. These results confirm that the local chemistry of the amide and hydride groups is preserved after annealing.

Furthermore, the same T_1 ^{1}H value (46 s) for both signals supports the formation of a solid solution since it indicates that spin diffusion is active. This is only possible if they belong to the same phase, or in the case of homogeneous samples on a nanometre scale.[174]

Direct evidence for the formation of a solid solution is provided by the ^{1}H DQ MAS SSNMR experiment (Fig. 3.25). Indeed, the strong DQ correlation between the KNH_2 (−3.2 ppm) and KH (4.8 ppm) signals observed for the annealed sample (Fig. 3.25-b) implies that they are in close spatial proximity to each other (less than 5 Å). This is only possible if they are in close contact, as in a solid solution.[175] A similar correlation, although much weaker, is observed for the sample before annealing (Fig. 3.25-a), which can be explained with the formation of a small fraction of solid solution as the sample temperature slightly increased during the NMR experiment.

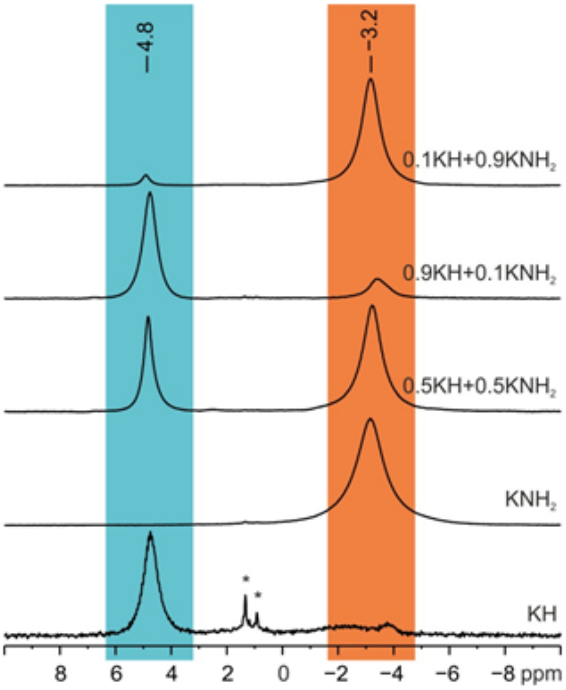

Figure 3.24: ^{1}H (400.23 MHz) MAS SSNMR spectra of the starting reagents (KH and KNH_2) and xKNH_2 + (1-x)KH samples at different compositions (x = $\{0.1, 0.5, 0.9\}$) after annealing recorded with a spinning speed of 32 kHz. Asterisks denote impurities. Santoru et al., Chem. Commun., 2016, 52, 11760-11763 - Published by The Royal Society of Chemistry.[150]

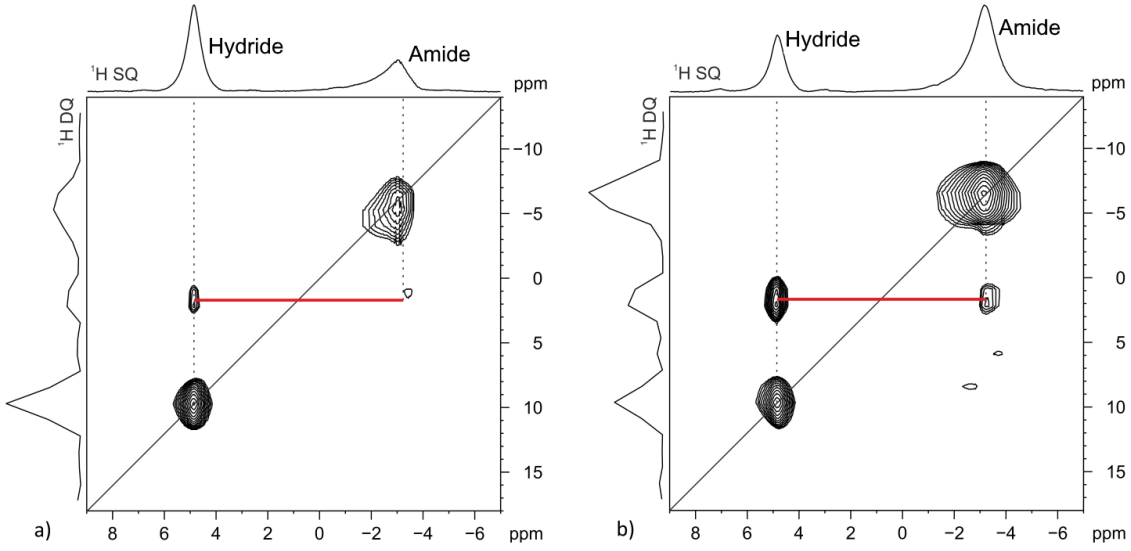

Figure 3.25: 2D ^{1}H (400.23 MHz) DQ MAS SSNMR spectra of the 0.5 KNH_2 + 0.5 KH sample after hand grinding (a) and after annealing (b) recorded with a spinning speed of 32 kHz. The red line highlights the DQ correlation between the KH and KNH_2 signals. Readapted from Santoru et al., Chem. Commun., 2016, 52, 11760-11763 - Published by The Royal Society of Chemistry.[150]

3.3.5 KNH_2-KH system: general discussion and summary

The results of the XPD (*in situ* and *ex situ*), NPD and SSNMR analysis provided complementary proofs, confirming the formation of a potassium amide-hydride solid solution and explaining the unexpected behaviour observed in sections 3.1.3 and 3.2

Between *ex situ* and *in situ* diffraction data, some similarities are observed. Indeed, also the *ex situ* data discussed in section 3.3.1 show absence of tetragonal or monoclinic phases after ball milling or annealing for x $= \{0.1, 0.3, 0.5, 0.7\}$ (Fig. 3.18). The main difference between the two sets of data is that in the *in situ* SR-XPD investigation the formation of a single cubic phase, which appears stable until RT, is visible; conversely, the diffractograms collected *ex situ* at RT show coexistence of two different phases. The diffraction data collected at 270 °C (Fig. 3.26) clearly prove that a single phase is formed, indicating full solubility at this temperature.

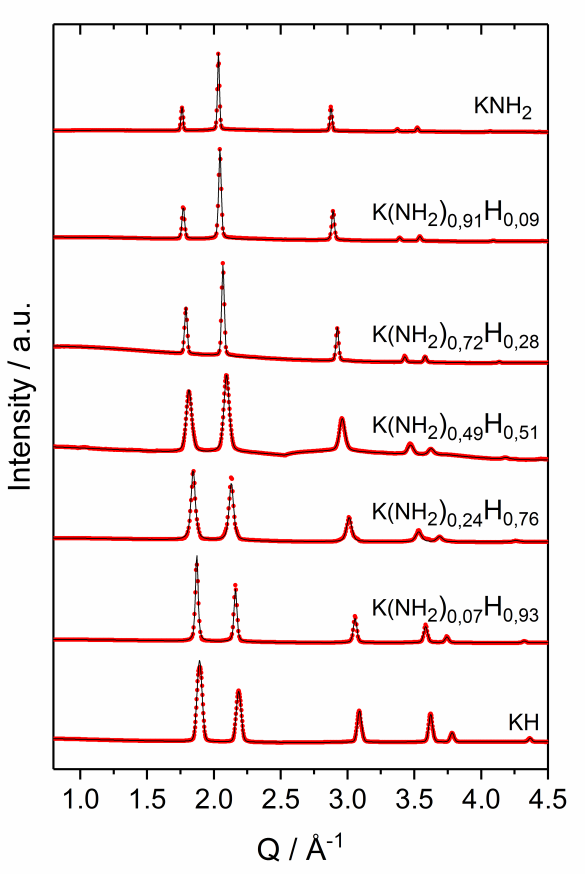

Figure 3.26: Rietveld refinements of the SR-XPD patterns collected at 270 °C for different compositions after hand-grinding (additional information on sample preparation in section 2.1.3). Diffractograms of KH and $K(NH_2)_{0.49}H_{0.51}$ acquired at MAX-lab ($\lambda = 0.9941$ Å and $\lambda = 0.995\,48$ Å, respectively), all other measurements performed at PETRA III ($\lambda = 0.2075$ Å for KNH_2, $\lambda = 0.207\,79$ Å for the others). Readapted from Santoru et al., Chem. Commun., 2016, 52, 11760-11763 - Published by The Royal Society of Chemistry.[150]

The coexistence of two phases, as revealed by *ex situ* XPD data acquired at RT several hours after the thermal treatment, suggests that at RT partial segregation occurs, which is too slow to take place during the cooling process of the *in situ* SR-XPD experiment.

Another interesting aspect can be noticed by the comparison of *in situ* and *ex situ* data for the sample x = 0.9. For this composition, a polymorphic change from cubic to tetragonal is already visible in the cooling process of the *in situ* SR-XPD measurement. However the diffractogram collected *ex situ* exhibits coexistence of monoclinic and cubic phase. In light of what discussed just above, it can be inferred that, for the composition x = 0.9, the tetragonal phase is a metastable phase at RT and it segregates to form monoclinic KNH_2 and cubic $K(NH_2)_xH_{1-x}$, with a process that is too slow compared to the time scale of the *in situ* diffraction experiment.

The general picture that can be drawn by combination of *in situ* and *ex situ* XPD data shows full solubility at RT only for low amounts of KNH_2 (x = 0.1). Increasing the content of KNH_2, the formation of two distinct cubic phases indicates a miscibility gap, probably due to the fact that, at RT, the stable polymorph of KNH_2 is monoclinic. Indeed, increasing the fraction of KNH_2 even further (x = 0.9), also the monoclinic phase is present after thermal treatment (Fig. 3.18), indicating that it is not possible to dissolve such a high content of KNH_2 into the cubic lattice of KH. On the other side, the SR-XPD patterns collected at 270 °C show one single cubic phase for all compositions (Fig. 3.26); a progressive shift to lower Q-values and a gradual change of the relative intensities of the Bragg peaks of this phase is observed in the corresponding diffractograms, indicating that the anionic substitution process takes place as expected and causes expansion of the crystalline lattice.

The complete solubility observed at 270 °C is probably due to the fact that at high temperature (T > 80 °C) the cubic polymorph of KNH_2 is the most stable and its similarity with the crystal structure of KH facilitates the dissolution process.

To the best of our knowledge an amide-hydride solid solution was never reported before in literature. Owing to this interesting feature, potassium amide differs significantly from the amides of the lighter alkali metals. Indeed, differently from lithium and sodium amide, the formation of potassium amide involves an exchange of amide and hydride anions rather than just a direct reaction with ammonia, as evidenced in section 3.1. The same mechanism is also involved in the desorption process of the K-Mg-N-H system (section 3.2), with the difference that the amide anions are provided from the reaction partner, rather than from gaseous ammonia. In this case the formation of $K(NH_2)_xH_{1-x}$ occurs as a continuous process already at low temperatures (100 °C < T < 200 °C). Interestingly, this new mechanism of anionic exchange is compatible with the two reaction mechanisms that are known from the literature (i.e. "direct interaction" and "ammonia-mediated"), as already illustrated in Fig. 3.17. Another interesting aspect is that the formation of non-stoichiometric phases does

not preclude, but rather precedes, the formation of phases with a defined composition (e.g $KMgNH_2NH$) previously reported.

Rb-additives have been investigated only after the effect of K-additives was discovered. For this reason the Rb-Mg-N-H system is still relatively unexplored, compared to the K-Mg-N-H system. Considering that the amides of potassium and rubidium present very similar crystal chemistry, it is interesting, at this point, to determine whether an ordered bimetallic amide-imide phase and a disordered amide-hydride phase can be formed also in the Rb-Mg-N-H and Rb-N-H systems, respectively. These questions are addressed in the next chapter.

3.4 New phases in the Rb-Mg-N-H and Rb-N-H systems

Recently, the total or partial replacement of potassium- with rubidium-based additives was proven to be a successful step to further improve the performance of Li-Mg-N-H systems.[118, 119, 121, 122, 120, 123] Furthermore, it was reported that the enhanced sorption properties of these systems derives from an alteration of the thermodynamic stability and kinetic behaviour, caused by the addition of small amounts of RbF or RbH.[118, 121] Despite the fact that possible reaction pathways were proposed, the key reaction product formed from the additive, $RbMgNH_2NH$, at that time was still unknown from the structural point of view. This section describes the synthesis of this compound and the determination of its crystal structure. Additionally, a new intermediate of the Rb-N-H system, which is likely to be found in future Rb-containing amide/hydride systems, is described. Finally, a general discussion of the structural analogies and differences between the potassium and the rubidium case is also presented.

3.4.1 Synthesis of $RbMgNH_2NH$

It was previously reported that a 1:1 mixture of $Mg(NH_2)_2$ and RbH forms $RbMgNH_2NH$ while releasing an equivalent mole of H_2 when heated to 250 °C. Therefore, the following reaction was proposed:[118]

$$Mg(NH_2)_2 + RbH \longrightarrow RbMgNH_2NH + H_2 \tag{3.20}$$

In fact, the XPD analysis of the product obtained in the present work, after annealing a 1:1 mixture of $Mg(NH_2)_2$ and RbH (reported in Fig. 3.27-a) shows that it is not possible to identify the Bragg reflections of the starting materials. Except from some $Rb_2Mg(NH_2)_4$, the other peaks are not attributable to any known Rb-containing amide, imide or nitride phases. In order to synthesize $RbMgNH_2NH$, an alternative and possibly more convenient synthesis

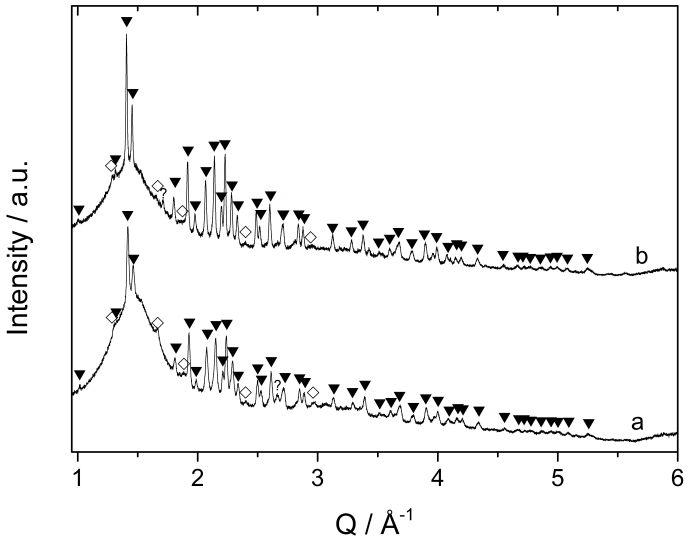

Figure 3.27: Room temperature XPD pattern of the product obtained after annealing of $Mg(NH_2)_2$ + RbH (a) and $Rb_2Mg(NH_2)_4$ + MgH_2 (b), collected with the Bruker D8 Discover (λ = 1.541 84 Å). ▼ = New phase, ◇ = $Rb_2Mg(NH_2)_4$, ? = spurious peaks. Reprinted with permission from Santoru et al., Inorg. Chem. 57, 6, 3197-3205. Copyright 2018 American Chemical Society.[176]

route was considered (reaction 3.21).

$$Rb_2Mg(NH_2)_4 + MgH_2 \longrightarrow 2\,RbMgNH_2NH + 2\,H_2 \tag{3.21}$$

According to the diffractogram in Fig. 3.27-b, the main reaction product is the same.

The deuterated compound $RbMgND_2ND$ was also synthesized, using the second synthesis route, i.e. starting from $Rb_2Mg(ND_2)_4$ and MgD_2. The reaction products were characterized by ATR-IR (Fig. 3.28). For the $RbMgNH_2NH$ phase, the stretching signals of the N-H bonds are found at 3319 cm^{-1} and 3261 cm^{-1}, similarly to the values of 3317 cm^{-1} and 3260 cm^{-1} reported from Li C. et al, thus confirming the reproducibility of the synthesis.[118] As predictable, the isotopic effect causes a red-shift of about 840 cm^{-1} for the stretching signals of the N-D bonds in the deuterated compounds.

3.4.2 Structure solution

As anticipated, the formation of $RbMgNH_2NH$ was reported to be an important step for the reduced reaction enthalpy of Rb-doped Li-Mg-N-H systems.[118] Considering that increasing attention has been devoted to the study of similar systems, it is important to determine the structural features of this phase, which in turn will provide a starting point for the development of plausible reaction mechanisms. This could help in the identification of the $RbMgNH_2NH$ as component of other hydrogen storage systems that will be developed in the future. In

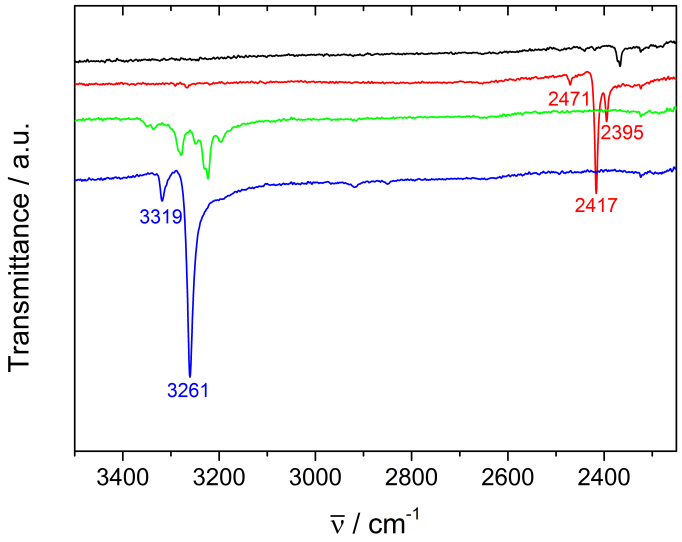

Figure 3.28: ATR-IR spectra of the samples (from the top) $Rb_2Mg(ND_2)_4$ + MgD_2 after grinding (black), after annealing (red), $Rb_2Mg(NH_2)_4$ + MgH_2 after grinding (green) and after annealing (blue). Reprinted with permission from Santoru et al., Inorg. Chem. 57, 6, 3197-3205. Copyright 2018 American Chemical Society.[176]

order to attempt a structural characterization of the obtained product, a synchrotron XPD pattern was collected at the SNBL at ESRF. The high crystallinity of the sample coupled with the high quality of the measurement, allowed the identification of the reflections belonging to the main phase, which were indexed in the orthorhombic crystal system with unit cell parameters: $a = 9.6282$, $b = 3.7120$ and $c = 10.1164$ Å. From the systematic absences the possible space group candidates were restricted to *Pnma* and $Pna2_1$. The structure was solved using FOX with the global optimization algorithm, excluding hydrogen atoms. For NPD data collected with the deuterated sample, the same procedure was used, but including free deuterium atoms (see section 2.2.5 for more details). For both space groups the global optimization provided very similar structural models, with the formula unit $RbMgN_2D_3$, in agreement with the stoichiometry predicted by Li et al.[118] Owing to the extremely similar structures of the two space group candidates, which differ only by the presence or absence of the inversion center, the differences in the Rietveld refinements are not significant, indicating that the higher symmetry (*Pnma*) is the best choice. Finally, a combined Rietveld refinement of both XPD and NPD patterns was performed for the *Pnma* space group. The corresponding graphs are presented in Fig. 3.29 and Fig. 3.30, respectively. Moreover, the final structural model obtained after combined refinement is presented in Fig. 3.31.

A total of 4 formula units are contained in the unit cell of $RbMgNH_2NH$, which gives a density of 2.67 g/cm^3, similar to that of α-$RbNH_2$ (2.59 g/cm^3) and comparable to that of $Rb_2Mg(NH_2)_4$ (2.31 g/cm^3). Furthermore, $RbMgND_2ND$ is isostructural to $KMgND_2ND$. A

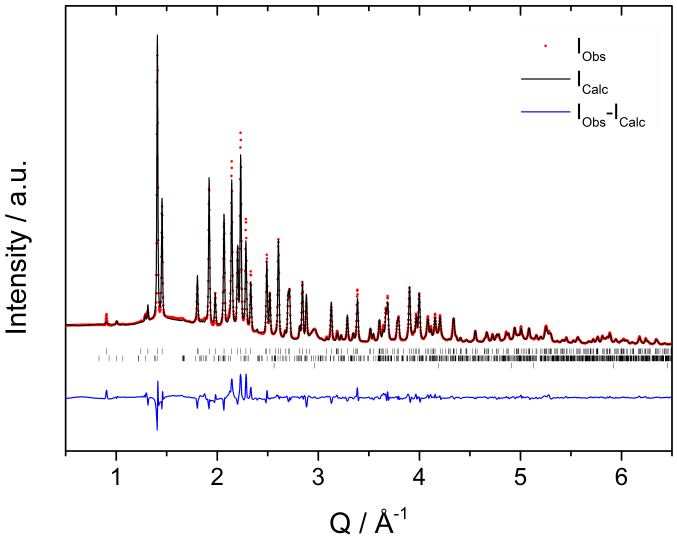

Figure 3.29: Rietveld refinement of the RT synchrotron XPD data collected at SNBL (ESRF, λ = 0.8212 Å) on the product obtained after annealing the $Rb_2Mg(ND_2)_4$ + MgD_2 sample. The figure shows the observed intensities (red dots), the calculated curve (black line) and the difference plot (observed – calculated intensities, blue line). The vertical marks shown correspond, from top to bottom, to the structural models of $RbMgNH_2NH$, $Rb_2Mg(NH_2)_4$ and MgO. Rwp(%) = 6.89 (corrected for background). Adapted with permission from Santoru et al., Inorg. Chem. 57, 6, 3197-3205. Copyright 2018 American Chemical Society.[176]

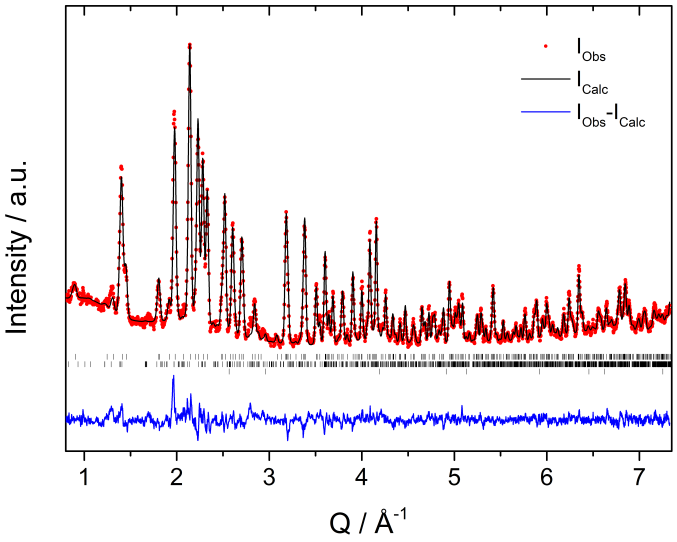

Figure 3.30: Rietveld refinement of the NPD pattern acquired at RT on the annealed $Rb_2Mg(ND_2)_4$ + MgD_2 product (IFE, PUS instrument, λ = 1.553 57 Å). The figure shows the observed intensities (red dots), the calculated curve (black line) and the difference plot (observed – calculated intensities, blue line). The Bragg reflections of the $RbMgND_2ND$ structure, $Rb_2Mg(NH_2)_4$ and MgO are shown as vertical marks, from top to bottom, respectively. Rwp(%) = 5.56 (corrected for background). Adapted with permission from Santoru et al., Inorg. Chem. 57, 6, 3197-3205. Copyright 2018 American Chemical Society.[176]

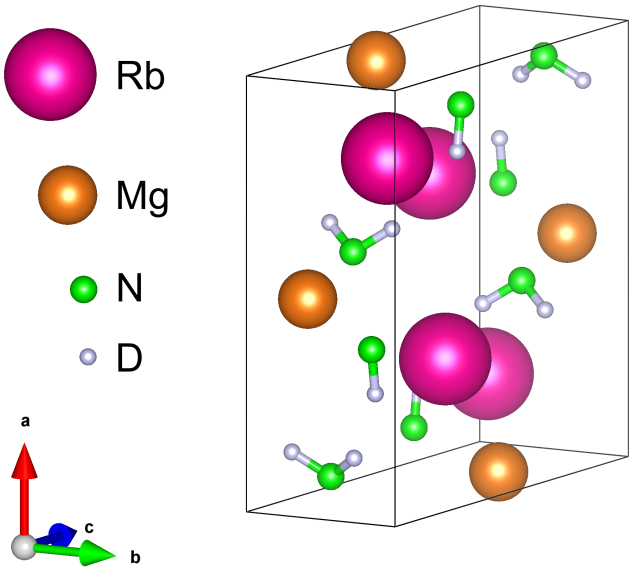

Figure 3.31: Structural model of $RbMgND_2ND$ as obtained after combined Rietveld refinement of NPD and XPD data. Reprinted with permission from Santoru et al., Inorg. Chem. 57, 6, 3197-3205. Copyright 2018 American Chemical Society.[176]

comparison of the unit cell parameters of the two compounds is presented in Tab. 3.1 and the crystal structure parameters of $RbMgND_2ND$ are summarized in Tab. 3.2.

Table 3.1: Unit cell parameters and unit cell volume of the $RbMgND_2ND$ phase as obtained after combined Rietveld refinement of the NPD and XPD data. The values for $KMgND_2ND$ were taken from the work of Napolitano et al.[111] and are shown for comparison.

Compound	a/Å	b/Å	c/Å	V/Å^3
$KMgND_2ND$	9.3497(3)	3.6631(1)	9.8901(3)	338.72(2)
$RbMgND_2ND$	9.55256(31)	3.70772(11)	10.08308(32)	357.125(24)

The unit cell volume is noticeably bigger in the case of $RbMgND_2ND$, which is reasonable considering the bigger ionic radius of rubidium compared to potassium. From Tab. 3.3 it can be noticed that all but one of the M^+-N distances are longer for the $RbMgND_2ND$ phase as compared to $KMgND_2ND$. Therefore, a bi-capped trigonal prism of amide and imide anions coordinating Rb^+, can be identified in this case (Fig. 3.32-a) as compared to the mono-capped trigonal prism reported for the $KMgND_2ND$. A possible explanation for this difference is that, due to the longer radius, i.e. bigger coordination sphere (see average M^+-N distance in Tab. 3.3), an additional amide group coordinates the Rb^+ in $RbMgND_2ND$. Conversely, the additional amide group is excluded from the first coordination sphere of K^+, because the shorter ionic radius is associated with a smaller coordination sphere and,

Table 3.2: Structural parameters of $RbMgND_2ND$, obtained by combined Rietveld refinement of the XPD and NPD data.

Atom type	Label	Wyckoff site	x	y	z	$B_{iso}/Å^2$
Rb	Rb1	4*c*	0.18408(19)	1/4	0.87445(19)	2.45(6)
Mg	Mg1	4*c*	0.47980(31)	1/4	0.10325(31)	0.63(6)
N	N1	4*c*	0.11203(28)	1/4	0.55890(25)	0.88(5)
D	D1	4*c*	0.2157(5)	1/4	0.5745(4)	2.98(9)
N	N2	4*c*	0.05703(29)	1/4	0.20248(27)	1.84(6)
D	D2	8*d*	0.1116(4)	0.0412(9)	0.16907(31)	5.00(10)

therefore, shorter interatomic distances (stronger repulsions) between the amide and imide groups. Indeed, an average N-N distance of 4.7763(6) Å and 4.8781(7) Å can be calculated for the K- and Rb-phases, respectively. The nitrogen atoms considered for the calculation of the average N-N distance are displayed in Fig. 3.32-a.

Table 3.3: Selected M^+-N distances ($d < 3.92$ Å) obtained from the structural models of $RbMgND_2ND$ (Santoru et al.[176]) and $KMgND_2ND$ (Napolitano et al.[111]).

Label	d_1, d_2	d_3, d_4	d_5	d_6, d_7	d_8	Average
Multiplicity	2	2	1	2	1	-
$d_{K-N}/Å$	3.071(6)	3.378(6)	3.097(7)	2.937(6)	3.910(7)	3.222(2)
$d_{Rb-N}/Å$	3.269(3)	3.544(3)	3.255(4)	3.057(3)	3.523(4)	3.3148(12)

The surrounding of the amide anion can be described considering the octahedral geometry proposed in Fig. 3.32-b. It is also possible to identify a triangular antiprism Rb_3Mg_3 around the imide anion (Fig. 3.32-c). This coordination entity is very similar in both the $KMgND_2ND$ and $RbMgND_2ND$ phases. Another interesting structural aspect that the two compounds have in common is the tetrahedral coordination of Mg^{2+} to one ND_2^- and three ND^{2-} anions (Fig. 3.32-d). In fact, rather than displaying $[Mg(ND_2)(ND)_3]^{5-}$ isolated tetrahedrons, each imide anion coordinates to other three magnesium cations, building an infinite anionic chain in the [010] direction, counterbalanced by Rb^+ (Fig. 3.33). Similar features can be found in the structure of some double-cation tetrahydroborates.[177]

In this case, the amide anions completing the tetrahedral units are in terminal (i.e. "non-bridging") positions because of an insufficient number of free electron pairs (Fig. 3.33). The deuterium atoms of the imide groups are equidistant (2.190(6) Å) from the closer deuterium

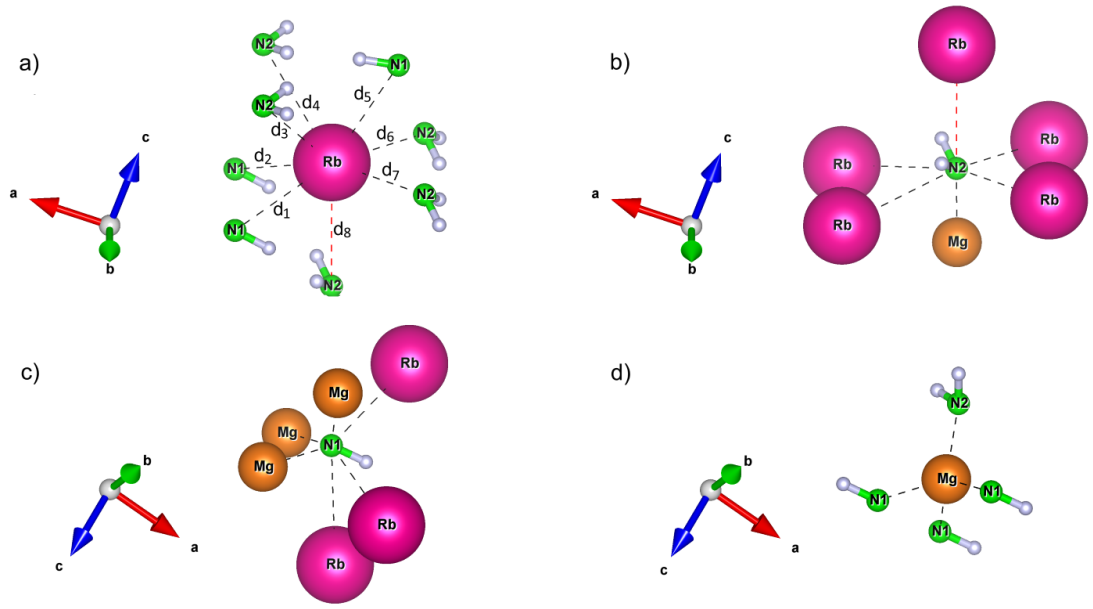

Figure 3.32: Structural coordination of (a) Rb^{+} (bi-capped trigonal prism), (b) $ND_2{}^{-}$ (octahedron), (c) ND^{2-} (trigonal prism) and (d) Mg^{2+} (tetrahedron). All the geometries present considerable distortion as compared to the ideal case. The Rb-N distance of 3.523(4) Å is indicated by a dotted red line in (a) and (b). Reprinted with permission from Santoru et al., Inorg. Chem. 57, 6, 3197-3205. Copyright 2018 American Chemical Society.[176]

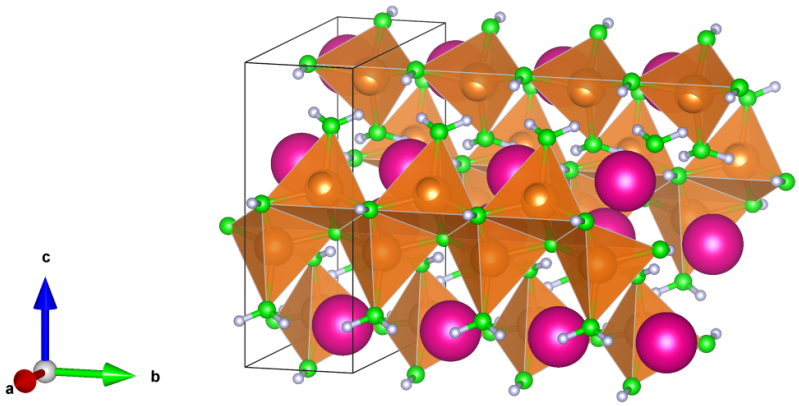

Figure 3.33: Infinite anionic chain of edge-sharing $[Mg(ND_2)(ND)_3]$ tetrahedrons develops in the [010] direction. Reprinted with permission from Santoru et al., Inorg. Chem. 57, 6, 3197-3205. Copyright 2018 American Chemical Society.[176]

atoms of each amide group in the adjacent chain and both amide and imide groups are oriented in order to minimize repulsions with the Rb^+ and Mg^{2+} cations.

3.4.3 Rb-N-H system

Structural similarities between compounds of potassium and rubidium are not a peculiarity of bimetallic M-Mg-N-H systems, as they also occur in other classes of compounds, e.g. metal amides (MNH_2) and metal hydrides (MH). The new intermediates identified in the K-N-H system (section 3.3) are the first example of a metal amide/hydride solid solution. Here a a systematic study of the $RbNH_2$-RbH system is presented, in order to reveal the main similarities and differences with the KNH_2-KH case study.

Mixtures of $RbNH_2$ and RbH were prepared in different molar ratios ($x = \{0, 0.1, 0.3, 0.5, 0.7, 0.9, 1\}$; with x indicating the molar fraction of $RbNH_2$), annealed and then characterized by *ex situ* XPD (Fig. 3.34).

From the diffraction patterns collected after annealing, it is not possible to identify the Bragg reflections of the RT modification of $RbNH_2$ (monoclinic, s.g. $P2_1/m$) for the intermediate compositions 0.1, 0.3, 0.5 and 0.7. The diffractograms of these annealed samples are similar to the pattern of RbH ($x = 0$), except for a significant shift of the peak positions to lower Q-values and altered relative intensities. For $x = 0.9$ the peaks of both monoclinic and cubic phases can be identified.

In order to reveal how the starting components interacted during the annealing process, an *in situ* SR-XPD experiment was performed on a 1:1 molar mixture of $RbNH_2$ and RbH (Fig. 3.35).

In the diffraction pattern acquired at RT, the peaks of the monoclinic $RbNH_2$ are clearly visible (Fig. 3.35). Furthermore, the reflections of two cubic phases are also noticeable. The positions and relative intensities of the peaks of the two cubic phases, are similar to the values expected for RbH and the cubic polymorph of $RbNH_2$. When increasing the temperature, the phase transformation from the monoclinic polymorph of $RbNH_2$ to the cubic one occurs at ca. 65 °C. After the phase transformation, the peaks of these three cubic phases undergo a gradual shift and broadening, until they converge to a single set of sharp reflections. The shift of the diffraction peaks in Fig. 3.35 suggests that, owing to mutual solubility, a continuous change of the amide/hydride content takes place in each phase until a single phase-composition is achieved at 270 °C. Indeed, all three intermediate cubic phases, as well as the final single phase product, can be successfully fitted taking into account NH_2^-/H^- substitution and cell expansion in the structural model of RbH (Fig. 3.36). The final cubic phase formed at 270 °C is retained during the entire cooling process to RT (Fig. 3.35).

The *in situ* SR-XPD experiments were performed for all the examined compositions (Fig.

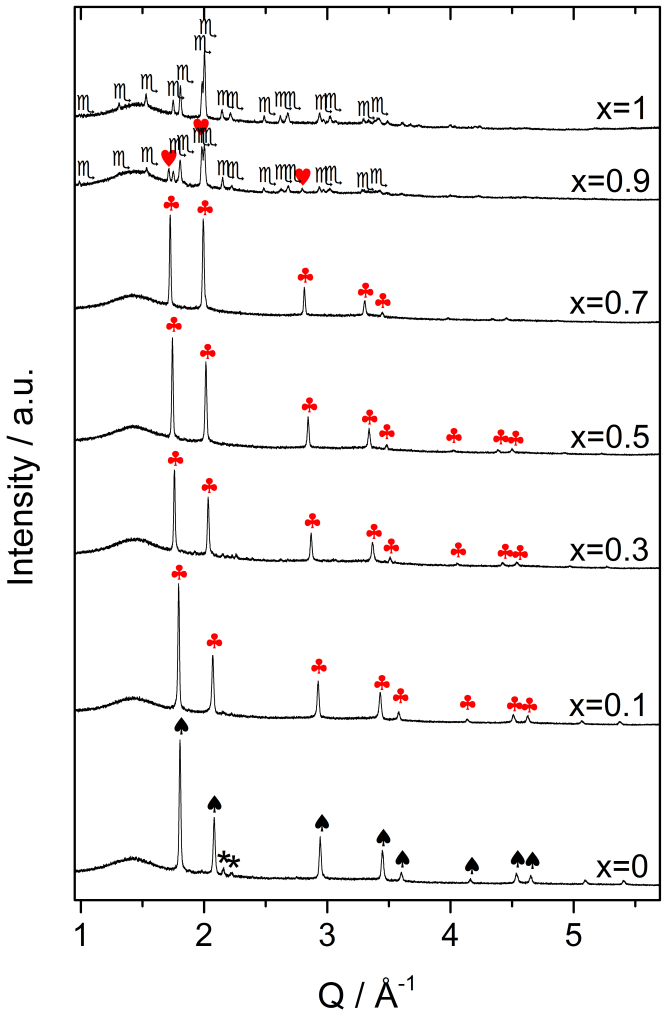

Figure 3.34: RT diffractograms of the annealed $xRbNH_2$ + (1-x)RbH samples acquired with the Bruker D8 Discover, $\lambda = 1.541\,84$ Å. ♠ = RbH ($Fm\bar{3}m$), ♣ = $Rb(NH_2)_xH_{(1-x)}$ ($Fm\bar{3}m$, full solubility), ♥ = $RbNH_2$-like phase ($Fm\bar{3}m$), ♏ = $RbNH_2$ ($P2_1/m$), ♏ = RbOH ($P2_1/m$). Reprinted with permission from Santoru et al., Inorg. Chem. 57, 6, 3197-3205. Copyright 2018 American Chemical Society.[176]

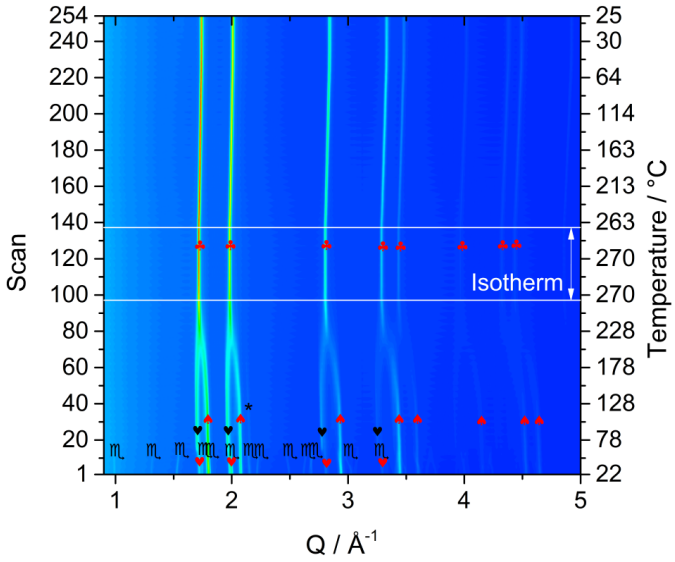

Figure 3.35: *In situ* XPD patterns acquired at PETRA III (P07, $\lambda = 0.142\,35$ Å) for the sample $0.5\,RbNH_2 + 0.5\,RbH$. ♠ = RbH-like phase ($Fm\bar{3}m$), ♥ = $RbNH_2$-like phase ($Fm\bar{3}m$), ♏ = $RbNH_2$ ($P2_1/m$), ♥ = $RbNH_2$ ($Fm\bar{3}m$), ♏ = RbOH ($P2_1/m$), ♣ = $Rb(NH_2)_xH_{(1-x)}$ ($Fm\bar{3}m$, full solubility). Adapted with permission from Santoru et al., Inorg. Chem. 57, 6, 3197-3205. Copyright 2018 American Chemical Society.[176]

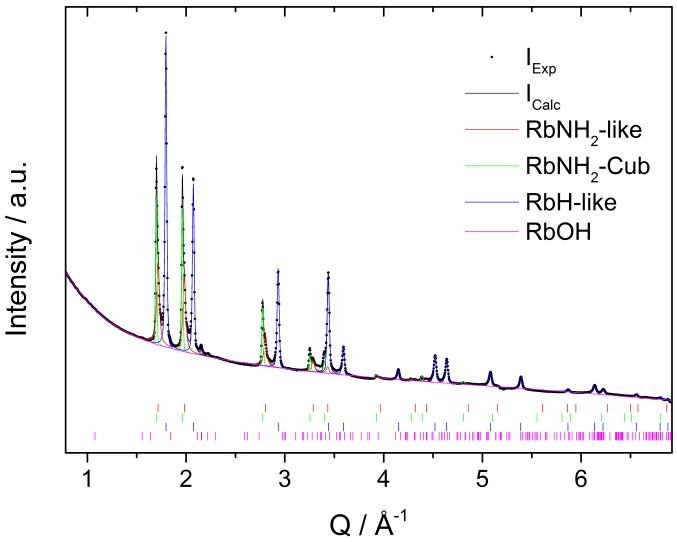

Figure 3.36: Rietveld refinement of the SR-XPD pattern of the sample $0.5\,RbNH_2 + 0.5\,RbH$ collected *in situ* (Scan 19, T = 75 °C) at the beamline P07 of PETRA III ($\lambda = 0.142\,35$ Å). Rwp(%) = 3.60 (corrected for background). Adapted with permission from Santoru et al., Inorg. Chem. 57, 6, 3197-3205. Copyright 2018 American Chemical Society.[176]

3.37). In every case the formation of a single phase composition is achieved at 270 °C.

For the composition x = 0.9, the formation of a single cubic phase is achieved at 270 °C, but after the cooling process some new peaks appeared at RT. Unfortunately, it is not possible to fit the peaks with the monoclinic model of $RbNH_2$ or to attempt a structure solution, due to the low intensity and small number of Bragg reflections available. Nonetheless, it can be noticed that the appearance of the new peaks is associated with a decrease in the intensity of the pre-existing peaks of the cubic phase. The changes in the XPD patterns suggest that a slow partial segregation process started to take place, involving an intermediate structure. This structure, after some time, may be transformed into the monoclinic phase of $RbNH_2$, as visible in the *ex situ* experiments at RT (Fig. 3.34). Therefore, at RT, full solubility into the cubic phase seems to be achievable, except when the content of amide phase (monoclinic at RT) is too high ($x \geqslant 0.9$).

Comparing the diffraction patterns acquired at 270 °C for all the different compositions (Fig. 3.38) it is possible to notice a progressive shift of the Bragg peaks to lower Q-values and a change of their relative intensities, as the amount of $RbNH_2$ phase increases. These results are very similar to the ones previously reported for the K-N-H system (section 3.3.2). Therefore, it is possible to conclude that, in both K-N-H and Rb-N-H systems, the amide/hydride substitution causes an expansion of the crystal lattice over the entire compositional range.

As a further confirmation, a SSNMR investigation on the composition x = 0.5 hand-ground and annealed samples was carried out to independently assess the formation of solid solutions rather than heterogeneous mixtures. In the ^1H MAS spectra (Fig. 3.39), no significant shifts are observed on passing from the starting materials to the annealed and ground samples (Tab. 3.4). The broadening of the hydride signals in the grinded sample

Table 3.4: ^1H chemical shifts (ppm) with assignments and T_1 ^1H (s) values for the samples RbH, $RbNH_2$, 0.5 $RbNH_2$ + 0.5 RbH annealed and 0.5 $RbNH_2$ + 0.5 RbH ground.

	Hydride peak		Amide peak	
Sample	δ/ppm	T_1 ^1H/s	δ/ppm	T_1 ^1H/s
RbH	6.1	7.8	-	-
$RbNH_2$	-	-	−3.2	30.6
$x = 0.5$ (ground)	6.6	7.4	−3.2	26.4
$x = 0.5$ (annealed)	6.5	4.9	−3.3	4.4

(FWHM ca. 790 Hz) prevents any reliable signal integration which results underestimated. This line width is similar to that of pure RbH indicating a similar chemical environment, while in the annealed sample is smaller (FWHM is ca. 350 Hz). The broadening of the hydride signal can be caused by residual dipolar coupling to the quadrupolar nucleus (Rb-85 and Rb-87

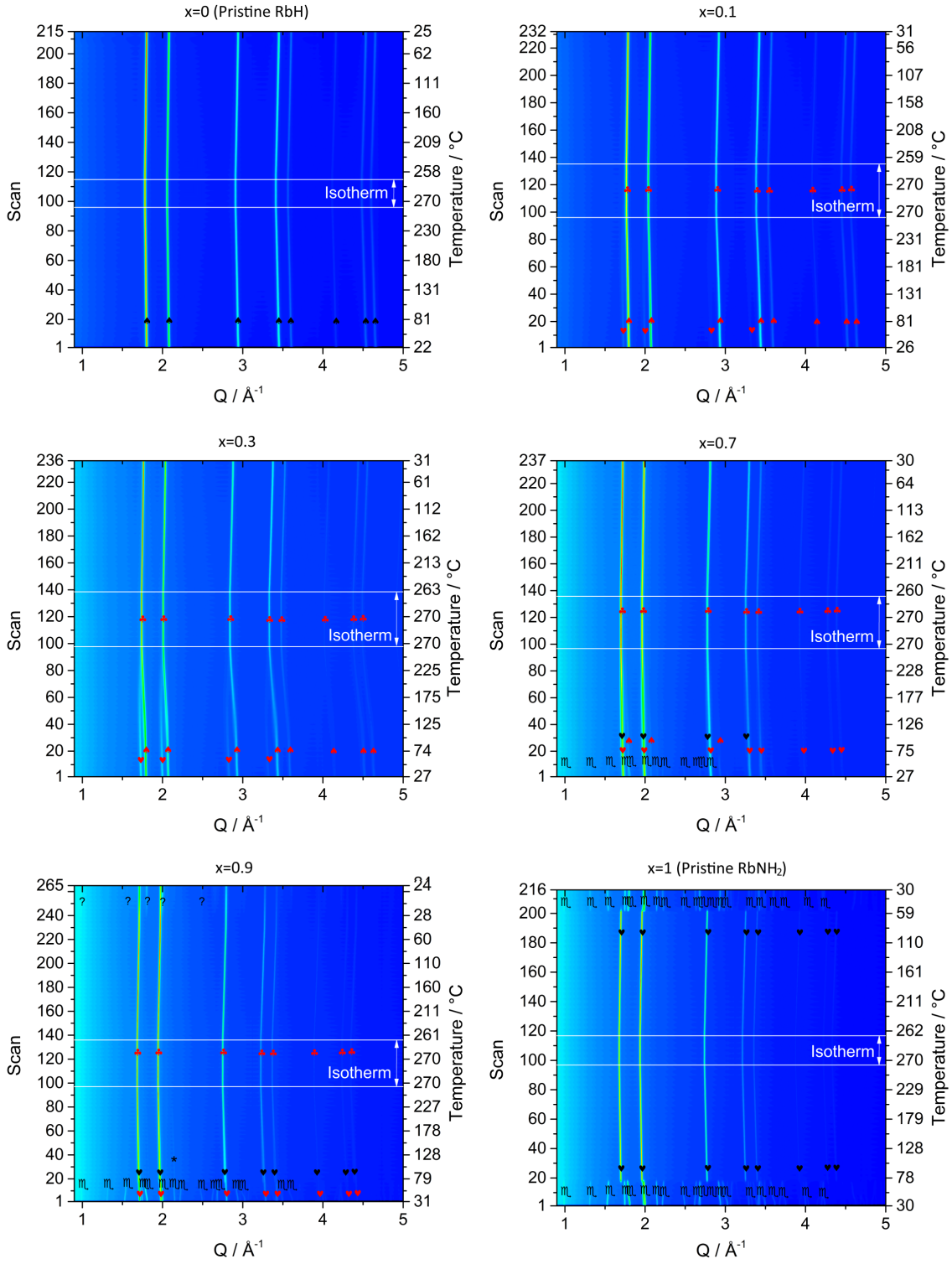

Figure 3.37: *In situ* SR-XPD experiments on the x$RbNH_2$ + (1-x)RbH system, performed at PETRA III (Beamline P07, $\lambda = 0.142\,35$ Å). ♏ = $RbNH_2$ ($P2_1/m$), ♥ = $RbNH_2$ ($Fm\bar{3}m$), ♥ = $RbNH_2$-like phase ($Fm\bar{3}m$) ♠ = RbH ($Fm\bar{3}m$), ♠ = RbH-like phase ($Fm\bar{3}m$), ♣ = $Rb(NH_2)_xH_{1-x}$ (full solubility). Adapted with permission from Santoru et al., Inorg. Chem. 57, 6, 3197-3205. Copyright 2018 American Chemical Society.[176]

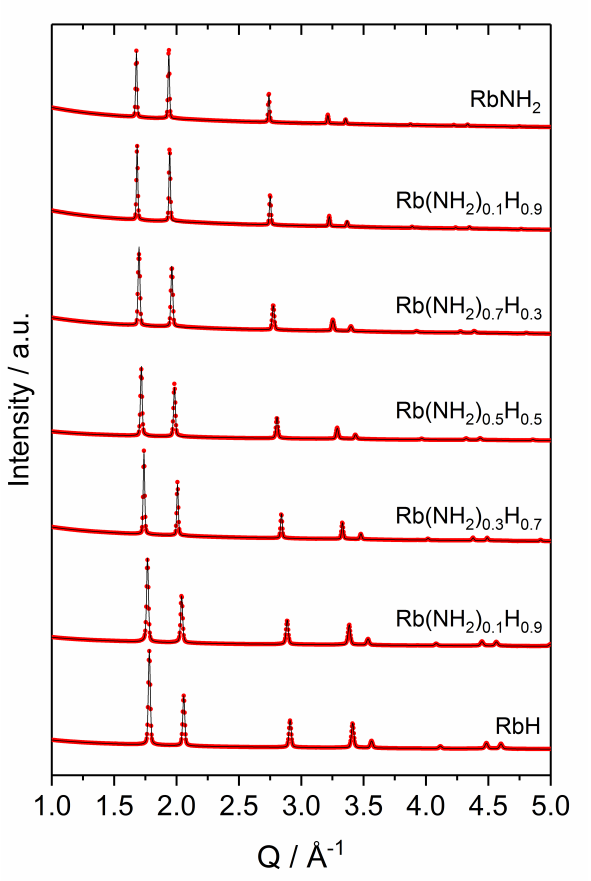

Figure 3.38: Rietveld refinements of the SR-XPD patterns collected at 270 °C for different compositions. Data from PETRA III, beamline P07, $\lambda = 0.142\,35$ Å.

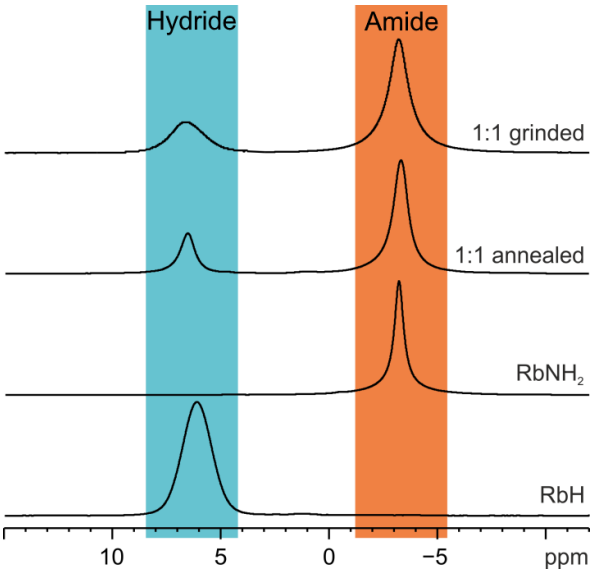

Figure 3.39: ^{1}H (400.23 MHz) MAS SSNMR spectra of of starting reagents (RbH and $RbNH_2$), 0.5 $RbNH_2$ + 0.5 RbH annealed and 0.5 $RbNH_2$ + 0.5 RbH ground recorded with a spinning speed of 32 kHz. Reprinted with permission from Santoru et al., Inorg. Chem. 57, 6, 3197-3205. Copyright 2018 American Chemical Society.[176]

spin 5/2 and 3/2, respectively) and static or dynamic disorder. T_1 ^{1}H relaxation measurements (Tab. 3.4) on the annealed sample show almost the same value for the hydride and amide resonances (4.9 and 4.4 s, respectively) compared to those of the starting compounds (7.8 and 30.6 s, respectively). This is only possible when a spin diffusion process is active, i.e. if the protons belong to the same phase, or in the case of homogeneous samples on a nanometre scale.[174]

Direct evidence of the solid solution formation is provided by the ^{1}H DQ MAS SSNMR experiment (Fig. 3.40-b). Certainly, the observed DQ correlation ($\delta_{DQ} = 3.2$ ppm) between the hydride (6.5 ppm) and amide (−3.3 ppm) signals implies that the two anions are in close spatial proximity to each other (less than 5 Å). This is possible only if they are intimately related, as in a solid solution.[175]

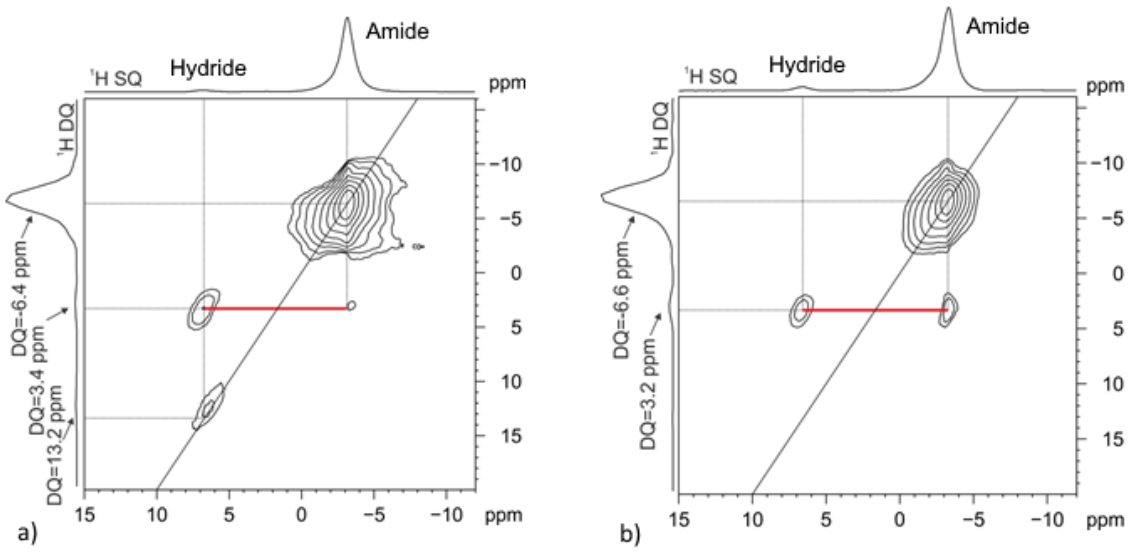

Figure 3.40: 2D ^{1}H (400.23 MHz) DQ MAS SSNMR spectra of the 0.5 $RbNH_2$ + 0.5 RbH sample after hand grinding (a) and after annealing (b) recorded with a spinning speed of 32 kHz. The red line highlights the DQ correlation between the RbH and $RbNH_2$ signals. Adapted with permission from Santoru et al., Inorg. Chem. 57, 6, 3197-3205. Copyright 2018 American Chemical Society.[176]

A similar correlation is also observed for the ground sample (Fig. 3.40-a), which can be explained with the formation of a solid solution already without annealing. Interestingly, the degree of mixing of RbH and $RbNH_2$ in this case seems to be much lower compared to the annealed sample: in fact, an auto-peak ($\delta_{DQ} = 13.2$ ppm) in the ^{1}H DQ MAS spectrum, highlights proximity between RbH protons. This signal, not present in the annealed sample, indicates that the RbH unit cells are organized in clusters and are mixed with clusters of $RbNH_2$ unit cells. This is supported in the T_1 ^{1}H relaxation measurements (Tab. 3.4), which show different T_1 values for the hydride and amide resonances (7.4 and 26.4 s, respectively) indicating the presence of distinct RbH and $RbNH_2$ domains much larger than 100 Å.

3.4.4 Rb-Mg-N-H system: general discussion and summary

The results presented just above define two new cases of structural analogies between potassium and rubidium amide based systems: the MNH_2-MH solid solution and the $MMgNH_2NH$ phase (M = {K, Rb}).

For both KNH_2 and $RbNH_2$ a low temperature (monoclinic, s.g. $P2_1/m$)[178, 135] and a high temperature (cubic, s.g. $Fm\bar{3}m$)[92, 93] polymorphs are known. However, in the case of potassium, Jacobs and von Osten reported the existence of an additional polymorph (tetragonal, s.g. $P4/nmm$) as intermediate structure between the high and low temperature modifications (Fig. 3.41).[157] For $RbNH_2$, in the same study, this structural modification was not observed, in agreement with our *in situ* SR-XPD experiments (presented in the previous section).[157] Moreover, for KNH_2 the phase transformation into cubic takes place at about

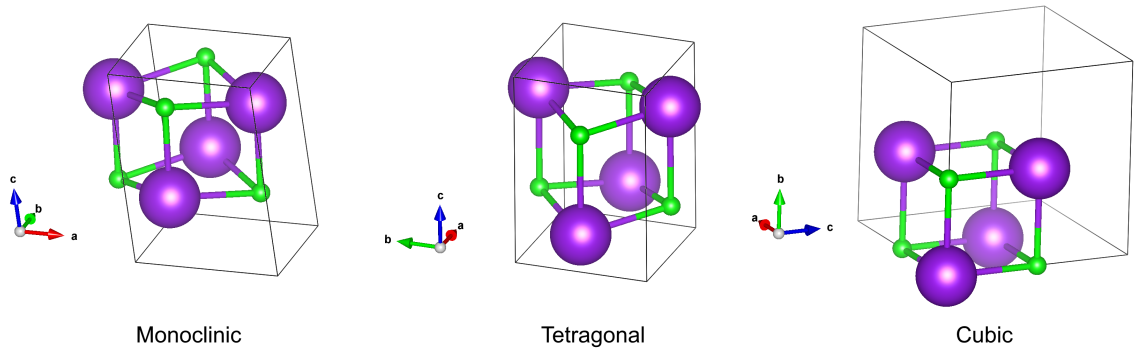

Figure 3.41: Different polymorphs of KNH_2. It is possible to identify a distorted cubic element within the tetragonal and monoclinic structures. The monoclinic and cubic structures of KNH_2 and $RbNH_2$ are isotypical. For $RbNH_2$ a direct phase transformation from monoclinic to cubic occurs. Readapted from Santoru et al., Chem. Commun., 2016, 52, 11760-11763 - Published by The Royal Society of Chemistry.[150]

75 °C[157], while in the case of $RbNH_2$ it occurs already at 65 °C (present work) or even at lower temperatures (40-45 °C in the pioneering studies).[93] For $CsNH_2$, the low temperature modification is tetragonal (s.g. $P4/nmm$) rather than monoclinic and the polymorphic change to cubic (s.g. $Pm\bar{3}m$) occurs already at 30-35 °C.[93] Therefore, the lower limit of the stability range of the cubic phase is progressively shifted to lower temperatures in the order: K, Rb, Cs. Interestingly, the melting point of the pure metals (63.2, 38 and 30 °C for K, Rb and Cs, respectively) follows the same trend.[179] The size of the cation seems to affect also the solubility of the MNH_2-MH system at RT. For the KNH_2-KH system full solubility was achieved at RT only when the content of the amide phase was very low ($x = 0.1$). In this case it is possible to achieve full solubility for all compositions, except for $x = 0.9$ (Fig. 3.34). This aspect is probably related to the fact that the bigger cation causes a stabilization of the cubic phase of the metal amide at lower temperature, which appears to be a fundamental step

toward the formation of the solid solution. In fact, at 270 °C, when for both the MNH_2 and the MH phases the cubic structure is present, it is possible to achieve full solubility for all the compositions.

The cation seems to have an effect also on the reactivity of the solid solution. In the KNH_2-KH system the peaks of the solid solution were not present or barely detectable after hand grinding, and the sample consisted essentially of unreacted KNH_2 and KH (Fig. 3.20 and Fig. 3.21). However, in the diffractograms of the $RbNH_2$-RbH system (Fig. 3.35 and Fig. 3.37), strong peaks belonging to the intermediate compositions are present already after hand grinding at RT, for all the mixed samples ($x = \{0.1, 0.3, 0.5, 0.7, 0.9\}$). These results suggest that the larger cation hastens the kinetics of the dissolution process at RT.

In both cases the amide/hydride anionic substitution causes an increase of the unit cell dimensions (Fig. 3.42), which explains the singular behaviour previously evidenced in the *in situ* SR-XPD measurements of the K–Mg–N–H system (section 3.2). Comparing the potassium and rubidium based amide/hydride systems, significantly larger cell parameters were found for M = Rb, which had to be expected considering the bigger ionic radius of Rb^+.

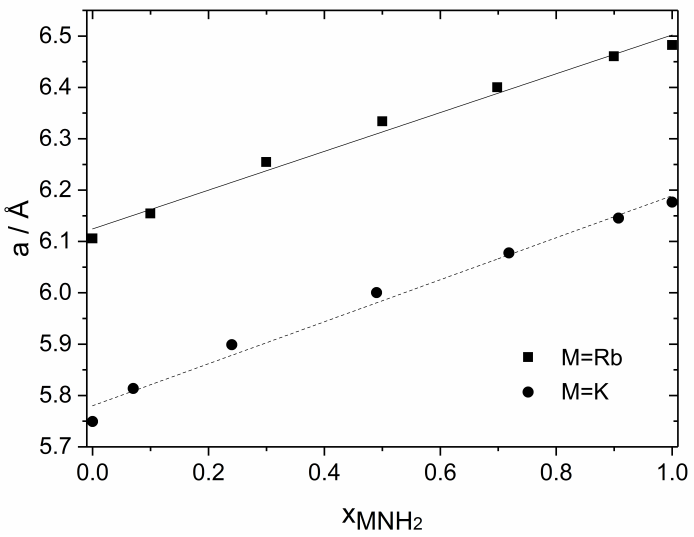

Figure 3.42: Unit cell parameters as a function of the MNH_2 content (expressed as molar fraction), obtained from Rietveld refinement of the XPD patterns acquired at 270 °C (circles and squares) and corresponding linear fit (dotted and solid lines), for M = {K, Rb}, respectively.

The structural properties of the $RbMgNH_2NH$ phase, as experimentally determined in the present work, fit very well in the crystal chemistry of metal amides. Among the known alkali and alkaline-earth metal amides with the formula $M_2Mg(NH_2)_4$ (M = {K, Rb, Cs}), only for (M = {K, Rb}) isotypic phases are formed.[99, 98] With the present work, the isostructurality of $MMgNH_2NH$ phases is also demonstrated for M = {K, Rb}. The main

differences are the increased unit cell volume and the coordination number of the monovalent cation; they are both a consequence of the different ionic radius of the monovalent cation (M^+).

Taking into account the isostructurality of $KMgNH_2NH$/$RbMgNH_2NH$ and the effects that Rb-based additives have on the hydrogen sorption kinetics of Li-Mg-N-H systems, it is interesting to recall the possible mechanisms previously proposed for the $KMgNH_2NH$ phase.[111] Both structures show more dense packing along the [100] and [001] directions (Fig. 3.43), while along the [010] direction the presence of voids and channels could promote the diffusion of hydrogen and increase the total active surface area, thus mitigating the negative impact of sintering and particle growth.

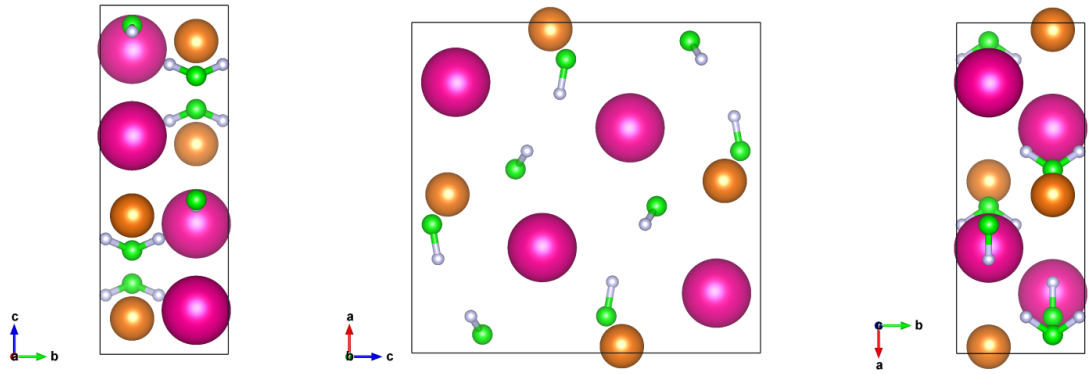

Figure 3.43: From left to right: projection along the crystallographic direction [100], [010] and [001] respectively, for the structural model of $RbMgND_2ND$. Reprinted with permission from Santoru et al., Inorg. Chem. 57, 6, 3197-3205. Copyright 2018 American Chemical Society.[176]

Moreover, the b-axis of the orthorhombic unit cell is significantly smaller than the other two axes, and also smaller than the interatomic distances between atoms of the same type within the unit cell. Thus, considering the same type of atoms, the longest atomic chain with the shortest interatomic distances runs along the b-axis. For this reason the [010] direction would probably be the most favourite pathway if diffusion by vacancies occurred.

3.5 Overall discussion

The results reported in the previous sections demonstrate numerous analogies and differences among amide-hydride systems of alkali and alkaline-earth metals. In this chapter the possible implications for K- or Rb-containing amide/hydride based composites for hydrogen storage are discussed. Moreover, the most important findings derived from the present work are presented with a broader perspective and depicted within the crystal chemistry of metal

amides.

3.5.1 Possible mechanisms of hydrogen release

The most noticeable insight gained from the *in situ* SR-XPD experiments presented in section 3.1 is certainly the difference in the ammonolysis process of potassium hydride, as compared to lithium and sodium hydride. Instead of the direct formation of the metal amide, the formation of non-stoichiometric amide-hydride cubic phases ($K(NH_2)_xH_{1-x}$) was hypothesized (Pistidda C., Santoru A. et al.[140]). In light of the follow-up study that demonstrated the correctness of this hypothesis (Santoru et al.[150]) the ammonolysis process of KH can be described according to reaction 3.22:

$$KH + xNH_3 \longrightarrow K(NH_2)_xH_{1-x} + xH_2 \tag{3.22}$$

In this case $K(NH_2)_xH_{1-x}$ is formed from the gas-solid interaction of NH_3 and KH. From the investigation conducted on the K-Mg-N-H system, reported in section 3.2 (Santoru et al.[163]), it appears clear that the same compounds can be formed also as a result of the solid-solid interaction of KNH_2 with MgH_2 or KH with $Mg(NH_2)_2$. Hence, an exchange of amide and hydride anions between the metal amide and its reaction partner occurs in the solid state. For this reason, these intermediates are not only involved in the synthesis of KNH_2 by ammonolysis of KH, but they also take part to the reaction pathway of the K-Mg-N-H hydrogen storage system and can be potentially formed in other K-containing amide/hydride composites. In the literature of the past 15 years, two main reaction mechanisms were proposed for the interaction of metal amides and metal hydrides leading to hydrogen release. The first one suggests a direct interaction of the $H^{\delta+}$ of the metal amide with the H^- anion of the metal hydride. The second mechanism considers a multi-step process mediated by ammonia: NH_3 released from the decomposition of the metal amide interacts with the metal hydride at the interface forming metal amide and releasing hydrogen; the process is repeated until all the amide is converted in the corresponding imide product.[33] The formation of $K(NH_2)_xH_{1-x}$ is compatible with both these mechanisms, since it can take place by direct anionic exchange or ammonia-mediated exchange as already discussed. The novelty of these findings however, concerns the coexistence of amide and hydride anions within the same crystal structure. In fact the existence of an amide-hydride solid solution was demonstrated, to the best of our knowledge for the first time, by the investigation presented in section 3.3 (Santoru et al.[163]). Similar results were also obtained for the Rb-N-H system, demonstrating the existence of $Rb(NH_2)_xH_{1-x}$, as reported in section 3.4 (Santoru et al.[176]). The replacement of potassium with rubidium in the amide phase causes the phase transition

monoclinic $\longrightarrow$ cubic to occur at lower temperature and without an intermediate tetragonal polymorph. When considering the entire compositional range (x$RbNH_2$ + (1-x)RbH), the effects deriving from the different cation are: expansion of the cell volume, increased solubility range at RT and a stronger driving force toward the dissolution process in general. Moreover, beyond the specific similarities and differences evidenced comparing the KNH_2-KH and $RbNH_2$-RbH systems, these results are important because they show potential applicability and transferability of this work's findings to other amide-hydride based hydrogen storage systems containing K or Rb that will be developed in the future.

3.5.2 Implications for K- and Rb-doped systems

The studies carried out to understand the role of K-based additives in the Li-Mg-N-H system evidenced the formation of several bimetallic compounds (e.g. $K_2Mg(NH_2)_4$, $KLi_3(NH_2)_4$, $KMgNH_2NH$)[110, 134, 115, 114] and the effect of the interaction of KH with $Mg(NH_2)_2$ at the interface[110, 134]. Our results show that $K(NH_2)_xH_{1-x}$ can be formed at the interface between KH and $Mg(NH_2)_2$ in the first stage of the desorption process. When considering the overall composite (Li-Mg-N-H system with K-based additives) the mechanism might be more complicated due to the presence of Li as additional variable in the chemistry of the system. Nevertheless, similar performances were obtained with K- and Rb-based additives[121, 122, 123] and the present work confirms and expands the comparable crystal chemistry of K-N-H and Rb-N-H systems. Moreover, the structural similarities between compounds of potassium and rubidium are not limited to M-N-H systems but can be further expanded also to M-Mg-N-H systems. In this regard, solving the crystal structure of $RbMgND_2ND$ allowed us to prove its isostructurality to $KMgND_2ND$ and to suggest possible mechanisms for the release and uptake of hydrogen. This perspective suggests that the similar hydrogen storage performance of K- and Rb-doped systems depends to some extent from the crystallographic analogies found in the possible reaction products and intermediates. Therefore taking into account structural similarities can be a precious strategy for finding new suitable additives (or co-additives), narrowing (or at least prioritizing) the screening window of the most promising candidates.

3.5.3 Origin of the structural analogies and differences

The explanation for the different crystal chemistry of K and Rb, as compared to Li and Na can be found in the periodic trend of the molar volumes, as pointed out in the pioneering work of Juza.[180] An updated plot is reported in Fig. 3.44, expanding this approach to include metal hydrides and bimetallic mixed amide imides.

Essentially, considering the trend of the molar volumes of ionic compounds of alkali

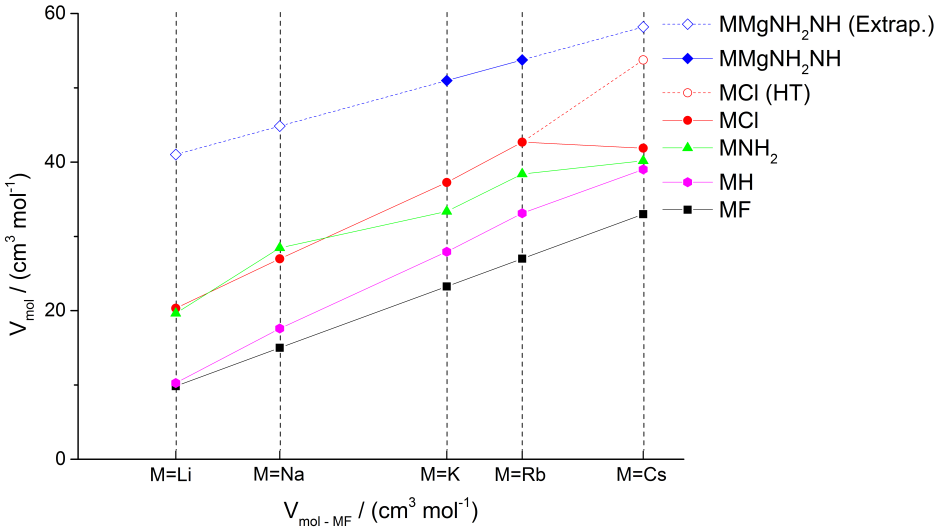

Figure 3.44: Molar volumes of alkali metal fluorides (MF), chlorides (MCl) and amides (MNH_2), as a function of the molar volume of alkali metal fluorides (MF), calculated from the cell volumes reported in the ICSD. The experimental values of $KMgND_2ND$ (Napolitano et al.[111]) and $RbMgND_2ND$ (Santoru et al.[176]) are also reported; the other values of $MMgND_2ND$ are extrapolated assuming a linear behaviour.

metals as a function of the molar volume of the alkali metal fluorides (which are taken as reference), any time this trend deviates too much from the reference, a change in the coordination number is expected, in order to avoid unstable structures (with not optimal packing density).[180]

Metal hydrides are isostructural to metal fluorides (c.n. = 6) and in fact display linear behaviour, but their slope is rather steeper then the reference curve (Fig. 3.44). For this reason a phase transition to a more dense structure (c.n. = 8) occurs at high pressure for NaH, KH, RbH and CsH. The transformation takes place at different pressures in the order $P_{CsH} < P_{RbH} < P_{KH} < P_{NaH}$ [181, 182], as predictable accordingly to this trend (the larger the deviation from the reference line, the more favourable the phase transformation to a higher density polymorph).

The trend of metal chlorides is comparable to the one of metal hydrides, indeed they are also isostructural to metal fluorides, except for CsCl. Being CsCl the extreme member, the deviation from the ideal behaviour is too large, therefore the coordination changes to 8, to achieve a smaller molar volume. Nonetheless the structure with c.n. = 6 exists above 445 °C[183], since higher temperatures thermodynamically favour the formation of less dense phases.

For metal amides, a change in the coordination number can be noticed, every time the slope of the line changes. Lithium amide and sodium amide have both c.n. = 4. However the trend is already too steep to have a stable KNH_2 with c.n. = 4. For K and Rb a coordination

number of 6 is required, for achieving a higher packing density. For caesium amide a coordination number of 8 is necessary, for the same reason. From the structural point of view, this is the key explanation for the formation of amide/hydride solid solutions. KNH_2 and $RbNH_2$ have both c.n. = 6, the same of KH and RbH, and their RT structure can be considered a distorted NaCl-type structure (Fig. 3.41).

Considering $KMgNH_2NH$, $RbMgNH_2NH$ the trend is rather parallel to the ideal one, only slightly less steeper, therefore it is possible that a $CsMgNH_2NH$ phase exists with a similar crystal structure. Conversely, the values extrapolated for $LiMgNH_2NH$ and $NaMgNH_2NH$, are more distant from the reference line and this might be the reason why the existence of these two compounds was not proven so far.

4 Outlook

The results presented in this work shed new light on the structural properties of several alkali and alkaline-earth metal amide/hydride systems and their reaction mechanism. Therefore, the present work can constitute the basis for further investigations, aiming at expanding this research line and finding similarities with other systems.

The experimental evidences discussed in this work allowed to suggest a new reaction mechanism of amide/hydride anionic exchange. These considerations provide some new ground for further discussion on the mechanistic effect of K- and Rb-based additives on the sorption properties of the Li-Mg-N-H system at atomic level. In fact, it is likely that $M(NH_2)_xH_{1-x}$ phases are formed at the first stage of the interface reaction between $Mg(NH_2)_2$ and MH, helping the transfer of amide/hydride anions between the main reaction partners ($Mg(NH_2)_2$ and LiH) through a mechanism of anionic exchange and then further reacting to form the bimetallic phases previously mentioned (e.g. $KMgND_2ND$ and $RbMgND_2ND$). The problem is challenging since the material requirements necessary to improve the hydrogen storage performance (e.g. low amount of additive, nanostructured and/or amorphous particles, fast reactions) are not optimal for conventional diffraction experiments that aim to detailed structural characterizations (e.g. single phase products, high crystallinity, long exposure times). Different experimental approaches (e.g. TEM, *in situ* EXAFS) and simulations could help to determine whether or not this mechanism takes place in the nanoscale, when small amounts of additive are considered and the material underwent the prolonged and energetic mechanochemical processing necessary to reach good cyclability.

Additional structural aspects are worth of further attention, not necessarily focusing on the role of the additives, but also on the major components of the most promising systems. For example, it is known that $Mg(NH_2)_2$ undergoes complete amorphization during high energy ball milling, however, to the best of my knowledge, little is known on the amorphous structure of this important component, other than the necessary assumption that the long range periodicity of the original crystal structure is lost. It would be interesting to determine its amorphous structure by Pair Distribution Function (PDF) analysis and clarify whether its amorphization is beneficial or not in terms of hydrogen storage properties, particularly desorption kinetics.

Another interesting aspect derived by this work is the isostructurality of $KMgNH_2NH$ and

$RbMgNH_2NH$. Considering that Cs-based additives have recently shown interesting results and that the formation of a $CsMgNH_2NH$ phase was suggested[124, 125], it is important to solve and compare its crystal structure, with respect to those of of $KMgNH_2NH$ and $RbMgNH_2NH$. This would allow to determine whether any common structural features can be identified and to compare the experimental value of its molar volume to the the extrapolated trend in Fig. 3.44.

These considerations will help the scientific community in the design of new additives for the Li-Mg-N-H system, in the identification of previously unknown components simply by conventional diffraction methods and in the understanding of reaction mechanisms at nano-scale. However, complementary research on the microstructural properties of the materials, as well as the engineering and economical challenges associated with the scale-up process, are also very important aspects that must be taken into account, in order to successfully develop industrially competitive solid state hydrogen storage systems. In this sense, interesting results have already been obtained by other team members at Helmholtz-Zentrum Geesthacht, and the research activities continue through the use of advanced experimental techniques, simulations and testing facilities in order to assess the material distribution, heat management and cycle life of prototype storage tanks.

5 Summary

The present work constitutes, besides a confirmation, also a thorough investigation of some of the main aspects of the chemistry of common alkali and alkaline-earth metal amides; its originality and innovative content is demonstrated by the numerous new findings that are summarized in this section.

Concerning the *in situ* study of the ammonolysis process, the direct formation of lithium amide and sodium amide from the corresponding hydrides was attested. On the other hand, the formation of potassium amide takes place through non-stoichiometric phases of intermediate composition, as attested from the unexpected formation of a cubic KNH_2-like phase almost at RT. The importance of the high pressure polymorph of magnesium hydride in the ammonolysis process of magnesium amide was also demonstrated, evidencing its higher reactivity at low temperatures and its primary involvement in the formation of $Mg(NH_2)_2$, probably due to its metastability and smaller particle size. This evidence suggests that ball milling can be used effectively to increase the yield of the ammonolysis process. Concerning the Ca-N-H system, the formation of calcium imide rather then its amide occurred as predictable, however, intermediate compositions are probably formed at high temperature due to its further interaction with the unreacted calcium hydride: the structural similarities between the calcium imide (CaNH) and calcium nitride hydride (Ca_2NH) might favour the formation of these intermediates. All alkali metals showed a pronounced reactivity towards ammonia, since the reactions started to take place at RT, while the alkaline-earth metals were less reactive, requiring higher temperatures to initiate the ammonolysis process.

The same phases found during the ammonolysis process of potassium hydride play also a major role in the desorption process of $K-Mg-N-H$ systems. For this reason a mechanism of anionic exchange was formulated, involving the formation of K-N-H phases with variable composition, as a result of the exchange of amide/hydride anions at the interface between $Mg(NH_2)_2$ and KH; the same K-N-H phases could be formed also following an ammonia-mediated mechanism: the ammonia released from the amide interacts with the potassium hydride releasing hydrogen by ammonolysis. Moreover, the formation of crystalline bimetallic mixed amide/imide, imide and nitride phases of potassium and magnesium ($K_2Mg(NH_2)_2(NH)$, $K_2Mg(NH)_2$ and KMgN, respectively), reported in previous studies, was disproved. Interestingly the formation of K-N-H phases with intermediate composition seems

to occur simultaneously with the release of hydrogen. In particular, the formation of these compounds started just above 100 °C from the interaction of KH and $Mg(NH_2)_2$, while in case of KNH_2 and MgH_2 at least 200 °C were necessary to initiate the process. Therefore, the interaction at the $Mg(NH_2)_2$-KH interface seems to be easier, compared to KNH_2-MgH_2, which further supports the role of KH in lowering the desorption temperature of the $Mg(NH_2)$ + 2 LiH system by facilitating the interface reaction.

Through the use of complementary techniques, the K-N-H phases with intermediate amide/hydride compositions evidenced during the ammonolysis process of potassium hydride and the desorption pathways of K-Mg-N-H systems were isolated and identified, as the first known example of a metal amide/hydride solid solution. The results suggest that at RT only a limited amount of amide phase is soluble in the hydride phase, probably due to the structural difference between the stable polymorphs of the starting components. Conversely, full solubility is achieved at 270 °C, after the phase transformation of KNH_2. The fact that the single cubic phase is preserved during the cooling process of the *in situ* experiments is most likely due to the kinetic inertia of the segregation process.

The rubidium system was proven to be able to form amide/hydride solid solutions even at RT, simply by hand grinding. Moreover, after annealing and cooling, full solubility was maintained at RT, for almost all the compositions explored, implying a much wider solubility range. Moreover, for both the potassium and rubidium systems, the segregation was only partial and didn't reach the formation of the pure starting components (MNH_2 and MH).

$RbMgND_2ND$ was synthesized and its crystal structure solved, demonstrating its isostructurality to the $KMgND_2ND$ phase. The expanded unit cell volume and different coordination of the monovalent cation can be associated to the different ionic radius of K^+ and Rb^+. $KMgND_2ND$ and $RbMgND_2ND$ are the first and only example of a bimetallic ordered amide/imide phase known so far, to the best of our knowledge.

Potassium and rubidium are so far the only elements to be proven able to form amide/hydride solid solutions and a bimetallic mixed amide imide of magnesium. These compounds are important reactants, intermediates and products of promising hydrogen storage systems. The reason for the peculiarities attested for $K(NH_2)_xH_{1-x}$/$Rb(NH_2)_xH_{1-x}$ and $KMgNH_2NH$/$RbMgNH_2NH$ was found in the crystal chemistry of metal amides. In this sense, the previous knowledge was used to formulate explanations for the new analogies and differences emerged from this work. Moreover, the structural similarities of K and Rb, further attested from the formation of isostructural phases as $MMgNH_2NH$ and $M(NH_2)_xH_{1-x}$ is most likely the reason why both KH- and RbH-doped hydrogen storage systems display similar absorption/desorption temperatures and why potassium and rubidium-based compounds can effectively work together as co-dopants, which suggests a possible strategy for the design of other additives.

Bibliography

[1] Jean-Baptiste Joseph Fourier. Mémoire sur les temperatures du globe terrestre et des espaces planétaires. *Mémoires de l'Académie des sciences de l'Institut de France*, 7:569–604, 1827.

[2] J. Tyndall. On the transmission of heat of different qualities through gases of different kinds. *Proceedings of the Royal Institution*, 3:155–158, 1859.

[3] J. Tyndall. On the absorption and radiation of heat by gases and vapours, and on the physical connexion of radiation, absorption and conduction. *Philosophical Magazine*, 22:169–194, 1861.

[4] J. Tyndall. On the absorption and radiation of heat by gases and vapours, and on the physical connexion of radiation, absorption and conduction. *Philosophical Magazine*, 22:273–285, 1861.

[5] Mike Hulme. On the origin of 'the greenhouse effect': John Tyndall's 1859 interrogation of nature. *Weather*, 64(5):121–123, 2009.

[6] S. Arrhenius. On the influence of carbonic acid in the air upon the temperature of the ground. *Philosophical Magazine and Journal of Science*, 41:237–276, 1896.

[7] S. Arrhenius and H. Borns. *Worlds in the making: the evolution of the universe*. Harper, 1908.

[8] James Rodger Fleming. Arrhenius and current climate concerns: Continuity or a 100-year gap? *Eos, Transactions American Geophysical Union*, 79(34):405–410, 1998.

[9] H. Rubens and E. Aschkinass. Beobachtungen über Absorption und Emission von Wasserdampf und Kohlensäure im ultrarothen Spectrum. *Annalen der Physik*, 300(3):584–601, 1898.

[10] G. S. Callendar. The artificial production of carbon dioxide and its influence on temperature. *Quarterly Journal of the Royal Meteorological Society*, 64(275):223–240, 1938.

[11] G. S. Callendar. On the amount of carbon dioxide in the atmosphere. *Tellus*, 10(2):243–248, 1958.

[12] G. S. Callendar. Temperature fluctuations and trends over the earth. *Quarterly Journal of the Royal Meteorological Society*, 87(371):1–12, 1961.

[13] Julia Uppenbrink. Arrhenius and global warming. *Science*, 272(5265):1122, 1996.

[14] Thomas R. Anderson, Ed Hawkins, and Philip D. Jones. CO_2, the greenhouse effect and global warming: from the pioneering work of Arrhenius and Callendar to today's Earth System Models. *Endeavour*, 40(3):178–187, 2016.

[15] Roger Revelle and Hans E. Suess. Carbon dioxide exchange between atmosphere and ocean and the question of an increase of atmospheric CO_2 during the past decades. *Tellus*, 9(1):18–27, 1957.

[16] C. MacFarling Meure, D. Etheridge, C. Trudinger, P. Steele, R. Langenfelds, T. van Ommen, A. Smith, and J. Elkins. Law Dome CO_2, CH_4 and N_2O ice core records extended to 2000 years BP. *Geophysical Research Letters*, 33(14), 2006.

[17] Ed Hawkins and Phil D. Jones. On increasing global temperatures: 75 years after callendar. *Quarterly Journal of the Royal Meteorological Society*, 139(677):1961–1963, 2013.

[18] M. King Hubbert. Energy from fossil fuels. *Science*, 109(2823):103, 1949.

[19] Hugh Odishaw. International geophysical year. *Science*, 127(3290):115, 1958.

[20] Hugh Odishaw. International geophysical year. *Science*, 128(3339):1599, 1958.

[21] Hugh Odishaw. International geophysical year. *Science*, 129(3340):14, 1959.

[22] Charles D. Keeling, Robert B. Bacastow, Arnold E. Bainbridge, Carl A. Ekdahl, Peter R. Guenther, Lee S. Waterman, and John F. S. Chin. Atmospheric carbon dioxide variations at Mauna Loa Observatory, Hawaii. *Tellus*, 28(6):538–551, 1976.

[23] Peter Lynch. The origins of computer weather prediction and climate modeling. *Journal of Computational Physics*, 227(7):3431–3444, 2008.

[24] Naomi Oreskes. The scientific consensus on climate change. *Science*, 306(5702):1686, 2004.

[25] L.A. Pachauri, R.K.; Meyer. IPCC, 2014: Climate change 2014: Synthesis report. Contribution of working groups I, II and III to the fifth assessment report of the Intergovernmental Panel on Climate Change. 2014.

[26] International Energy Agency. World energy balances: Overview, 2017.

[27] Louis Schlapbach and Andreas Züttel. Hydrogen-storage materials for mobile applications. *Nature*, 414:353, 2001.

[28] A. A. Evers. *The Hydrogen Society: More Than Just a Vision?* Hydrogeit Verlag, 2010.

[29] Brian C. H. Steele and Angelika Heinzel. Materials for fuel-cell technologies. *Nature*, 414:345, 2001.

[30] A. Bauen and D. Hart. Assessment of the environmental benefits of transport and stationary fuel cells. *Journal of Power Sources*, 86(1):482–494, 2000.

[31] George W. Crabtree, Mildred S. Dresselhaus, and Michelle V. Buchanan. The hydrogen economy. *Physics Today*, 57(12):39–44, 2004.

[32] S. C. Singhal. Advances in solid oxide fuel cell technology. *Solid State Ionics*, 135(1):305–313, 2000.

[33] M. Hirscher and K. Hirose. *Handbook of Hydrogen Storage: New Materials for Future Energy Storage*. Wiley, 2010.

[34] Ulrich Eberle, Michael Felderhoff, and Ferdi Schüth. Chemical and physical solutions for hydrogen storage. *Angewandte Chemie International Edition*, 48(36):6608–6630, 2009.

[35] D. P. Broom, C. J. Webb, K. E. Hurst, P. A. Parilla, T. Gennett, C. M. Brown, R. Zacharia, E. Tylianakis, E. Klontzas, G. E. Froudakis, Th A. Steriotis, P. N. Trikalitis, D. L. Anton, B. Hardy, D. Tamburello, C. Corgnale, B. A. van Hassel, D. Cossement, R. Chahine, and M. Hirscher. Outlook and challenges for hydrogen storage in nanoporous materials. *Applied Physics A*, 122(3):151, 2016.

[36] Gagik Barkhordarian, Thomas Klassen, and Rüdiger Bormann. Fast hydrogen sorption kinetics of nanocrystalline Mg using Nb_2O_5 as catalyst. *Scripta Materialia*, 49(3):213–217, 2003.

[37] M. Dornheim, N. Eigen, G. Barkhordarian, T. Klassen, and R. Bormann. Tailoring hydrogen storage materials towards application. *Advanced Engineering Materials*, 8(5):377–385, 2006. Cited By :153 Export Date: 23 January 2018.

[38] M. Dornheim. *Tailoring Reaction Enthalpies of Hydrides*, pages 184–214. 2010. Cited By :12 Export Date: 23 January 2018.

[39] T. Graham. On the absorption and dialytic separation of gases by colloid septa. *Phil. Trans. R. Soc. Lond.*, 156:399–439, 1866.

[40] Andrea Baldi, Tarun C. Narayan, Ai Leen Koh, and Jennifer A. Dionne. In situ detection of hydrogen-induced phase transitions in individual palladium nanocrystals. *Nature Materials*, 13:1143, 2014.

[41] Kazutoshi Miwa, Nobuko Ohba, Shin-ichi Towata, Yuko Nakamori, Andreas Züttel, and Shin-ichi Orimo. First-principles study on thermodynamical stability of metal borohydrides: Aluminum borohydride ($Al(BH_4)_3$. *Journal of Alloys and Compounds*, 446-447(Supplement C):310–314, 2007.

[42] D. Ravnsbœk, Y. Filinchuk, Y. Cerenius, H. J. Jakobsen, F. Besenbacher, J. Skibsted, and T. R. Jensen. A series of mixed-metal borohydrides. *Angewandte Chemie - International Edition*, 48(36):6659–6663, 2009. Cited By :167 Export Date: 23 January 2018.

[43] Dorthe B. Ravnsbæk, Lise H. Sørensen, Yaroslav Filinchuk, Flemming Besenbacher, and Torben R. Jensen. Screening of metal borohydrides by mechanochemistry and diffraction. *Angewandte Chemie International Edition*, 51(15):3582–3586, 2012.

[44] L. H. Rude, T. K. Nielsen, D. B. Ravnsbæk, U. Bösenberg, M. B. Ley, B. Richter, L. M. Arnbjerg, M. Dornheim, Y. Filinchuk, F. Besenbacher, and T. R. Jensen. Tailoring properties of borohydrides for hydrogen storage: A review. *Physica Status Solidi (A) Applications and Materials Science*, 208(8):1754–1773, 2011. Cited By :163 Export Date: 23 January 2018.

[45] L. H. Jepsen, M. B. Ley, Y. S. Lee, Y. W. Cho, M. Dornheim, J. O. Jensen, Y. Filinchuk, J. E. Jørgensen, F. Besenbacher, and T. R. Jensen. Boron-nitrogen based hydrides and reactive composites for hydrogen storage. *Materials Today*, 17(3):129–135, 2014. Cited By :84 Export Date: 23 January 2018.

[46] M. B. Ley, L. H. Jepsen, Y. S. Lee, Y. W. Cho, J. M. Bellosta Von Colbe, M. Dornheim, M. Rokni, J. O. Jensen, M. Sloth, Y. Filinchuk, J. E. Jørgensen, F. Besenbacher, and

T. R. Jensen. Complex hydrides for hydrogen storage - new perspectives. *Materials Today*, 17(3):122–128, 2014. Cited By :128 Export Date: 23 January 2018.

[47] L. H. Jepsen, M. B. Ley, Y. Filinchuk, F. Besenbacher, and T. R. Jensen. Tailoring the properties of ammine metal borohydrides for solid-state hydrogen storage. *ChemSusChem*, 8(8):1452–1463, 2015. Cited By :18 Export Date: 23 January 2018.

[48] B. R. S. Hansen, M. Paskevicius, H. W. Li, E. Akiba, and T. R. Jensen. Metal boranes: Progress and applications. *Coordination Chemistry Reviews*, 323:60–70, 2016. Cited By :20 Export Date: 23 January 2018.

[49] B. R. S. Hansen, N. Tumanov, A. Santoru, C. Pistidda, J. Bednarcik, T. Klassen, M. Dornheim, Y. Filinchuk, and T. R. Jensen. Synthesis, structures and thermal decomposition of ammine $M_xB_{12}H_{12}$ complexes (M = Li, Na, Ca). *Dalton Transactions*, 46(24):7770–7781, 2017. Export Date: 23 January 2018.

[50] Mark Paskevicius, Lars H. Jepsen, Pascal Schouwink, Radovan Černý, Dorthe B. Ravnsbaek, Yaroslav Filinchuk, Martin Dornheim, Flemming Besenbacher, and Torben R. Jensen. Metal borohydrides and derivatives - synthesis, structure and properties. *Chemical Society Reviews*, 46(5):1565–1634, 2017.

[51] Julián Puszkiel, Sebastiano Garroni, Chiara Milanese, Fabiana Gennari, Thomas Klassen, Martin Dornheim, and Claudio Pistidda. Tetrahydroborates: Development and potential as hydrogen storage medium. *Inorganics*, 5(4), 2017.

[52] Y. Filinchuk, D. Chernyshov, and V. Dmitriev. *Crystal chemistry of light metal borohydrides*, pages 137–164. 2011. Cited By :1 Export Date: 23 January 2018.

[53] R. Černý and Y. Filinchuk. Complex inorganic structures from powder diffraction: Case of tetrahydroborates of light metals. *Zeitschrift fur Kristallographie*, 226(12):882–891, 2011. Cited By :13 Export Date: 23 January 2018.

[54] R. Černý and P. Schouwink. The crystal chemistry of inorganic metal boro-hydrides and their relation to metal oxides. *Acta Crystallographica Section B: Structural Science, Crystal Engineering and Materials*, 71:619–640, 2015. Cited By :17 Export Date: 23 January 2018.

[55] Borislav Bogdanović and Manfred Schwickardi. Ti-doped alkali metal aluminium hydrides as potential novel reversible hydrogen storage materials1invited paper presented at the international symposium on metal-hydrogen systems, Les Diablerets, August

25-30, 1996, Switzerland.1. *Journal of Alloys and Compounds*, 253-254(Supplement C):1–9, 1997.

[56] James J. Reilly and Richard H. Wiswall. Reaction of hydrogen with alloys of magnesium and copper. *Inorganic Chemistry*, 6(12):2220–2223, 1967.

[57] G. Barkhordarian, T. Klassen, and R. Bormann. Wasserstoff speicherndes Kompositmaterial sowie Vorrichtung zur reversiblen Speicherung von Wasserstoff, 2006.

[58] J. J. Vajo, F. O. Mertens, S. L. Skeith, and M. P. Balogh. Reversible hydrogen storage system and methods for use thereof, 2005.

[59] John J. Vajo, Sky L. Skeith, and Florian Mertens. Reversible storage of hydrogen in destabilized $LiBH_4$. *The Journal of Physical Chemistry B*, 109(9):3719–3722, 2005.

[60] Gagik Barkhordarian, Thomas Klassen, Martin Dornheim, and Rüdiger Bormann. Unexpected kinetic effect of MgB_2 in reactive hydride composites containing complex borohydrides. *Journal of Alloys and Compounds*, 440(1):L18–L21, 2007.

[61] Ulrike Bösenberg, Dorthe B. Ravnsbæk, Hans Hagemann, Vincenza D'Anna, Christian Bonatto Minella, Claudio Pistidda, Wouter van Beek, Torben R. Jensen, Rüdiger Bormann, and Martin Dornheim. Pressure and temperature influence on the desorption pathway of the MgH_2-$LiBH_4$ composite system. *The Journal of Physical Chemistry C*, 114(35):15212–15217, 2010.

[62] Ulrike Bösenberg, Stefania Doppiu, Lene Mosegaard, Gagik Barkhordarian, Nico Eigen, Andreas Borgschulte, Torben R. Jensen, Yngve Cerenius, Oliver Gutfleisch, Thomas Klassen, Martin Dornheim, and Rüdiger Bormann. Hydrogen sorption properties of MgH_2-$LiBH_4$ composites. *Acta Materialia*, 55(11):3951–3958, 2007.

[63] S. Garroni, C. Milanese, A. Girella, A. Marini, G. Mulas, E. Menéndez, C. Pistidda, M. Dornheim, S. Suriñach, and M. D. Baró. Sorption properties of $NaBH_4/MH_2$ (M=Mg, Ti) powder systems. *International Journal of Hydrogen Energy*, 35(11):5434–5441, 2010.

[64] Claudio Pistidda, Sebastiano Garroni, Christian Bonatto Minella, Francesco Dolci, Torben R. Jensen, Pau Nolis, Ulrike Bösenberg, Yngve Cerenius, Wiebke Lohstroh, Maximilian Fichtner, Maria Dolores Baró, Rüdiger Bormann, and Martin Dornheim. Pressure effect on the $2\,NaH + MgB_2$ hydrogen absorption reaction. *The Journal of Physical Chemistry C*, 114(49):21816–21823, 2010.

[65] Christian Bonatto Minella, Sebastiano Garroni, David Olid, Francesc Teixidor, Claudio Pistidda, Inge Lindemann, Oliver Gutfleisch, Maria Dolores Baró, Rüdiger Bormann, Thomas Klassen, and Martin Dornheim. Experimental evidence of $Ca[B_{12}H_{12}]$ formation during decomposition of a $Ca(BH_4)_2 + MgH_2$ based reactive hydride composite. *The Journal of Physical Chemistry C*, 115(36):18010–18014, 2011.

[66] U. Bösenberg, J. W. Kim, D. Gosslar, N. Eigen, T. R. Jensen, J. M. Bellosta von Colbe, Y. Zhou, M. Dahms, D. H. Kim, R. Günther, Y. W. Cho, K. H. Oh, T. Klassen, R. Bormann, and M. Dornheim. Role of additives in MgH_2-$LiBH_4$ reactive hydride composites for sorption kinetics. *Acta Materialia*, 58(9):3381–3389, 2010.

[67] Humphry Davy. I. the bakerian lecture, on some new phenomena of chemical changes produced by electricity, particularly the decomposition of the fixed alkalies, and the exhibition of the new substances which constitute their bases; and on the general nature of alkaline bodies. *Phil. Trans. R. Soc. Lond.*, 98:1–44, 1808.

[68] L. J. Gay-Lussac, J. L.; Thénard. Notiz über das Kali - und das Natron - Metall. *Annalen der Physik*, 32(5):23–39, 1809.

[69] L. J. Gay-Lussac, J. L.; Thénard. Recherches physico-chimiques, faites sur la pile, sur la préparation chimique et les propriétés du potassium et du sodium, sur la décomposition de l'acide boracique, sur les acides fluorique, muriatique et muriatique oxigéné, sur l'action chimique de la lumière, sur l'analyse végétale et animale. *Recherches Physicochimiques (I)*, pages 337–342, 1811.

[70] L. J. Gay-Lussac, J. L.; Thénard. Recherches physico-chimiques, faites sur la pile, sur la préparation chimique et les propriétés du potassium et du sodium, sur la décomposition de l'acide boracique, sur les acides fluorique, muriatique et muriatique oxigéné, sur l'action chimique de la lumière, sur l'analyse végétale et animale. *Recherches Physicochimiques (I)*, pages 354–356, 1811.

[71] Humphry Davy. III. The Bakerian Lecture. an account of some new analytical researches on the nature of certain bodies, particularly the alkalies, phosphorus, sulphur, carbonaceous matter, and the acids hitherto undecompounded; with some general observations on chemical theory. *Phil. Trans. R. Soc. Lond.*, 99:39–104, 1809.

[72] Humphry Davy. On a combination of oxymuriatic gas and oxygene gas. *Philosophical Transactions of the Royal Society of London*, 101:155–162, 1811.

[73] F. Wöhler. Ueber künstliche Bildung des Harnstoffs. *Annalen der Physik*, 88(2):253–256, 1828.

[74] Peter J. Ramberg. The death of vitalism and the birth of organic chemistry: Wohler's urea synthesis and the disciplinary identity of organic chemistry. *Ambix*, 47(3):170–195, 2000.

[75] F. Beilstein and A. Geuther. Ueber das Natriumamid. *Justus Liebigs Annalen der Chemie*, 108(1):88–102, 1858.

[76] M. Baumert and H. Landolt. Ueber die Einwirkung des Kaliumamids auf einige organische Verbindungen. *Justus Liebigs Annalen der Chemie*, 111(1):1–11, 1859.

[77] Arthur W. Titherley. XLV.-Sodium, potassium, and lithium amides. *Journal of the Chemical Society, Transactions*, 65(0):504–522, 1894.

[78] Arthur W. Titherley. XLVI.-Rubidamide. *Journal of the Chemical Society, Transactions*, 71(0):469–471, 1897.

[79] Henri Moissan. Préparation et propriétés de l'azoture de calcium. *Compt. Rend.*, 127:497–501, 1898.

[80] E. Rengade. Sur l'amidure de caesium. *Compt. Rend.*, 140:1183–1185, 1905.

[81] Edward Curtis Franklin. Potassium ammonomagnesate, $Mg(NHK)_2 \cdot 2\,NH_3$. *Journal of the American Chemical Society*, 35(10):1455–1464, 1913.

[82] F. W. Bergstrom and W. Conrad Fernelius. The chemistry of the alkali amides. *Chemical Reviews*, 12(1):43–179, 1933.

[83] Otto Ruff and Emil Geisel. Ueber die Natur der sogenannten Metallammoniumverbindungen. *Berichte der deutschen chemischen Gesellschaft*, 39(1):828–843, 1906.

[84] F. W. Dafert and R. Miklauz. Über einige neue Verbindungen von Stickstoff und Wasserstoff mit Lithium. *Monatshefte für Chemie und verwandte Teile anderer Wissenschaften*, 31(9):981–996, 1910.

[85] Otto Ruff and Hans Goerges. Über das Lithium-imid und einige Bemerkungen zu der Arbeit von Dafert und Miklauz: "Über einige neue Verbindungen von Stickstoff und Wasserstoff mit Lithium". *Berichte der deutschen chemischen Gesellschaft*, 44(1):502–506, 1911.

[86] F. D. Miles. XI - The reaction between sodamide and hydrogen. *Proceedings of the Royal Society of Edinburgh*, 35:134–137, 1915.

[87] F. Guntz, A.; Benoit. *Bull. soc. chim.*, 41(4):434–438, 1927.

[88] Robert Juza. Über die Amide der 1. und 2. Gruppe des periodischen Systems. Metallamide. I. Mitteilung. *Zeitschrift für anorganische und allgemeine Chemie*, 231(1-2):121–135, 1937.

[89] R. Juza, K. Fasold, and Chr Haeberle. Untersuchungen über die Amide der Alkalimetalle Metallamide. II. Mitteilung. *Zeitschrift für anorganische und allgemeine Chemie*, 234(1):75–85, 1937.

[90] Robert Juza and Karl Opp. Metallamide und Metallnitride, 24. Mitteilung. Die Kristallstruktur des Lithiumamides. *Zeitschrift für anorganische und allgemeine Chemie*, 266(6):313–324, 1951.

[91] Robert Juza, Hans Hermann Weber, and Karl Opp. Kristallstruktur des Natriumamids. *Zeitschrift für anorganische und allgemeine Chemie*, 284(1-3):73–82, 1956.

[92] Robert Juza and Hans Liedtke. Zur Kenntnis des Kaliumamids. *Zeitschrift für anorganische und allgemeine Chemie*, 290(3-4):205–208, 1957.

[93] Robert Juza and Artur Mehne. Zur Kristallstruktur der Alkalimetallamide. *Zeitschrift für anorganische und allgemeine Chemie*, 299(1-2):33–40, 1959.

[94] Robert Juza and Harm Schumacher. Zur Kenntnis der Erdalkalimetallamide. *Zeitschrift für anorganische und allgemeine Chemie*, 324(5-6):278–286, 1963.

[95] H. Jacobs. Die Kristallstruktur des Magnesiumamids. *Zeitschrift für anorganische und allgemeine Chemie*, 382(2):97–109, 1971.

[96] Pierre Palvadeau and Jean Rouxel. L'amidure ternaire $K_2Mg(NH_2)_4$, l'imidure $K_2Mg(NH)_2$ et le nitrure double KMgN. *C. R. Acad. Sc. Paris*, 266:1605–1607, 1968.

[97] Pierre Palvadeau and Jean Rouxel. Préparation et caractérisation structurale d'amidures doubles de magnésium et de métaux alcalins: les dérivés $M_2Mg(NH_2)_4$. *Bulletin de la Société Chimique de France*, 2:480–485, 1970.

[98] H. Jacobs, J. Birkenbeul, and J. Kockelkorn. Darstellung und Eigenschaften der amidomagnesate des Kaliums und Rubidiums $K_2[Mg(NH_2)_4]$- und $Rb_2[Mg(NH_2)_4]$-Verbindungen mit isolierten $[Mg(NH_2)_4]^{2-}$-Tetraedern. *Journal of the Less Common Metals*, 97(Supplement C):205–214, 1984.

[99] Herbert Jacobs, Jürgen Birkenbeul, and Dieter Schmitz. Strukturverwandtschaft des dicaesiumamidomagnesats, $Cs_2[Mg(NH_2)_4]$, zum β-K_2SO_4-Typ. *Journal of the Less Common Metals*, 85(Supplement C):79–86, 1982.

[100] H. Jacobs, J. Kockelkorn, and J. Birkenbeul. Struktur und Eigenschaften der ternären Metallamide $NaCa(NH_2)_3$, $KBa(NH_2)_3$, $RbBa(NH_2)_3$, $RbEu(NH_2)_3$ und $RbSr(NH_2)_3$. *Journal of the Less Common Metals*, 87(2):215–224, 1982.

[101] Ping Chen, Zhitao Xiong, Jizhong Luo, Jianyi Lin, and Kuang Lee Tan. Interaction of hydrogen with metal nitrides and imides. *Nature*, 420:302, 2002.

[102] Yuko Nakamori and Shin-ichi Orimo. Destabilization of Li-based complex hydrides. *Journal of Alloys and Compounds*, 370(1):271–275, 2004.

[103] Y. Nakamori, G. Kitahara, K. Miwa, S. Towata, and S. Orimo. Reversible hydrogen-storage functions for mixtures of Li_3N and Mg_3N_2. *Applied Physics A*, 80(1):1–3, 2005.

[104] Haiyan Y. Leng, Takayuki Ichikawa, Satoshi Hino, Nobuko Hanada, Shigehito Isobe, and Hironobu Fujii. New Metal-N-H system composed of $Mg(NH_2)_2$and LiH for hydrogen storage. *The Journal of Physical Chemistry B*, 108(26):8763–8765, 2004.

[105] Weifang Luo. ($LiNH_2$-MgH_2): a viable hydrogen storage system. *Journal of Alloys and Compounds*, 381(1):284–287, 2004.

[106] Z. Xiong, G. Wu, J. Hu, and P. Chen. Ternary imides for hydrogen storage. *Advanced Materials*, 16(17):1522–1525, 2004.

[107] Zhitao Xiong, Jianjiang Hu, Guotao Wu, Ping Chen, Weifang Luo, Karl Gross, and James Wang. Thermodynamic and kinetic investigations of the hydrogen storage in the Li-Mg-N-H system. *Journal of Alloys and Compounds*, 398(1):235–239, 2005.

[108] Jianjiang Hu, Yongfeng Liu, Guotao Wu, Zhitao Xiong, and Ping Chen. Structural and compositional changes during hydrogenation/dehydrogenation of the Li-Mg-N-H system. *The Journal of Physical Chemistry C*, 111(49):18439–18443, 2007.

[109] Jianhui Wang, Tao Liu, Guotao Wu, Wen Li, Yongfeng Liu, Moysés C. Araújo, Ralph H. Scheicher, Andreas Blomqvist, Rajeev Ahuja, Zhitao Xiong, Ping Yang, Mingxia Gao, Hongge Pan, and Ping Chen. Potassium-modified $Mg(NH_2)_2$/2 LiH system for hydrogen storage. *Angewandte Chemie International Edition*, 48(32):5828–5832, 2009.

[110] Jianhui Wang, Guotao Wu, Yong Shen Chua, Jianping Guo, Zhitao Xiong, Yao Zhang, Mingxia Gao, Hongge Pan, and Ping Chen. Hydrogen sorption from the $Mg(NH_2)_2$-KH system and synthesis of an amide-imide complex of $KMg(NH)(NH_2)$. *ChemSusChem*, 4(11):1622–1628, 2011.

[111] Emilio Napolitano, Francesco Dolci, Renato Campesi, Claudio Pistidda, Markus Hoelzel, Pietro Moretto, and Stefano Enzo. Crystal structure solution of $KMg(ND)(ND_2)$: An ordered mixed amide/imide compound. *International Journal of Hydrogen Energy*, 39(2):868–876, 2014.

[112] Weifang Luo, Vitalie Stavila, and Leonard E. Klebanoff. New insights into the mechanism of activation and hydrogen absorption of ($2\,LiNH_2$-MgH_2). *International Journal of Hydrogen Energy*, 37(8):6646–6652, 2012.

[113] Tolulope Durojaiye and Andrew Goudy. Desorption kinetics of lithium amide/magnesium hydride systems at constant pressure thermodynamic driving forces. *International Journal of Hydrogen Energy*, 37(4):3298–3304, 2012.

[114] Yongfeng Liu, Chao Li, Bo Li, Mingxia Gao, and Hongge Pan. Metathesis reaction-induced significant improvement in hydrogen storage properties of the KF-added $Mg(NH_2)_2$-2LiH system. *The Journal of Physical Chemistry C*, 117(2):866–875, 2013.

[115] Chu Liang, Yongfeng Liu, Mingxia Gao, and Hongge Pan. Understanding the role of K in the significantly improved hydrogen storage properties of a KOH-doped Li-Mg-N-H system. *Journal of Materials Chemistry A*, 1(16):5031–5036, 2013.

[116] Chao Li, Yongfeng Liu, Yanjing Yang, Mingxia Gao, and Hongge Pan. High-temperature failure behaviour and mechanism of K-based additives in Li-Mg-N-H hydrogen storage systems. *Journal of Materials Chemistry A*, 2(20):7345–7353, 2014.

[117] Huai-Jun Lin, Hai-Wen Li, Biswajit Paik, Jianhui Wang, and Etsuo Akiba. Improvement of hydrogen storage property of three-component $Mg(NH_2)_2$-$LiNH_2$-LiH composites by additives. *Dalton Transactions*, 45(39):15374–15381, 2016.

[118] Chao Li, Yongfeng Liu, Yingjie Gu, Mingxia Gao, and Hongge Pan. Improved hydrogen-storage thermodynamics and kinetics for an RbF-doped $Mg(NH_2)_2$-$2\,LiH$ system. *Chemistry - An Asian Journal*, 8(9):2136–2143, 2013.

[119] Tolulope Durojaiye, Jalaal Hayes, and Andrew Goudy. Rubidium hydride: An exceptional dehydrogenation catalyst for the lithium amide/magnesium hydride system. *The Journal of Physical Chemistry C*, 117(13):6554–6560, 2013.

[120] Jalaal Hayes, Tolulope Durojaiye, and Andrew Goudy. Hydriding and dehydriding kinetics of RbH-doped $2\,LiNH_2/MgH_2$ hydrogen storage system. *Journal of Alloys and Compounds*, 645(Supplement 1):S496–S499, 2015.

[121] Chao Li, Yongfeng Liu, Ruijun Ma, Xin Zhang, You Li, Mingxia Gao, and Hongge Pan. Superior dehydrogenation/hydrogenation kinetics and long-term cycling performance of K and Rb cocatalyzed $Mg(NH_2)_2$-2LiH system. *ACS Applied Materials & Interfaces*, 6(19):17024–17033, 2014.

[122] Tolulope Durojaiye, Jalaal Hayes, and Andrew Goudy. Potassium, rubidium and cesium hydrides as dehydrogenation catalysts for the lithium amide/magnesium hydride system. *International Journal of Hydrogen Energy*, 40(5):2266–2273, 2015.

[123] Jalaal Hayes and Andrew Goudy. Thermodynamics, kinetics and modeling studies of KH- RbH- and CsH-doped 2 $LiNH_2/MgH_2$ hydrogen storage systems. *International Journal of Hydrogen Energy*, 40(36):12336–12342, 2015.

[124] Jiaxun Zhang, Yongfeng Liu, Xin Zhang, Yaxiong Yang, Qihang Zhang, Ting Jin, Yuxuan Wang, Mingxia Gao, Lixian Sun, and Hongge Pan. Synthesis of CsH and its effect on the hydrogen storage properties of the $Mg(NH_2)_2$-2 LiH system. *International Journal of Hydrogen Energy*, 41(26):11264–11274, 2016.

[125] Jiaxun Zhang, Yiqi Wang, Min Zhang, Zihan Leng, Mingxia Gao, Jianjiang Hu, Yongfeng Liu, and Hongge Pan. Improved overall hydrogen storage properties of a CsH and KH co-doped $Mg(NH_2)_2$/2LiH system by forming mixed amides of Li-K and Cs-Mg. *RSC Advances*, 7(48):30357–30364, 2017.

[126] Jianjiang Hu, Yongfeng Liu, Guotao Wu, Zhitao Xiong, Yong Shen Chua, and Ping Chen. Improvement of hydrogen storage properties of the Li-Mg-N-H system by addition of $LiBH_4$. *Chemistry of Materials*, 20(13):4398–4402, 2008.

[127] Hujun Cao, Guotao Wu, Yao Zhang, Zhitao Xiong, Jieshan Qiu, and Ping Chen. Effective thermodynamic alteration to $Mg(NH_2)_2$-LiH system: achieving near ambient-temperature hydrogen storage. *Journal of Materials Chemistry A*, 2(38):15816–15822, 2014.

[128] Hujun Cao, Weijin Zhang, Claudio Pistidda, Julian Puszkiel, Chiara Milanese, Antonio Santoru, Fahim Karimi, Maria Victoria Castro Riglos, Gokhan Gizer, Edmund Welter, Jozef Bednarcik, Martin Etter, Ping Chen, Thomas Klassen, and Martin Dornheim. Kinetic alteration of the 6 $Mg(NH_2)_2$-9 LiH-$LiBH_4$ system by co-adding YCl_3 and Li_3N. *Physical Chemistry Chemical Physics*, 19(47):32105–32115, 2017.

[129] Han Wang, Guotao Wu, Hujun Cao, Claudio Pistidda, Anna-Lisa Chaudhary, Sebastiano Garroni, Martin Dornheim, and Ping Chen. Near ambient condition hydrogen

storage in a synergized tricomponent hydride system. *Advanced Energy Materials*, 7(13):1602456, 2017.

[130] Han Wang, Hujun Cao, Claudio Pistidda, Sebastiano Garroni, Guotao Wu, Thomas Klassen, Martin Dorheim, and Ping Chen. Effects of stoichiometry on the H_2-storage properties of $Mg(NH_2)_2$-LiH-$LiBH_4$ tri-component systems. *Chemistry - An Asian Journal*, 12(14):1758–1764, 2017.

[131] Hujun Cao, Theresia M. M. Richter, Claudio Pistidda, Anna-Lisa Chaudhary, Antonio Santoru, Gökhan Gizer, Rainer Niewa, Ping Chen, Thomas Klassen, and Martin Dornheim. Ternary amides containing transition metals for hydrogen storage: A case study with alkali metal amidozincates. *ChemSusChem*, 8(22):3777–3782, 2015.

[132] Hujun Cao, Antonio Santoru, Claudio Pistidda, Theresia M. M. Richter, Anna-Lisa Chaudhary, Gokhan Gizer, Rainer Niewa, Ping Chen, Thomas Klassen, and Martin Dornheim. New synthesis route for ternary transition metal amides as well as ultrafast amide-hydride hydrogen storage materials. *Chemical Communications*, 52(29):5100–5103, 2016.

[133] Hujun Cao, Claudio Pistidda, Theresia M. M. Richter, Antonio Santoru, Chiara Milanese, Sebastiano Garroni, Jozef Bednarcik, Anna-Lisa Chaudhary, Gökhan Gizer, Hanns-Peter Liermann, Rainer Niewa, Chen Ping, Thomas Klassen, and Martin Dornheim. In situ X-ray diffraction studies on the de/rehydrogenation processes of the $K_2[Zn(NH_2)_4]$-8 LiH system. *The Journal of Physical Chemistry C*, 121(3):1546–1551, 2017.

[134] Jianhui Wang, Ping Chen, Hongge Pan, Zhitao Xiong, Mingxia Gao, Guotao Wu, Chu Liang, Cao Li, Bo Li, and Jieru Wang. Solid-solid heterogeneous catalysis: The role of potassium in promoting the dehydrogenation of the $Mg(NH_2)_2$/2 LiH composite. *ChemSusChem*, 6(11):2181–2189, 2013.

[135] R. Juza, H. Jacobs, and W. Klose. Die Kristallstrukturen der Tieftemperaturmodifikationen von Kalium- und Rubidiumamid. *Zeitschrift für anorganische und allgemeine Chemie*, 338(3-4):171–178, 1965.

[136] Y. Cerenius, K. Stahl, L. A. Svensson, T. Ursby, A. Oskarsson, J. Albertsson, and A. Liljas. The crystallography beamline I711 at MAX II. *Journal of Synchrotron Radiation*, 7(4):203–208, 2000.

[137] Ann-Christin Dippel, Hanns-Peter Liermann, Jan Torben Delitz, Peter Walter, Horst Schulte-Schrepping, Oliver H. Seeck, and Hermann Franz. Beamline P02.1 at PETRA

III for high-resolution and high-energy powder diffraction. *Journal of Synchrotron Radiation*, 22(3):675–687, 2015.

[138] R. V. Martins, N. Schell, T. Lippmann, F. Beckmann, H. U. Ruhnau, R. Kiehn, and A. Schreyer. The status of GKSS' High Energy Materials Science beamline at PETRA III. *Acta Crystallographica Section A*, 63(a1):s246, 2007.

[139] Ulrike Bösenberg, Claudio Pistidda, Martin Tolkiehn, Nina Busch, Ivan Saldan, Karina Suarez-Alcantara, Anna Arendarska, Thomas Klassen, and Martin Dornheim. Characterization of metal hydrides by in-situ XRD. *International Journal of Hydrogen Energy*, 39(18):9899–9903, 2014.

[140] C. Pistidda, A. Santoru, S. Garroni, N. Bergemann, A. Rzeszutek, C. Horstmann, D. Thomas, T. Klassen, and M. Dornheim. First direct study of the ammonolysis reaction in the most common alkaline and alkaline earth metal hydrides by in situ SR-PXD. *The Journal of Physical Chemistry C*, 119(2):934–943, 2015.

[141] A. P. Hammersley, S. O. Svensson, M. Hanfland, A. N. Fitch, and D. Hausermann. Two-dimensional detector software: From real detector to idealised image or two-theta scan. *High Pressure Research*, 14(4-6):235–248, 1996.

[142] E. Seifert. OriginPro 9.1: Scientific data analysis and graphing software-software review. *Journal of Chemical Information and Modeling*, 54(5):1552–1552, 2014.

[143] H. Rietveld. Line profiles of neutron powder-diffraction peaks for structure refinement. *Acta Crystallographica*, 22(1):151–152, 1967.

[144] H. Rietveld. A profile refinement method for nuclear and magnetic structures. *Journal of Applied Crystallography*, 2(2):65–71, 1969.

[145] L. Lutterotti, S. Matthies, H. R. Wenk, A. S. Schultz, and J. W. Richardson. Combined texture and structure analysis of deformed limestone from time-of-flight neutron diffraction spectra. *Journal of Applied Physics*, 81(2):594–600, 1997.

[146] Vadim Dyadkin, Philip Pattison, Vladimir Dmitriev, and Dmitry Chernyshov. A new multipurpose diffractometer PILATUS@SNBL. *Journal of Synchrotron Radiation*, 23(3):825–829, 2016.

[147] Vincent Favre-Nicolin and Radovan Černý. FOX, 'free objects for crystallography': a modular approach to ab initio structure determination from powder diffraction. *Journal of Applied Crystallography*, 35(6):734–743, 2002.

[148] Bjørn C. Hauback, Helmer Fjellvåg, Olav Steinsvoll, Kjell Johansson, Ole Tore Buset, and Johny Jørgensen. The high resolution Powder Neutron Diffractometer PUS at the JEEP II reactor at Kjeller in Norway. *Journal of Neutron Research*, 8(3):215–232, 2000.

[149] Varley F. Sears. Neutron scattering lengths and cross sections. *Neutron News*, 3(3):26–37, 1992.

[150] Antonio Santoru, Claudio Pistidda, Magnus H. Sørby, Michele R. Chierotti, Sebastiano Garroni, Eugenio Pinatel, Fahim Karimi, Hujun Cao, Nils Bergemann, Thi T. Le, Julián Puszkiel, Roberto Gobetto, Marcello Baricco, Bjørn C. Hauback, Thomas Klassen, and Martin Dornheim. KNH_2-KH: a metal amide-hydride solid solution. *Chemical Communications*, 52(79):11760–11763, 2016.

[151] Allen C. Larson and Robert B. Von Dreele. General Structure Analysis System (GSAS). Report, Los Alamos National Laboratory, 2000.

[152] Brian Toby. EXPGUI, a graphical user interface for GSAS. *Journal of Applied Crystallography*, 34(2):210–213, 2001.

[153] Koichi Momma and Fujio Izumi. VESTA 3 for three-dimensional visualization of crystal, volumetric and morphology data. *Journal of Applied Crystallography*, 44(6):1272–1276, 2011.

[154] William I. F. David, Martin O. Jones, Duncan H. Gregory, Catherine M. Jewell, Simon R. Johnson, Allan Walton, and Peter P. Edwards. A mechanism for non-stoichiometry in the lithium amide/lithium imide hydrogen storage reaction. *Journal of the American Chemical Society*, 129(6):1594–1601, 2007.

[155] Joshua W. Makepeace, Martin O. Jones, Samantha K. Callear, Peter P. Edwards, and William I. F. David. In situ X-ray powder diffraction studies of hydrogen storage and release in the Li-N-H system. *Physical Chemistry Chemical Physics*, 16(9):4061–4070, 2014.

[156] J. M. McGee. The preparation and properties of sodium amide. *Journal of the American Chemical Society*, 43(3):586–591, 1921.

[157] H. Jacobs Osten and E. Von. Die Kristallstruktur einer neuen Modifikation des Kaliumamids, KNH_2. *Z. Naturforsch.*, 31b:385–386, 1976.

[158] Satoshi Hino, Takayuki Ichikawa, Haiyan Leng, and Hironobu Fujii. Hydrogen desorption properties of the Ca-N-H system. *Journal of Alloys and Compounds*, 398(1):62–66, 2005.

[159] Lars H. Jepsen, Peikun Wang, Guotao Wu, Zhitao Xiong, Flemming Besenbacher, Ping Chen, and Torben R. Jensen. Thermal decomposition of sodium amide, $NaNH_2$, and sodium amide hydroxide composites, $NaNH_2$-NaOH. *Physical Chemistry Chemical Physics*, 18(36):25257–25264, 2016.

[160] R. A. Varin, T. Czujko, and Z. Wronski. Particle size, grain size and γ-MgH_2 effects on the desorption properties of nanocrystalline commercial magnesium hydride processed by controlled mechanical milling. *Nanotechnology*, 17(15):3856, 2006.

[161] Hikaru Yamamoto, Hiroki Miyaoka, Satoshi Hino, Haruyuki Nakanishi, Takayuki Ichikawa, and Yoshitsugu Kojima. Recyclable hydrogen storage system composed of ammonia and alkali metal hydride. *International Journal of Hydrogen Energy*, 34(24):9760–9764, 2009.

[162] Morten B. Ley, Mariem Meggouh, Romain Moury, Kateryna Peinecke, and Michael Felderhoff. Development of hydrogen storage tank systems based on complex metal hydrides. *Materials*, 8(9):5891–5921, 2015. materials-08-05280[PII] 28793541[pmid] Materials (Basel).

[163] A. Santoru, S. Garroni, C. Pistidda, C. Milanese, A. Girella, A. Marini, E. Masolo, A. Valentoni, N. Bergemann, T. T. Le, H. Cao, D. Haase, O. Balmes, K. Taube, G. Mulas, S. Enzo, T. Klassen, and M. Dornheim. A new potassium-based intermediate and its role in the desorption properties of the K-Mg-N-H system. *Physical Chemistry Chemical Physics*, 18(5):3910–3920, 2016.

[164] Francesco Dolci, Emilio Napolitano, Eveline Weidner, Stefano Enzo, Pietro Moretto, Michela Brunelli, Thomas Hansen, Maximilian Fichtner, and Wiebke Lohstroh. Magnesium imide: Synthesis and structure determination of an unconventional alkaline earth imide from decomposition of magnesium amide. *Inorganic Chemistry*, 50(3):1116–1122, 2011.

[165] V. G. Kuznetsov and M. M. Shkrabkina. X-ray diffraction study of NaH and KH at temperatures from 20 to 400°C. *Journal of Structural Chemistry*, 3(5):532–537, 1962.

[166] Lene Mosegaard Arnbjerg and Torben R. Jensen. New compounds in the potassium-aluminium-hydrogen system observed during release and uptake of hydrogen. *International Journal of Hydrogen Energy*, 37(1):345–356, 2012.

[167] Jianjiang Hu, Zhitao Xiong, Guotao Wu, Ping Chen, Kenji Murata, and Ko Sakata. Effects of ball-milling conditions on dehydrogenation of $Mg(NH_2)_2$-MgH_2. *Journal of Power Sources*, 159(1):120–125, 2006.

[168] G. Aylward Findlay and T. *Thermodynamic database: SI chemical data*. Wiley, 1998.

[169] Uri Ash-Kurlander, Gennady E. Shter, Shifi Kababya, Asher Schmidt, and Gideon S. Grader. Playing hardball with hydrogen: Metastable mechanochemical hydrogenation of magnesium nitride. *The Journal of Physical Chemistry C*, 117(3):1237–1246, 2013.

[170] M. Müller, B. Asmussen, W. Press, J. Senker, H. Jacobs, H. Büttner, W. Kockelmann, and R. M. Ibberson. Dynamics of the amide ions in potassium amide: Orientational order and disorder. *Physica B: Condensed Matter*, 234-236:45–47, 1997.

[171] M. Müller, J. Senker, B. Asmussen, W. Press, H. Jacobs, W. Kockelmann, H. M. Mayer, and R. M. Ibberson. Orientational order and rotational dynamics of the amide ions in potassium amide. I. Neutron diffraction. *The Journal of Chemical Physics*, 107(7):2363–2373, 1997.

[172] M. Müller, B. Asmussen, W. Press, J. Senker, H. Jacobs, H. Büttner, and H. Schober. Orientational order and rotational dynamics of the amide ions in potassium amide. II. Quasielastic neutron scattering. *The Journal of Chemical Physics*, 109(9):3559–3567, 1998.

[173] J. Senker. Molecular dynamics of amide ions in potassium amide (KNH_2) studied with orientation-dependent deuterium spin lattice relaxation. *Solid State Nuclear Magnetic Resonance*, 26(1):22–35, 2004.

[174] K. Gaglioti, M. R. Chierotti, F. Grifasi, R. Gobetto, U. J. Griesser, D. Hasa, and D. Voinovich. Improvement of the water solubility of tolfenamic acid by new multiple-component crystals produced by mechanochemical methods. *CrystEngComm*, 16(35):8252–8262, 2014.

[175] Michele R. Chierotti and Roberto Gobetto. NMR crystallography: the use of dipolar interactions in polymorph and co-crystal investigation. *CrystEngComm*, 15(43):8599–8612, 2013.

[176] Antonio Santoru, Claudio Pistidda, Matteo Brighi, Michele R. Chierotti, Michael Heere, Fahim Karimi, Hujun Cao, Giovanni Capurso, Anna-Lisa Chaudhary, Gökhan Gizer, Sebastiano Garroni, Magnus H. Sørby, Bjørn C. Hauback, Radovan Černý, Thomas Klassen, and Martin Dornheim. Insights into the Rb-Mg-N-H system: an ordered

mixed amide/imide phase and a disordered amide/hydride solid solution. *Inorganic Chemistry*, 57(6):3197–3205, 2018.

[177] Pascal Schouwink, Lubomir Smrcok, and Radovan Černý. Role of the Li^+ node in the Li-BH_4 substructure of double-cation tetrahydroborates. *Acta Crystallographica Section B*, 70(5):871–878, 2014.

[178] R. Juza, H. Jacobs, and W. Klose. Die Kristallstrukturen der Tieftemperaturmodifikationen von $RbNH_2$ und KNH_2. *Naturwissenschaften*, 49(2):35–36, 1962.

[179] O. Kubaschewski and C. B. Alcock. *Metallurgical thermochemistry*. Pergamon International Library. Pergamon Press, 1979.

[180] R. Juza. Amides of the alkali and the alkaline earth metals. *Angewandte Chemie International Edition in English*, 3(7):471–481, 1964.

[181] H. D. Hochheimer, K. Strössner, W. Hönle, B. Baranowski, and F. Filipek. High pressure x-ray investigation of the alkali hydrides NaH, KH, RbH, and CsH, 1985.

[182] James Hooper, Pio Baettig, and Eva Zurek. Pressure induced structural transitions in KH, RbH, and CsH. *Journal of Applied Physics*, 111(11):112611, 2012.

[183] M. Watanabe, M. Tokonami, and N. Morimoto. The transition mechanism between the CsCl-type and NaCl-type structures in CsCl. *Acta Crystallographica Section A*, 33(2):294–298, 1977.

Acknowledgements

The research leading to these results has received funding from the European Marie Curie Actions under ECOSTORE grant agreement no. 607040. I want to thank Dr. Klaus Taube, coordinator of the ECOSTORE project, for providing the necessary networking opportunities and Sigrid Wulff for all the help with the administrative and bureaucratic issues. The beamline scientists Francisco Martinez Casado, Dorthe Haase, Olivier Balmes, (MAX-lab - Lund, Sweden), Norbert Schell, Martin Etter and Jozef Bednarcik (DESY - Hamburg, Germany) and the Swiss- Norwegian Beamlines of ESRF are thankfully acknowledged for the allocation of beamtime and their excellent support with data collection. Additionally, I thank Prof. Dr.-Ing. Karsten Meier, Dr.-Ing. Tobias Redlich and their collaborators for the kind support during my studies at the Helmut-Schmidt-Universität, Nils Bergemann for helping me during our studies together and Dr.-Ing. Julian Jepsen for assisting me with the final submission of the thesis. I want to express my gratitude towards the colleagues at the research groups of the University of Turin, University of Pavia, University of Sassari, University of Geneva, Institute for Energy Technology (IFE, Norway) and here at the Helmholtz-Zentrum Geesthacht for all the interesting discussions and fruitful collaborations; moreover, I thank Dr. Claudio Pistidda, Dr. Martin Dornheim and Prof. Thomas Klassen for the kind supervision.

Aside from the professional context, I thank the friends from HZG, the friends from the ECOSTORE network and my old friends from Italy for all the laughters; all of you helped me to enjoy the last four years, filling them with a lot of happy moments.

Finally, I thank my family, particularly my parents, my brother and sister, Pino, Vanna, Francesca, Fabrizio and Roberta, for staying close to me the whole time and for encouraging me during the difficult moments.

Publications

Parts of this thesis were presented in the following peer-reviewed publications:

- C. Pistidda, A. Santoru, S. Garroni, N. Bergemann, A. Rzeszutek, C. Horstmann, D. Thomas, T. Klassen, and M. Dornheim. First direct study of the ammonolysis reaction in the most common alkaline and alkaline earth metal hydrides by in situ SR-PXD. *The Journal of Physical Chemistry C*, 119(2):934–943, 2015.

- A. Santoru, S. Garroni, C. Pistidda, C. Milanese, A. Girella, A. Marini, E. Masolo, A. Valentoni, N. Bergemann, T. T. Le, H. Cao, D. Haase, O. Balmes, K. Taube, G. Mulas, S. Enzo, T. Klassen, and M. Dornheim. A new potassium-based intermediate and its role in the desorption properties of the K-Mg-N-H system. *Physical Chemistry Chemical Physics*, 18(5):3910–3920, 2016.

- A. Santoru, C. Pistidda, M. H. Sørby, M. R. Chierotti, S. Garroni, E. Pinatel, F. Karimi, H. Cao, N. Bergemann, T. T. Le, J. Puszkiel, R. Gobetto, M. Baricco, B. C. Hauback, T. Klassen, and M. Dornheim. KNH_2-KH: a metal amide-hydride solid solution. *Chemical Communications*, 52(79):11760–11763, 2016.

- A. Santoru, C. Pistidda, M. Brighi, M. R. Chierotti, M. Heere, F. Karimi, H. Cao, G. Capurso, A.-L. Chaudhary, G. Gizer, S. Garroni, M. H. Sørby, B. C. Hauback, R. Černý, T. Klassen, and M. Dornheim. Insights into the Rb-Mg-N-H system: an ordered mixed amide/imide phase and a disordered amide/hydride solid solution. *Inorganic Chemistry*, 57(6):3197–3205, 2018.

Curriculum vitae

Personal information

Name: Antonio Santoru	Nationality: Italian
Date of birth: 14.09.1988	Place of birth: Sassari, Italy

Professional experience

03/2014 - today	Helmholtz-Zentrum Geesthacht Institute of Materials Research / Department of Nanotechnology Scientific researcher

University studies

Material science (Ph.D. student)

03/2014 - today	Helmut-Schmidt-University Target degree: Ph.D.

Chemical Sciences (student)

10/2011 - 10/2011	University of Sassari Degree: Master Degree

Chemistry (student)

09/2007 - 10/2011	University of Sassari Degree: Bachelor Degree

School education

09/2002 - 07/2007	Liceo Scientifico G. Spano Degree: Diploma - Istruzione Secondaria Superiore ad indirizzo scientifico